Imperial College of Science, Technology and Medicine
Department of Mechanical Engineering

Wildfire Simulations to Protect Rural Communities and Avoid Dire Evacuations

Nikolaos Kalogeropoulos

Supervised by Prof. Guillermo Rein, March 2025

Submitted in part fulfilment of the requirements for the degree of
Doctor of Philosophy in Mechanical Engineering, March 2025

Abstract

Large and fast wildfires can have catastrophic effects on lives, property, and the environment. Changing wildfire regimes create more destructive wildfires globally, increasing the number of people placed in danger. Evacuations from wildfires are a dramatic, disruptive, yet sometimes necessary last step to ensure people are removed from danger when other layers of wildfire protection are insufficient. Evacuations that start too late may become dire, without enough time for people to evacuate safely, exposing them to the growing hazard. It is imperative that dire evacuations be avoided. This thesis provides a definition of dire evacuations and ways to plan against them, using calculations of wildfire spread. The core effort resides in trigger boundaries, imaginary lines around communities at risk of wildfires, which when crossed by the flames denote the last safe evacuation chance. For this purpose, the k-PERIL model was developed, the first to conduct probabilistic trigger boundary calculations, and applied to the communities of Roxborough Park in Colorado, USA, Mati in Greece and Fort McMurray in Canada. With wildfire spread rate having paramount importance on the validity of trigger boundaries, even state-of-the-art wildfire models were compared, first in a series of benchmark cases, then on probabilistic trigger boundaries, to estimate the effect of model choice on safety. An ensemble approach, considering all the models combined, is required for accurate trigger boundary calculation. Moreover, an effect of wildfire that is rarely considered in evacuations is smoke. A ground-level smoke dispersion model was developed, Galini, that accounts for downwind terrain, flaming and smouldering combustion. This thesis proposes a framework to assess the danger of wildfires on communities via ensemble modelling inferred trigger boundaries, using coupled wildfire, evacuation and ground level smoke modelling. This provides quality and actionable means for communities to plan and prepare themselves for evacuations and improve community safety.

Acknowledgements

A number of great people have helped in the creation of this thesis. These people have helped in individual chapters and through the three and a half years of this PhD. I cannot thank them enough for their support.

For the thesis as a whole:

- Thank you to the Engineering and Physical Sciences Research Council (EPSRC) who funded this PhD in the form of a Doctoral Training studentship. Starting this PhD would have been impossible without their financial support.

- I would like to thank Prof. Guillermo Rein for his continued supervision. Guillermo took me in as a final year master's project student and started a collaboration whose conclusion is this thesis. His experience, generocity and open mindedness helped me turn this PhD to more than a collection of written works, and into an experience of a lifetime.

- The Hazelab research group was a great environment to work on, with its many researchers providing help, academic and spiritual, throughout my studies. Special thanks to (in no particular order) Harry Mitchell, Rikesh Amin, Francesca Lugaresi, Dwi Purnomo, Simona Dossi, Alexander Castagna, Auriane Javaloyes, Hafizha Mulyasih, Matt Bonner, Wuquan Cui, Ben Khoo and Hanna Berry.

- I could have done none of this were it not for my family and the foundation they helped me build. Thank you to my mother Elena, my father Nektarios and my brother Panagiotis for their constant multifaceted support, starting from way before this PhD commenced.

- Thank you to Anwesha De, who had to deal with my daily issues and struggles, even though she understood very little of it. Thank you for making sure I was fed and rested properly for the last few years of this PhD.

- Finally I want to thank my friends, who collectively go by the name Conferm, for reminding me that there is more to this life than just doing a PhD.

For chapter 3:

The authors thank the funding and support of National Institute of Standards and Technology (NIST) in USA, and National Research Council of Canada (NRC). We also thank the rest of the WUI-NITY team and the RACE-Wildfires team for their continued support through this project, including Amanda Kimball, Erica Kuligowski, Jonathan Wahlqvist, Arthur Rohaert, Max Kinateder, Noureddine Bénichou, and Aaron Westbury.

For chapter 4:

The authors would like to thank the Engineering and Physical Sciences Research Council (EPSRC, UK), National Research Council of Canada (NRC, Canada) and National Institute of Standards and Technology (NIST, USA) WUI-NITY project under award 60NANB22D179 from National Institute of Standards and Technology, U.S. Department of Commerce for funding this research. This work was also supported by an ARC Future Fellowship by the Australian Government through the Australian Research Council (Grant No. FT220100618). The authors would like to thank the WUI-NITY team for their continued guidance and support, Giorgos Papachristodoulou of Imperial College London for collecting data for the Mati fire simulations, Dr. Francesca Lugaresi for support with figure design, and the rest of the Hazelab research group for advice and proofreading. The authors would also like to thank Thomas J. Cova for being the first to bring attention to this area of research.

For chapter 5:

The authors thank the funding and support of National Institute of Standards and Technology (NIST) in USA, the Society of Fire Protection Engineers (SFPE), and National Research Council of Canada (NRC). This work was done as part of an SFPE Student Grant project. The authors would like to thank John Burge, Matthew Bonanni and Matthias Ihme for their help with setting up and running the Google EPD and EPD-ConvLSTM models, Robert Bryce for his help in setting up WISE, Maria Theodori for her help in running ELMFIRE.

For chapter 6:

The authors thank the funding and support of National Institute of Standards and Technology (NIST) in USA, and National Research Council of Canada (NRC). The authors would like to thank John Burge, Matthew Bonanni and Matthias Ihme for their help with setting up and

running the Google EPD and EPD-ConvLSTM models, Robert Bryce for his help in setting up WISE, Maria Theodori for her help in running ELMFIRE.

For chapter 7:

The authors thank the funding and support of National Institute of Standards and Technology (NIST) in USA, and National Research Council of Canada (NRC). This work was done as part of the RACEwildfire project.

Prologue

Many works discussing fire science open with a remark on the the relationship between man and fire. In Greek mythology, Prometheus is credited with giving the gift of fire to humanity, a gift so powerful that, for his actions, we was punished by the gods with eternal torment. A powerful gift can bring great joy, and it can bring great harm, if it is not respected appropriately.

In our modern world this is as true as in the time of the ancient Greeks. Our modern world of globalized transport of mass, energy, and information, is made possible in great part by our ability to control fire and use it to power our buildings, appliances, and wider society. Almost in balance to our use of fire as a tool, comes fire as a destructive force, akin to divine punishment. We see urban fires, battery fires, building fires, and most pertinent to this work, wildfires spawning unexpectedly, and causing great detriment to life, property and the environment.

We view wildfires as something inherently destructive and evil. Every time wildfires are in the media, they are presented as a ravenous power. The firefighters are shown battling an enemy whose purpose is only to encroach to our homes and cause as much destruction as it can. To understand the goal of this thesis, and of the whole of wildfire science, it is important to understand that wildfires are not inherently evil, or a force of havoc. Wildfires simply are, just as natural and neutral as the morning dew on the grass in a cold day. Lightning strikes would cause wildfires in forests long before people started them with power line sparks and BBQs. Wildfires existed long before humans, and will probably exist for much longer than us. The scientist James Lovelock, in his book "Gaia", wondered if wildfires are the earth's way to restore a cosmic balance to the levels of oxygen and carbon dioxide, lest we forget that the roles of the two elements are reversed for plantlife. Is "evil" a state of nature, or does it exist only because humans believe it to exist?

While this thesis is part of a Philosophy Doctorate degree, it was developed in the Department of Mechanical Engineering at Imperial College London. It will not seek out to answer the origins and root of evil, but will instead look at wildfires in the way engineers are trained to: treat it as a problem and seek a solution. To solve any problem, one can take an immediate or a long-term solution. To me, these two approaches are best explained through my years' experience as a football player, specifically a goalkeeper.

As a goalkeeper, you are the last line of defense of your team. Many times, the ball ends up at

your feet, passed back from a teammate. This is a problem; if you lose the ball to an attacker, from a challenge or a missed pass, nothing separates the ball from your open goal, risking the game. One solution is simple and can work immediately: launch the ball with full force, and send it as far away from you and your goal as possible. The immediate danger disappears, and to an audience it will look like you handled the danger well. The ball will fly far, but will probably end up to the opposing team, meaning the danger is just postponed, and may come back with greater might.

There is another solution, one that will not work immediately, one that will put you at risk in the short term, but if you train and practice for long enough, will bring great results. You can control the ball, think about who of your closest players is best placed to receive it, and pass it to them. Start a structured, coordinated attack towards the other side. A great goalkeeper is one that can do exactly this, coordinate his team and control the ball. Without practice and experience, this can be incredibly risky, with one wrong pass, either too weak or off target, giving the attacker an opportunity to score.

This is the dilemma of solving any problem. There always exists an immediate and cheap solution that will alleviate the problem but not solve it. There also exist a long-term solution, that is more expensive, but will ultimately be more effective in alleviating the effects of, and dealing with the root causes of, the problem.

Societies have figured out their immediate response to the wildfire problem, by throwing as much water and manpower as is economically and physically possible. This thesis is an argument for the more long-term solutions to wildfire, ones that ensure a societal co-existence with wildfires. Instead of viewing wildfires as an unavoidable and constant threat, we can study and understand them, to make our communities and our homes more fire resilient.

Wildfires are a complex problem that requires a multifaceted solution. This work offers some ways that we can implement long-term wildfire resilience plans, to learn from past tragedies, and make sure we do not repeat our mistakes.

Copywrite Statement

The copyright of this thesis rests with the author. Unless otherwise indicated, its contents are licensed under a Creative Commons Attribution-Non Commercial 4.0 International Licence (CC BY-NC). Under this licence, you may copy and redistribute the material in any medium or format. You may also create and distribute modified versions of the work. This is on the condition that: you credit the author and do not use it, or any derivative works, for a commercial purpose. When reusing or sharing this work, ensure you make the licence terms clear to others by naming the licence and linking to the licence text. Where a work has been adapted, you should indicate that the work has been changed and describe those changes. Please seek permission from the copyright holder for uses of this work that are not included in this licence or permitted under UK Copyright Law.

Statement of Originality

All work in this thesis, unless otherwise stated, is original work by me. While multiple collaborators have contributed in each chapter of their thesis, their involvement will be clearly highlighted in relevant areas and in the acknowledgment sections.

Contents

Abstract **i**

Acknowledgements **iii**

Prologue **vii**

Copywrite Statement **ix**

Statement of Originality **ix**

1 Introduction **1**

1.1 The six layers of Wildfire Protection 3

1.2 The 2018 Mati Fire 5

1.3 The WUI-NITY Project 6

1.4 Thesis Structure 8

1.5 Publications 8

2 Literature review **10**

2.1 Dire Evacuations 10

2.2 Trigger Boundaries 14

3 Probabilistic Trigger Boundaries **20**

3.1 The k-PERIL model 20

3.2 Results applied to Roxborough Park, USA 26

3.3 Conclusion 33

4 Quantifying dire evacuations and 2018 Mati wildfire in Greece 35

4.1 Probabilistic Distributions of WASET and WRSET 36

4.2 Evacuation safety factor and dire evacuations 37

4.3 Application of evacuation safety factor to the 2018 Mati fire 41

4.4 Conclusion 44

5 Benchmarking of Wildfire Spread Models 48

5.1 Operational Wildfire Spread Modelling 49

5.2 Selected Models 50

5.3 Methodology 52

5.4 Results 54

5.4.1 Verification 54

5.4.2 The 2018 Mati Wildfire 57

5.4.3 Ensemble modelling 60

5.5 Conclusion 62

6 Ensemble Probabilistic Trigger Boundaries 63

6.1 Introduction 63

6.2 Modelling Background 63

6.3 The Fort McMurray Case Study 64

6.4 Results 71

6.5 Discussion 79

6.6 Conclusion 82

7 Model of Gaussian Smoke Dispersion near the Ground **84**

7.1 Smoke Modelling 85

7.2 The Gaussian Dispersion Model 86

7.3 Galini Model 88

7.3.1 The Source Term 88

7.3.2 Downstream terrain effects 89

7.3.3 Injection Height 90

7.3.4 Flaming and Smouldering Fronts 92

7.3.5 Atmospheric Stability and Subgrid Modelling 93

7.4 Benchmarking and Verification 94

7.5 Conclusion 99

8 Conclusion **101**

A Mati Fuel Types **106**

B SB to CFFDRS Fuel Models Complete Table **108**

C SB to FCCS Fuel Model Conversion **111**

D Details on automatically using the ensemble models **113**

E Code Repositories **115**

Bibliography **115**

Chapter 1

Introduction

An ever increasing number of communities are impacted by the devastating effects of wildfires. The total burned area in wildfire prone, highly populated areas is increasing [1], [2]. Wildfires have been reaching record-breaking sizes in Europe [3] and equally record-breaking fatality numbers globally. The 2018 Mati fire in Greece [4], the 2018 Camp fire in the US [5], the 2023 Hawaii fires in the US [6], the 2025 Los Angeles Fires in the US [7] and the 2007 Black Saturday Fires in Australia [8] have a combined death toll of at least 486 people. Thousands of people are injured, physically or psychologically from wildfires, while the long term effects of smoke inhalation [9] and financial losses are beyond estimation.

These negative trends indicate a change in the global wildfire regimes, and subsequently a change in the way people are placed in danger. Although the number of recorded wildfires has not changed significantly, the resulting total burned area has increased [10] [11]. Four reasons have been identified that cause this change in the wildfire regime [12]. Firstly, climate change has a direct effect, with warmer and dryer summers creating environmental conditions that favor extreme wildfire behavior. The phenomenon of "climate whiplash" [13] causes rapid and sudden changes in climate, with incredibly wet seasons followed by abnormally dry summers. The wet seasons increase the vegetation load in the the wildlands, while the dry summers make this increased fuel load easy to ignite and quickly develop into unmanageable wildfires. The effect of the rise of ambient humidity at night, once considered sufficient to stop or significantly hinder wildfires, has been deteriorating [14], allowing wildfires to burn through the night more frequently than in the past.

Secondly, population movement has a profound effect on the societal impacts of wildfires, and to the changing wildfire regime. On the one hand, urbanization leads to the abandonment of farmlands and managed forests. Farmlands and managed forests have a reduced vegetation load and a higher average moisture content due to frequent irrigation, provide an earlier opportunity to detect wildfires, and more immediate means of suppressing them. Once abandoned, they

turn to unmanaged forests, which are difficult to access and monitor.

On the other hand, there is a simultaneous exodus from urban centers towards the countryside, with new developments and human activities closer to forests providing more opportunities for ignitions close to inhabited areas. Newly developed electrical infrastructure, human activity, and entertainment areas close to forests, can cause wildfires that develop very quickly and place humans in danger.

The final reason is the phenomenon of fire exclusion. Wildfires are a natural phenomenon, with many ecosystems placing wildfires in a critical part of their restoration and re-germination cycles [15]. Communities close to forested areas broke this cycle of frequent wildfires to protect their homes. Dead vegetation that would have naturally burned instead accumulates on the forest floor. As this fuel accumulates and is not burned, it provides more opportunities for ignition, and will provide the fire with more energy, making it harder to tackle. Decades of fire exclusion and fuel accumulation result in the extreme fire behavior witnessed today, where wildfires fully develop and approach communities with such power as to render most firefighting means ineffective.

The four causes of changing wildfire regime suggest that this trend will not stop in the near future. Wildfires threatening communities are a problem that needs to be adressed, as they are only projected to be worse. The communities most impacted by wildfires are in the wildland-urban interface (WUI) areas, which can be defined as the areas where wildland vegetation meets or mixes with humans and their development, including houses and infrastructure [16]. In the US, communities in the WUI have increased by over 33% in terms of both size and population from 1990 to 2010 [17]. There is an increased risk of ignition due human activity, and an elevated risk of wildfires reaching and threatening human habitation. The term WUI will be used scarcely through this thesis but is used often in the literature.

Wildfires spread via heat transfer [18]. Vegetation that is currently on fire is heating unburned vegetation primarily via convection of hot gases, radiation of the flames, direct flame contact between flaming and unburned vegetation, and firebrands, small pieces of burning vegetation that are lofted by the fire and deposited downwind, starting new ignition spots [19]. Wildfire spread needs to be studied in the smallest scales of heat transfer to be fully predicted, but can be adequately understood by considering the three controlling factors. Firstly, the direction and magnitude of the wind has a direct effect on the speed of wildfire spread, tilting the flames towards unburned fuels, promoting heat transfer and accelerating the ignition of unburned fuels [20]. Secondly, the slope of the terrain has an effect similar to that of wind. Flames spreading upwards are closer to the unburned vegetation, promoting heat transfer. Thirdly, fuel structure and humidity control the rate of wildfire spread. Thick, wet fuels are hard to ignite and have a low net heat of combustion. Thin, dry fuels are very easy to ignite and release more energy, thus controlling the ignition and speed of wildfire [21]. Understanding these three factors allows for

reasonable estimation of wildfire spread without the need to solve the heat and mass transfer involved.

Understanding the fire behavior of the area surrounding a community is paramount in establishing effective layers of wildfire protection. Estimating wildfire parameters such as its rate of spread and its flame height directly inform a community's evacuation plans, the fire service's suppression tactics, and the forest service's forest management schemes. The rate of spread of the fire is one of the more critical fire behavior values, setting the timescales for all associated layers of fire protection [19]. For this reason, a number of computational models have been developed to estimate wildfire behavior based on a set of input parameters, relating to the three controlling factors of wildfire spread. These models started development in the 1960's as simple slide rules and empirical relations that can predict the linear rate of spread of a wildfire [22], and have since evolved to computational models predicting the 2D spread of wildfire and the 3D evolution of its smoke plumes [23], [24].

1.1 The six layers of Wildfire Protection

The best way to protect communities from wildfires is to adopt a multifaceted wildfire resilience strategy, inspired by the concept of layers of fire protection in the built environment [25]. A multilayered model of fire protection ensures that, should one layer be compromised, there are other layers present to prevent failure of the system, as illustrated in Fig. 1.1. The first layer, in order of activation, is prevention. Forests surrounding populated communities should be managed in such a way that wildfire ignition is unlikely. The second layer is detection, aiming to detect a wildfire as soon as possible, to allow for the most possible time for the other layers to take effect. The third layer is compartmentation, where the spread of wildfire is contained by both natural and man-made means, such as rivers, roads, and other artificial fuel breaks preventing fire spread. The fourth layer is suppression, using water and manpower to stop or delay the spread of wildfire towards communities. The fifth layer is evacuation, which aims to remove people from the area in danger of wildfire impact. The sixth and final layer is resilience, both in the short term, ensuring that buildings do not collapse and can be used as shelter, and in the long term, ensuring that the community and its infrastructures are setup to bounce back as fast as possible. All of these layers are critical on their own and in collaboration with each other.

If all other layers of fire protection fail, it is important to ensure that the community be evacuated from the area, and ensure residents are not harmed by the wildfire. If an evacuation order be issued, there should exist an information stream regarding a plan for the evacuation, including transportation strategies [26]. It is important to assess and quantify the required evacuation time of a community and compare it to the available time prior to the wildfires

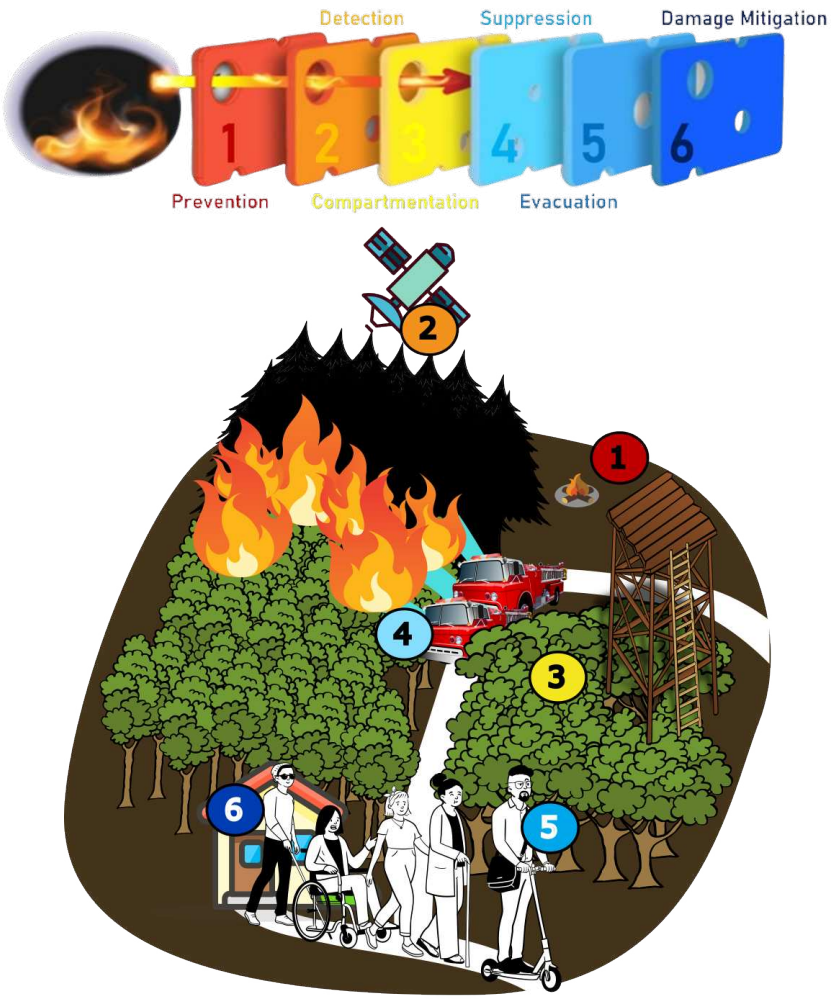


Figure 1.1: Top: The "Swiss cheese" model of the layers of fire protection, adapted from [25] Bottom: An illustration of each of the layers of fire protection.

arrival to the community. These two times are referred to as the Wildfire Required and Available Safe Egress Times (WRSET and WASET), terms adapted from fire engineering [27]. Safe evacuations require that the available time to evacuate (WASET) is greater than the required evacuation time (WRSET). This can be achieved by initiating evacuations when the wildfire front is away from the community and by minimizing the evacuation time, through tactics such as traffic management and notification systems [28], all before wildfire and smoke can impede evacuation. However, there are examples where evacuations have not been successful, resulting in entrapment and fatalities inside or near the community [29] Entrapment, in this context, refers to cases where the evacuation is hazardous, either because of the wildfire itself or because of the wildfire smoke. These evacuations, that started without enough time to be completed safely, are called dire evacuations [30], and are the most dangerous kind of evacuation. When they do occur, they place the evacuees at great danger of being harmed by the approaching wildfire. Dire evacuations must be avoided, either by starting evacuations early, or ensuring that homes and buildings can be used as refuge centers. Prior to this thesis, the concept of

dire evacuations has not been rigorously defined, and no method exists to predict when a dire evacuation may occur, or when "early" is, when starting an evacuation.

The increase in wildfire size has led to an increasing number of evacuees forced to flee from wildfires. With Canada as an example, using the data from Fig. 1.2, the number of evacuees is increasing by 2.5 % yearly. Extrapolating this globally yields an estimated total evacuee number of 620.000 per year by 2030. Many of these evacuations have the potential of becoming dire. As such, the wildfire safety layer of evacuation gets increasingly stressed, both in terms of its importance and in terms of the reliance people place upon it.

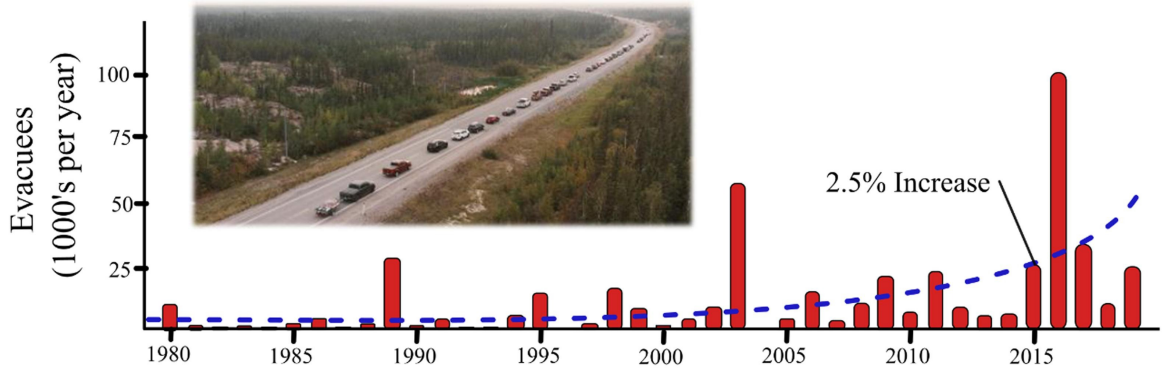


Figure 1.2: The number of people evacuating from wildfires in Canada annually. It has been steadily increasing, even though the burnt area has remained approximately the same in Canada. Data from [31]. More recent evacuation data is not available to the public. Also pictured: evacuation in progress of Yellowknife, capital of the Northwest territories of Canada, during the 2023 wildfire season (Pat Kane/Reuters 2023).

1.2 The 2018 Mati Fire

An important part of this thesis is the 2018 Mati fire near Athens, Greece. This wildfire was the deadliest in recent European history, resulting in 104 deaths and the decimation of the Mati community [4], [32]. On July 23rd 2018 a wildfire started in the mountains close to the Mati settlement, a few kilometers away from Athens, Greece. A long period of hot weather created ample amounts of dry fuel, while forest management was historically lacking, resulting in fuel accumulation and lack of robust firebreaks. Strong, dry catabatic winds [33] resulted in an average rate of spread of 35 m/min, with gust-driven increases up to 110 m/min [4]. Suppression resources were strained because of a prior nearby wildfire, while internal miscommunications meant firefighting efforts were scattered and inadequate to limit the wildfire spread. The rapid rate of spread, proximity to the local community and lack of an official evacuation notice resulted in a dire evacuation. The wildfire was a catalyst for radical change in the Greek wildfire strategy, especially around forest preparations and evacuations [34], [35].The location

of the wildfire and some of the resulting damage on the Mati community can be seen in Fig. 1.3. The extent of the wildfire can be seen in Fig. 1.4



Figure 1.3: (Left): The aftermath of the Mati wildfire. Cars, now in the middle of the road, were attempting to evacuate but were trapped as the networks got overwhelmed, most people chose to abandon their cars and head for the nearest beach. (AFP / Angelos Tzortzinis, 2018). (Right) Location of the Mati community in Attica, near Athens, Greece.

The Mati fire is selected as a case study in many parts of this thesis for a number of reasons. Primarily, the Mati fire caused a dire evacuation, with local residents spontaneously evacuating when they noticed the wildfire was putting them in danger. The dire evacuation of the community of Mati is the core example of the phenomenon this thesis is working on preventing. The author was affected by the wildfire and has family living in the area. Knowledge of the local vegetation and fuel loads, along with access to the affected area was critical in creating and collecting the datasets required for the studies in this thesis. The destructive effect it had on Greek society and the subsequent studies and investigations provide ample literature, in English and Greek, to understand the fire behavior of the area and the prevailing conditions during the fire. Lastly, the infamy of this fire has gathered scientific interest, resulting in multiple studies about the fire and the evacuation that took place. This plethora of data is what allowed the subsequent probabilistic studies to take place.

1.3 The WUI-NITY Project

A large part of this work was undertaken as part of the WUI-NITY project. WUI-NITY is a collaboration between a number of institutions, including Imperial College London (UK), Lund University (Sweden), Royal Melbourne Institute of Technology (RMIT), National Fire Protection Association (NFPA), and Movement Strategies, funded by the National Institute of Standards and Technology (NIST) and Natural Resources Canada (NRCan, through the RACEwildfire project). The goal is to create the first platform where evacuations due to wildfires can be simulated and planned with direct coupling of evacuation models and wildfire

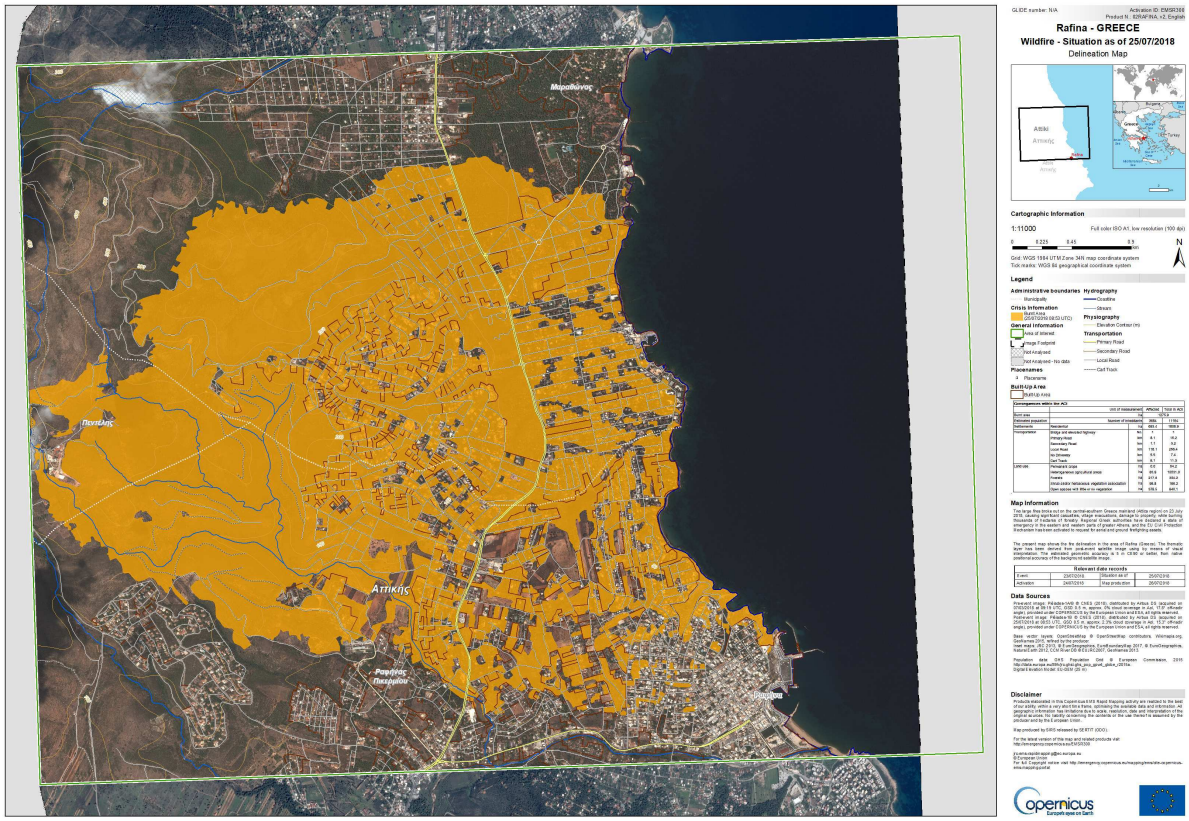


Figure 1.4: The wildfire scar of the 2018 Mati fire, as delineated by the Copernicus Mapping Service.

models. Traditionally, any sort of simulation-informed evacuation planning process involves the separate study of potential wildfire behavior and potential evacuation dynamics. The direct and pronounced influence of wildfire spread and smoke on evacuees' options and decisions was not studied, as it was not possible to simulate.

WUI-NITY aims to create a platform where evacuation simulations, smoke simulations and wildfire spread simulations run concurrently, so each of these simulation layers can affect the others in real time. It is purposefully made model agnostic, so any evacuation, wildfire and smoke model can be used interchangeably. It is the first project aiming to create a complete wildfire evacuation planning platform with pedestrian and vehicular evacuation, wildfire spread, and smoke dispersion, all while putting great focus on realistic visualisation of the results, with VR capabilities. A number of reports have been published on the progress of the project itself [27], [36]–[40], and on progress relevant to the project [41]–[48]. All chapters of this thesis are part of the WUI-NITY and RACEwildfire projects, exploring ways of utilising the direct coupling of evacuation and wildfire models, and comparing multiple potential wildfire models that can be used in WUI-NITY.

1.4 Thesis Structure

This thesis aims to explore the use of wildfire modelling, and how models can be used to inform evacuation strategies. While the most direct use of wildfire models is to predict the spread of a potential or current wildfire, this thesis aims to use wildfire models to study the wildfire danger potential surrounding communities, with the goal of creating data-backed community evacuation simulations. Ultimately, the goal of this thesis is to create a framework to create safe community evacuation plans, based on wildfire modelling and probabilistic analysis.

The chapters of this thesis have been compiled in chronological order of the work conducted. This structure introduces each of the topics sequentially, as many of the chapters build upon or rely on previous work. In furthering work that was established in a previous chapter, some of the conclusions or meanings of the work change. While working on each chapter, the nature of the work done changes, evolves and is refined. To show this evolution of understanding, and make the communication of the contents of this thesis more straightforward, the chapters are written with the understanding at that time. Each chapter, especially the earlier ones, may not reflect the final conclusions of that part of the work, and may be expanded upon or changed in subsequent chapters.

Within the scope of this thesis, Chapter 2 will introduce theory related to wildfire spread, modelling and dire evacuations. Chapter 3 will introduce kPERIL, the initial iteration of a framework created to inform evacuation plans using trigger boundaries. Chapter 4 uses the trigger boundary methodology of chapter 3 to define the once undefined concept of dire evacuations, the most dangerous kind of wildfire evacuations, using kPERIL as a tool to predict and prevent them. Chapter 5 selects seven of the state-of-the-art wildfire models, to highlight the effect of model choice when modelling a specific wildfire, ultimately showing that ensemble modelling is required for adequate wildfire risk assessment. Chapter 6 combines ensemble modelling and kPERIL to extend chapter 5, showing that multiple models are required to fully understand the potential wildfire behavior and create evacuation plans for a community. Chapter 7 will present Galini, a fast computational model of smoke transport near a wildfire, which has a substantial effect on the evacuation of a community. Finally, chapter 8 will provide some conclusions and discussion of the results of this thesis.

1.5 Publications

The main chapters of this thesis are a compilation of publications, either already published, in peer review or in preparation for submission. These publications are:

- For Chapter 3: N. Kalogeropoulos, H. Mitchell, E. Ronchi, *et al.*, “Design of stochastic

trigger boundaries for rural communities evacuating from a wildfire," *Fire Safety Journal*, vol. 140, Oct. 2023, Publisher: Elsevier Ltd. DOI: 10.1016/j.firesaf.2023.103854

- For Chapter 4: N. Kalogeropoulos, H. Mitchell, E. Kuligowski, *et al.*, "Quantifying dire evacuations in case of wildfire using trigger boundaries and case study of the 2018 Mati wildfire in Greece," *Safety Science*, vol. 181, Jan. 2025, Publisher: Elsevier B.V.. DOI: 10.1016/j.ssci.2024.106691

- For Chapter 5: N. Kalogeropoulos and G. Rein, "Benchmarking of Semi-Empirical and Machine Learning Models of Wildfire Spread Outside their Calibration Region". Submitted to the Mediterranean Combustion Symposium in Corfu, Greece for publication in conference proceedings.

- For Chapter 6: N. Kalogeropoulos, H. Mitchell and G. Rein, "Using Ensemble Modelling Methodologies in Probabilistic Trigger Boundaries to Plan Wildfire Evacuations". Submitted to Interflam in Royal Holloway, UK for publication in conference proceedings.

- For Chapter 7: N. Kalogeropoulos, A. Castagna and G. Rein, "A Gaussian Dispersion Model for Haze Spread with Downwind Terrain Effects". Submitted to the International Symposium of Fire and Explosion Hazards in Rome, Italy for publication in conference proceedings.

Other publications that were aided as part of this PhD are:

- H. Mitchell, S. Gwynne, E. Ronchi, *et al.*, "Integrating wildfire spread and evacuation times to design safe triggers: Application to two rural communities using PERIL model," *Safety Science*, vol. 157, Jan. 2023, Publisher: Elsevier B.V.. DOI: 10.1016/j.ssci.2022.105914

- E. Ronchi, J. Wahlqvist, A. Rohaert, *et al.*, "WUI-NITY 2: The integration, verification, and validation of the wildfire evacuation platform WUI-NITY," Tech. Rep., 2021. [Online]. Available: www.nfpa.org/foundation

- E. Ronchi, J. Wahlqvist, A. Ardinge, *et al.*, "The verification of wildlandurban interface fire evacuation models," en, *Natural Hazards*, vol. 117, no. 2, pp. 1493–1519, Jun. 2023, ISSN: 0921-030X, 1573-0840. DOI: 10.1007/s11069-023-05913-2. [Online]. Available: https://link.springer.com/10.1007/s11069-023-05913-2 (visited on 01/28/2025)

Chapter 2

Literature review

2.1 Dire Evacuations

Dire evacuations are a core part of this thesis, defining evacuations that start without enough time to be completed safely. Dire evacuations place evacuees in great danger. There is limited literature on the concept of dire evacuations from wildfires. A literature review was conducted to identify papers that discussed wildfire evacuations and the potential of an evacuation becoming dire. Since dire evacuations is a recent term, other search terms were used such as late, failed, rushed and slow. Papers discussing wildfires with multiple fatalities caused by late evacuations were also identified. A total of 30 papers and reports were identified, each discussing dire evacuations to some extent, some more directly than others.

A set of case studies discusses wildfires where an evacuation took place [29]. The dataset identified 28 notable wildfires where evacuation was actioned, most in north America and Europe. While some of these wildfires are obvious examples of dire evacuations, such as the 2018 Camp fire in the western US, 10 of the 28 cases included details describing faults with the evacuation, ranging from car queuing to burnovers and entrapments. This shows that, even if they have not been directly identified, dire evacuations occur in a significant number of wildfires. Some of the most recent cases of dire evacuations are the Lahaina fire of 2023 in the USA, the Mati fire of 2018 in Greece and the Camp fire of 2018 in the USA. Fig. 2.1 shows post-fire photos of four critical dire evacuations. In all cases evacuees were forced to evacuate while the wildfire was approaching them, often leading to wildfire entrapment, vehicle failure and casualties. The commonality of these fires, where evacuation complications arise in dire evacuations, is a common pattern in high-casualty wildfires. In Lahaina, strong catabatic winds, flammable construction material and the failure of communication-related infrastructure resulted in late evacuation notice and a high rate of wildfire spread [49]. In Mati, the lack of an official evacuation notice meant people started evacuating late, in some instances when

the wildfire reached their location [4], [32], [50]–[52]. In the Camp fire, a series of wildfires started very near a community and very early in the morning, not allowing enough time for a full and organized evacuation [5], [53], [54]. The Tubbs fire of 2017 in the USA with 22 deaths, and the Pedrógão Grande fire of 2017 in Portugal, with 66 deaths, are also examples of dire evacuations, where most of the fatalities were caused by wildfire and smoke reaching and engulfing the evacuees during the evacuation. These examples can be characterized dire evacuations, as the evacuation process itself occurred too late, placing people in danger of being entrapped by the wildfire.



Figure 2.1: Photos of the aftermaths of dire evacuations. In each case, the wildfire overtook evacuees who either abandoned their vehicles or were unable to do so. Top left: 2023 Lahaina Fire (Tiffany Kidder Winn via AP). Top right: 2016 Fort McMurray Fire (Canadian Press). Bottom left: 2018 Camp Fire (Josh Edelson/AFP/Getty Images). Bottom right: 2017 Pedrógão Fire (Guillermo Martinez/Reuters)

Post-incident research focuses on identifying the factors that led to casualties [55], [56], along with factors that influence decision making, such as whether to evacuate or shelter in place [57]. One such study examines the evacuation guidance in Greece, which routinely faces wildfires that cause dire evacuations, concluding that while early evacuation is the safest choice for communities threatened by wildfire, stay-in-place may also be a viable strategy [58]. Similar research was conducted in Israel, following the wildfire that threatened Haifa in 2016 [57]. The researchers compared the demographic data with the individuals choice to evacuate or not and their preferred route, highlighting that a large number of people evacuated by first making intermediate stops in the city to help friends and family. A paper studying communities in the USA focused on the responses of a community that evacuated from the 2019 Kincade Fire and compared the results to the 2016 Chimney Tops 2 Fire [59], both wildfires that either were or were close to being dire. Differences in response type were observed between

the two communities, mostly attributed to differences in wildfire experience and preparedness. Such reports and research on human behavior and evacuation, along with data collection from real wildfires [41], have resulted in multilayer models such as WUI-NITY [27], [36]–[38] and frameworks that describe human behavior in wildfire evacuation, with the aim of integrating it into evacuation planning and strategy [60]. A number of studies have looked into national or international statistics to analyze whether particular demographics are more susceptible, or whether specific activities and preparation plans during a wildfire are more effective or detrimental [61]. Examples include studies on Greece [55], the Mediterranean [62], and Australia [56], [63].

Australia has comparatively more research in topics relevant to dire evacuations, owing to their policy shift following the 2009 Black Saturday Fires. Prior to 2009, the Australian policy was to instruct residents to either evacuate wildfire-prone areas well in advance of extreme fire risk days, or to stay inside their homes when a wildfire occurs (Prepare, stay and defend or leave early). A statistical analysis of fatalities from 1900 to 2008 revealed that a large number of civilian deaths were occurring near their houses or inside their vehicles, indicating entrapment [56], [63]. The policy of staying and defending if unable to evacuate early was followed until the 2009 Black Saturday fires, which resulted in the highest death toll of any wildfire globally, where the majority of deaths were recorded inside houses. Based on the findings of the 2009 Victoria Bushfires Royal Commission [8], and relevant research on the bushfire plan preparedness and application of Australian citizens [64], [65], the Australian fire and emergency service authority changed their guidance to The safest action to protect life is for people to be away from the bushfire or threat of bushfire as early as possible, discouraging the option of sheltering in place.

A seminal paper by [30] is the first paper identified in the literature that establishes the term dire evacuations in the context of wildfires. It establishes a framework to model dire evacuations in terms of the temporal evacuation stages. Using a direness index, Cova et. al. quantify the relationship between remaining evacuation and available time. The paper stresses the need to move away from evacuation research assuming ample time for preparation and initiation, and to adopt research frameworks to avoid dire evacuations. Based on this paper, two papers by Grajdura et al discuss dire evacuations, based on modelling and observations of the 2018 Camp Fire in the US. The first of the two papers [53] investigates the response of people during the Camp Fire, in relation to when the evacuees detected the wildfire and how long it took them to initiate evacuating. In the second paper [54], an agent-based evacuation model is presented. Conclusions are then drawn on the factors correlated with people being trapped, highlighting that age, gender, wealth, education and smartphone ownership were all factors that affected the chances of entrapment.

A report published by NIST [5] provides guidance for small and medium sized communities at risk of wildfires, in terms of planning and preparation. A large part of the report, and a

major highlight of it, is on the conditions that can cause a dire evacuation, a term explicitly mentioned in the report. It places emphasis on both early evacuation and methods to respond to dire evacuations. The report suggests that communities produce maps of the landscape around them, and designate different zones based on the expected WASET and WRSET (although the report avoids using these terms and instead refers to wildfire rate of spread and evacuation duration). Wildfires that are in the outermost identified zone may allow enough time for an evacuation, while wildfires past the first zone and into the inner zone will allow enough time only for partial evacuation, at which point other courses of action need to be adopted, such as instituting temporary refuge areas inside the community, to avoid dire conditions. This methodology draws upon the principles of trigger boundaries, which will be extensively discussed later in the paper.

In transportation network design, an important design parameter is the capability of the road network to accommodate evacuees during an emergency. While the term dire is not used, the alternative term no-notice is extensively used. Most such research is aimed at cases of nuclear accidents, chemical accidents, earthquakes and terrorism [66]–[71]. The term no-notice does not have a set definition, with total evacuation values ranging from a few minutes of notice [66] to 72 h [72]. Some papers on transportation network design focus on hurricane evacuations and discuss late evacuations [72], but the difference in evacuation time values between hurricanes and wildfires is significant. One paper [73] presents a transportation model used to analyse the entrapment behavior of the population.

The identified literature discussed three primary categories of research. The first category is human behavior, with specific research ranging from evacuation modelling, road network optimization, and studies of human behavior. The second category is real wildfires, either recent ones or historical. The third category is wildfire behavior (including its effect on evacuations). As part of this literature review, each paper was given a weighting based on its contributions to each , estimated qualitatively. Based on these weightings, a ternary plot was developed which shows each paper as a point based on the three categories. Fig. 2.2 is a ternary plot categorizing each examined source based on its core subject and its relation to dire evacuations. Fig. 2.2 shows the range of disciplines and areas of research related to dire evacuations, and the necessity for a balanced approach in studying the concept of dire evacuations in depth. There is limited overlap between categories and references. Each paper was also given a weighting based on its direct relevance to dire evacuations, displayed as a darker fill. Papers with low dire evacuation relevance discuss the possibility of late evacuations but it is not the main focus of the paper. Papers with high dire evacuation relevance discuss dire evacuation directly and as a core topic of the paper. Papers that discuss dire evacuations are multidisciplinary, towards the midpoint of the plot, containing a mixture of categories, as shown by the papers most directly discussing dire evacuations being in the center of the plot in Fig. 2.2. A balance between the three is needed for thorough understanding of dire evacuations. This figure can be used to show

that greater collaboration and interdisciplinarity is needed to understand dire evacuations.

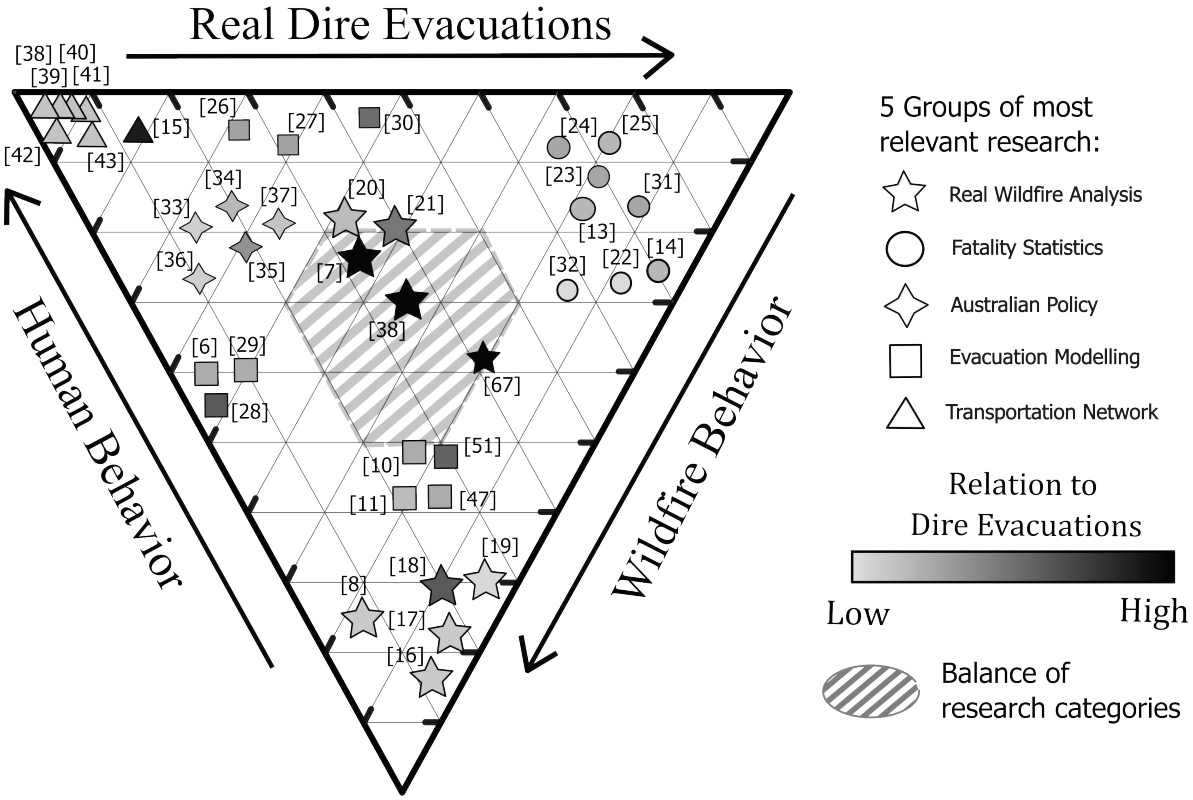


Figure 2.2: Arrangement of the literature on wildfire dire evacuations, in relation to the three main categories. The area in the middle represents a balance between the three research areas, where dire evacuation would be ideally integrated. The numbers of each point refer to the reference number in [45].

2.2 Trigger Boundaries

A critical tool for evacuation planning is trigger boundaries. Trigger boundaries are imaginary lines surrounding a community, informing the safety of a potential evacuations. Evacuations that start before a wildfire crosses this imaginary line are early enough to be completed safely before the wildfire reaches the community and places people at risk. If an evacuation starts after the wildfire crosses the trigger boundary, there will not be enough time to safely complete the evacuation.

The concept of trigger boundaries in wildfires comes from hurricane evacuations [74]. Emergency responders dealing with the landfall of hurricanes in coastal North America first used the concept of timing arcs, like the ones in Fig. 2.3, to relate the arrival time of a hurricane with its isochrones on a map. Timing arcs are circles away from a target community, indicating the location of a hurricane a certain amount of time away. While the time represented by the arcs is not associated with the evacuation process, this practice laid out the foundation for evacuation

hazard visualization, in associating a transient hazard with a spatial location. The introduction of a similar concept to wildfires is attributed to the group of Prof. Cova at the University of Utah, with their research on trigger boundaries (also called trigger buffers), calculated with the WUIVAC model, as seen in Fig. 2.3 [75]–[77]. They are an equivalent hazard visualization system to that of the timing arcs, made of a single boundary surrounding a community for a given wildfire, with the temporal aspect being the required evacuation time of the community.

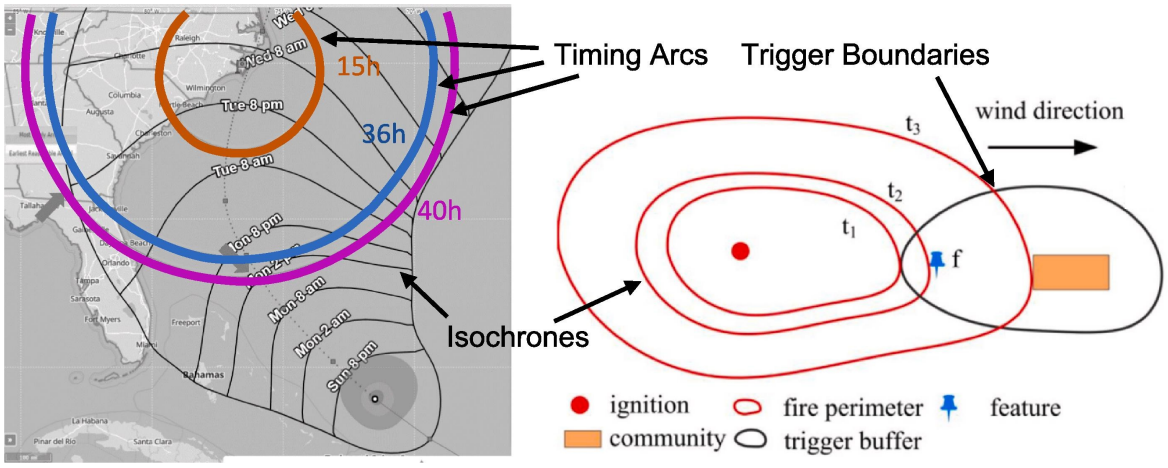


Figure 2.3: Illustrations of timing arcs used in hurricane research (adapted from [74]) and of evacuation trigger boundaries (adapted from [75]) Timing arcs mark the position of an impending hurricane at specific time intervals away from a target community. Trigger boundaries similarly mark the position of the wildfire at a time equal to the total evacuation time away from the community.

Trigger boundaries associate the spread rate and position of the wildfire with the evacuation progression. They suggest the latest safe time to evacuate by relating the position of the wildfire with its remaining travel time to the edge of the community. For a given wildfire and evacuation response, there exists a contour around a community where the available time is equal to the required time. The trigger boundary can be mathematically described as the locus of all the points in the landscape where the criterion in Eq. 2.1 is met.

$$WASET = WRSET \tag{2.1}$$

The way WASET and WRSET are obtained can be either through simulations or field data, though for most cases in the literature, models are used to predict the wildfire spread rate. Wildfire models are used to predict the spread based on inputs relating to the wind, the vegetation, and the topography around a community. Evacuation models estimate the egress of a pedestrian and vehicular population from a community under threat, using variables that represent the communitys response characteristics. The WASET of the wildfire is difficult to estimate directly, but for the purposes of this thesis can be approximated as the distance of the current wildfire perimeter to the community D, divided by the average rate of spread of the

wildfire ROS, as defined in Eq. 2.2.

$$WASET = \frac{D}{ROS} \tag{2.2}$$

Estimating the WASET of a potential wildfire requires understanding the wildfire behavior through a landscape, which is possible with wildfire spread models. The main goal of a wildfire model is to predict the evolution of the fire front over time, along with related information such as the flame length and fireline intensity at any given point in the fire front. Models can either start from the ignition of the fire or from an already developed fire front. A wide range of models have been developed in the literature to meet the different needs of wildfire science. Sullivan et. al. [78]–[80] have categorised existing models to a spectrum. Physical models solve fundamental equations of fluid motion and chemical kinetics to calculate wildfire progression [24]. These models are accurate but are typically very resource intensive; they are mostly used for fundamental research on fire spread mechanisms. On the other extreme are empirical models, which are based on experimental observations, data and regressions [81]. These models tend to be fast but inaccurate when used on anything other than the experimental conditions. In the middle between the two are semi-empirical and semi-physical models. These models incorporate aspects from both ends of the spectrum. Semi-physical models may neglect chemical kinetics equations and use lab data or heuristics instead, while semi-empirical models may employ physical equations with parameters fitted by experimentation [23], [82]. Recently, models based on machine learning have been developed, aiming to provide similar results to existing models but at a fraction of the computational cost and computation time [83]. Very few developed models account for the stochastic inputs of wind, weather, and fuel, instead opting either to use time-averaged values or specific, prescribed inputs. The variable effects of wildfires are thus not represented, only the average, or most probable, wildfire can be estimated with these models.

Estimating the WRSET of a community is possible through simulating the evacuation process. Evacuation models use different approaches, inputs and concepts to try and simulate human behaviour. A literature review by [84] and [85] identified 12 traffic and evacuation models that are in use today, and highlighted that only four of them are developed for emergency evacuations. The rest were made for steady-state traffic planning, illustrating that more research needs to be put into evacuation modelling. Evacuation traffic models are rare, and wildfire-coupled evacuation models are sparse. A vast minority of traffic models also consider and quantify the probabilistic nature of traffic due to the original stochastic conditions, especially so in wildfire evacuations. The wildfire progression also has an active effect on evacuation, whether that is through evacuation triggers like the smoke plume visibility, or through road blockages and limited visibility because of smoke. It is critical that specialised emergency evacuation models be developed so that WRSET values and the stochastic nature thereof can be accurately predicted

and quantified [27], [36]–[38].

Multiple factors affect the WRSET and WASET times. Factors affecting the wildfire behavior include variations in wind, weather, fuel moisture and fuel loading. These affect the spread rate and therefore the ASET [19]. Factors affecting human behavior include decision delays and traffic congestion, which increase the WRSET. Other factors are the pre-evacuation decision time [86], traffic congestion [41]and route choice [85]. All these factors have been reported to affect past evacuations and are detrimental to the evacuation process [41], [48], [59], [86]. Congestions appear when evacuees attempt to evacuate in larger numbers than the traffic network can accommodate, or when the ability of the network to accommodate the evacuees is compromised, in cases when there is reduced visibility because of smoke [87], fire-related road closures or vehicle breakdowns. The conditions that result in delays and congestion can be taken into account in WRSET calculations and therefore in trigger boundaries. A graphical representation of the two time scales, WRSET and WASET, is shown in 2.4.

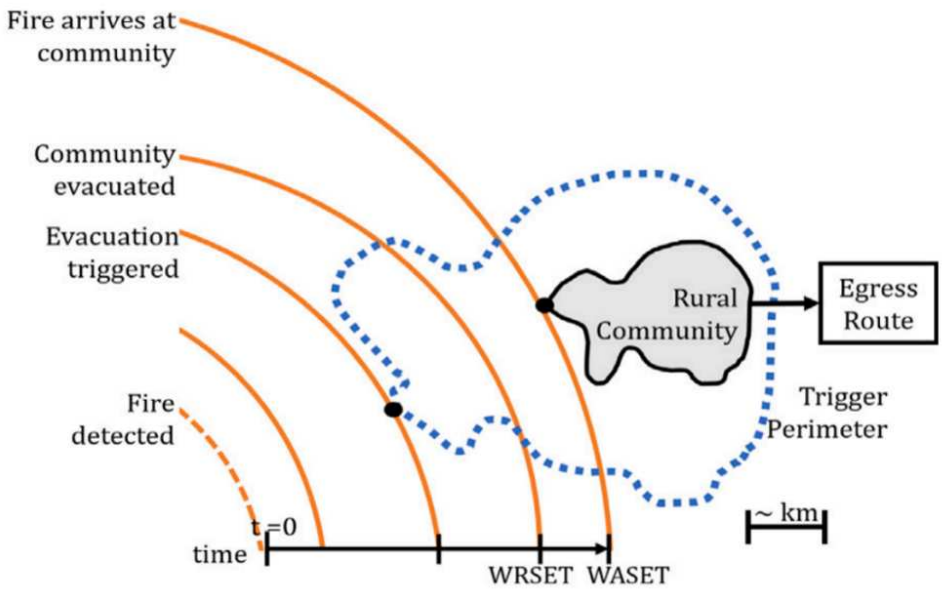


Figure 2.4: Schematic of the function of trigger boundaries (here referred to as trigger perimeters) [27] The time between the fire detection and the complete community evacuation is WRSET. The time between the fire detection and the fire arrival at the community is WASET.

Trigger boundary models use wildfire spread and evacuation simulations. They equate the WASET and WRSET of a specific wildfire event to denote the last safe evacuation opportunity, relating to the wildfire progression. A number of such models have been developed in the literature. One critical model is WUIVAC [75], [76], [88], a deterministic, open source model that works for one wildfire and evacuation scenario at a time. It uses the rate of spread values created by a wildfire simulation tool and accepts a set WRSET value by the user. WUIVAC has been used in applied test cases such as one involving the 2003 Cedar Creek fire [88], though none of them have been experimentally validated. Another critical model is Ramirez

et. als model [89], which calculates safety buffers using a stochastic model based on Monte-Carlo simulations. This probabilistic model simulates multiple wildfires, tracking the number of wildfires originating from every location around the community that manage to reach the urban area within an WRSET amount of time. Ramirez was the first to call for probabilistic trigger boundaries to be developed to depict the sensitivity of wildfires to initial conditions, and to tackle the deterministic nature of wildfire simulations. Finally PERIL is a trigger boundary calculation model relying on wildfire spread simulations and evacuation data [47]. It has been used to calculate trigger boundaries for a historic wildfire in the UK and for a community that practiced their evacuation plans, resulting in ample evacuation time data.

The first models used in calculating trigger boundaries, such as PERIL [47] and WUIVAC [76] were deterministic, where discrete input variables provide a repeatable, discrete result. Such studies are valuable to understand a previous wildfire but are insufficient to establish a long-term evacuation strategy. A large range of wildfires and evacuation responses is desirable to develop trigger boundaries for a wide range of possible conditions that can be used for planning. The result is probabilistic trigger boundaries, which can be explained and compared to stochastic trigger boundaries through 2.5.

Probabilistic wildfire spread models have been developed, especially when modelling spotting by firebrands as a stochastic effect, but the wildfire models most frequently used operationally are deterministic, with exceptions like FSPro and FSim, probabilistic 2D wildfire spread models used operationally in the United States. Obtaining probabilistic results from deterministic models can be accomplished by treating the input parameters as statistical distributions and using a pseudo-random method to sample different values from that distribution. Variables that can be sampled include the wind velocity and direction, the fuel moisture content, the fuel growth, and the overall management of the forest. The evacuation itself can be probabilistic but very few probabilistic evacuation models exist [48], [90]. Each single iteration is then used to produce a single trigger boundary. The process is repeated, with each generated boundary being compiled on an aggregate map. Once each subsequent iteration has negligible effect on the probabilistic results, convergence is achieved.

Probabilistic trigger boundary are an upgrade to simple trigger boundaries. While stochastic trigger boundaries apply for a specific wildfire and evacuation response, limiting their effectiveness in future planning, probabilistic trigger boundaries can apply for any applicable wildfire and following evacuation response. Probabilistic trigger boundaries can be used for future planning, allowing communities to create long term, data-driven evacuation plans.

The purpose of this thesis is to contribute to the WUI-NITY project, to create a tool that can be used to plan wildfire evacuations, with the ultimate goal of avoiding dire situations. An initial review of the literature showed that the topic of dire evacuations during wildfires is one that is not sufficiently explored, and needs further attention, as it places evacuees in

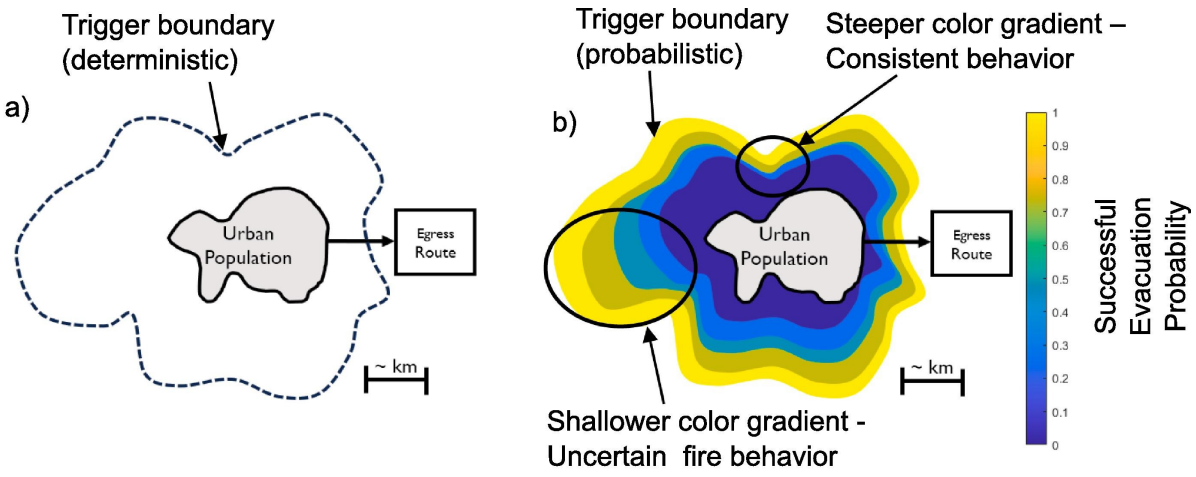


Figure 2.5: A) example of a deterministic trigger boundary surrounding an urban area [47]. b) The same area with probabilistic trigger buffers. Probabilistic trigger boundaries highlight areas with consistent or inconsistent fire behavior [43].

great danger. Trigger boundaries have a promise to aid as an evacuation planning tool, with current limitations on their applicability as long-term preparedness tools. This thesis discovers a critical link between probabilistic trigger boundaries and dire evacuations, bridging the gaps in the literature with regards to the understanding of dire evacuations and the availability of tools to plan against them. WUI-NITY is the first to offer simultaneous evacuation and wildfire simulations, enabling probabilistic trigger boundaries to be the pinnacle of this coupling. They are only possible because of this coupling. Probabilistic trigger boundaries can be used by communities to inform their evacuation plans, and quantify their evacuation capabilities.

Chapter 3

Probabilistic Trigger Boundaries

This chapter presents a methodology for generating probabilistic trigger boundaries called k-PERIL.[1] It is based on the PERIL algorithm [47] and has been upgraded to create probabilistic trigger boundaries through the use of multiple wildfire propagation and evacuation simulations, based on probabilistic simulations with normally distributed input variables. k-PERIL has been applied to a Wildland-Urban Interface area in Roxborough Park, CO, USA, that has undergone extensive evacuation testing and documenting as part of the WUI-NITY project [27], [36]–[38].

3.1 The k-PERIL model

Probabilistic trigger boundaries are a critical tool for long-term evacuation and community resilience planning. To that end, the k-PERIL model was developed. k-PERIL is a probabilistic trigger boundary calculation tool based on the mathematical principles of PERIL [47] a program created based in turn on the working principles of WUIVAC. k-PERIL, much like PERIL and WUIVAC, uses rate of spread and evacuation data, derived either numerically or experimentally.

The input data used by k-PERIL are a combination of raster data, to describe the landscape being investigated, and statistical data describing the weather and evacuation processes. Landscape raster data are matrix data, with each value prescribing a characteristic value for a square parcel of area. It is assumed that each such parcel, also called a cell, is internally homogeneous and can be accurately described by a single value. Examples include elevation, slope, vegetation, and tree stand height. They are essential in quantifying the wildfire behavior of the area. Weather data, specifically temperature, humidity and wind, are specified through mean values

[1] This chapter is based on the following publication: N. Kalogeropoulos, H. Mitchell, E. Ronchi, *et al.*, "Design of stochastic trigger boundaries for rural communities evacuating from a wildfire," *Fire Safety Journal*, vol. 140, Oct. 2023, Publisher: Elsevier Ltd. DOI: 10.1016/j.firesaf.2023.103854

and standard deviations. To obtain these values for a specific area, first the closest (or most appropriate) weather station is chosen. The data for the last 20 years or more is extracted, pertaining to hourly temperature, humidity and wind. The hottest and driest values of each year are recorded, along with the minimum temperature and humidity values of the same day, and the times at which they occur, resulting in 20 or more values of historic yearly maximum and minimum temperatures and humidities. The mean and standard deviation of each set of values is then calculated. This filtering of the maximum yearly values allows this study to account for the realistically worst case scenarios. Effects of long-term climate change are not reflected by this method. The wind values are simply collated with no filtering. These mean and standard deviation values are needed to conduct a probabilistic analysis for future planning. Finally, the urban area is marked in the landscape as a shapefile polygon. k-PERIL then interpolates between the polygon vertices to define a single polygon shape, representing the urban area.

To calculate probabilistic trigger boundaries, k-PERIL uses a large number of wildfire spread model scenarios and corresponding evacuation simulation scenarios. For each scenario, the provided raster data is used, along with randomly chosen values for wind magnitude, maximum daily temperature and humidity, minimum daily temperature and humidity, and times at which those occur, chosen based on the input statistical values. the maximum and minimum temperatures and humidities are used to interpolate a diurnal profile, to be used in the wildfire spread model. Subsequent studies with probabilistic trigger boundaries, after this chapter, use the diurnal profile to adjust the starting fuel moisture conditions, and simulate fire spread at peak temperature and minimum humidity.

The randomness of the input data coupled with a sufficiently large number of iterations will create a probabilistic trigger boundary that covers several realistic wildfire-evacuation scenarios. A graphical representation of the algorithm can be found in Fig. 3.1. In this study, the evacuation time, or WRSET, is prescribed in the beginning of the simulation as a statistical variable. Once k-PERIL is integrated into WUI-NITY, which uses integrated wildfire and evacuation simulation tools, it will be possible to calculate a WRSET value for each simulated wildfire scenario individually, generating more accurate results due to the better wildfire-evacuation coupling.

Each subsequent scenario is used to calculate the trigger boundary of the specific simulated wildfire and evacuation response. Once one iteration is finished, a new ignition spot is chosen, along with new values for the wind magnitude, maximum and minimum temperature and humidity, and times at which they occur, from the mean and standard deviation values of the historic data. One iteration is calculated at a time. Each individual trigger boundary is saved and superimposed, providing the probabilistic trigger boundary. This process of iterating and adding to the overall boundary continues until a convergence criterion is satisfied. In the case of trigger boundaries, convergence occurs when each subsequent iteration does not significantly

affect the overall probabilistic trigger boundary. In the case of k-PERIL, convergence is achieved when subsequent iterations cause a change of less than 2% on the overall boundary. The percent change is defined as the total area covered by the probabilistic boundary. The criterion is calculated for 10 deciles, and the maximum value is retained. In general, there has been no issue of non-convergence. In equation form, this criterion can be seen in 3.1:

$$\Delta B_{n+1} = \max_{m \in \{0, 0.1, \ldots, 1\}} \left(\frac{A_{n+1}^m - A_n^m}{A_{n+1}^m} \right) \tag{3.1}$$

Where ΔB_{n+1} is the error for iteration $n+1$, m is the decile value, A_n^m is the total trigger boundary area for the mth decile and nth iteration.The maximum value of 2% is chosen based on repeated testing, and requires approximately 300 iterations. This means that a set of 300 individual ignition locations, temperatures, humidities and wind magnitudes were used for this study, chosen from the historic mean and standard deviation values. This criterion is applied to all instances that k-PERIL is used. In Chapters 3 and 4, this criterion is used after computation is done, to check if the result represents a converged result. In Chapter 6, this criterion is actively used during computation, to stop the process when convergence is achieved.

The ignition location is chosen to be on the outskirts of the simulation domain, away from areas that restrict wildfire spread, such as built up areas and water bodies. The wind direction is then set so that the wind is driven from the ignition location towards the urban community, to reflect the worse case scenario. The wildfire simulation is then started. In this version of k-PERIL, Farsite was the wildfire spread model chosen. Farsite is a wildfire simulation model developed by the US Forest Service, based on the Rothermel semi-empirical wildfire rate of spread model. Farsite can estimate the wildfire rate from a single ignition point, for a given simulation duration [23], [91].

Once Farsite has calculated the wildfire spread rate for the area, the rate of spread data are saved. The first critical step of kPERIL is to calculate the rate of spread of the fire from each cell outwards to the 8 compass directions (N-S-E-W-NE-NW-SE-SW). k-PERIL achieves this by assuming that fire spreads elliptically from a point source, as has been implemented by many wildfire models [91]–[93]. Specifically, the ellipse model from [94], modified by [91] is used to interpolate the directional rate of spread values from the primary rate of spread vector. The equations are repeated in Equations 3.7.

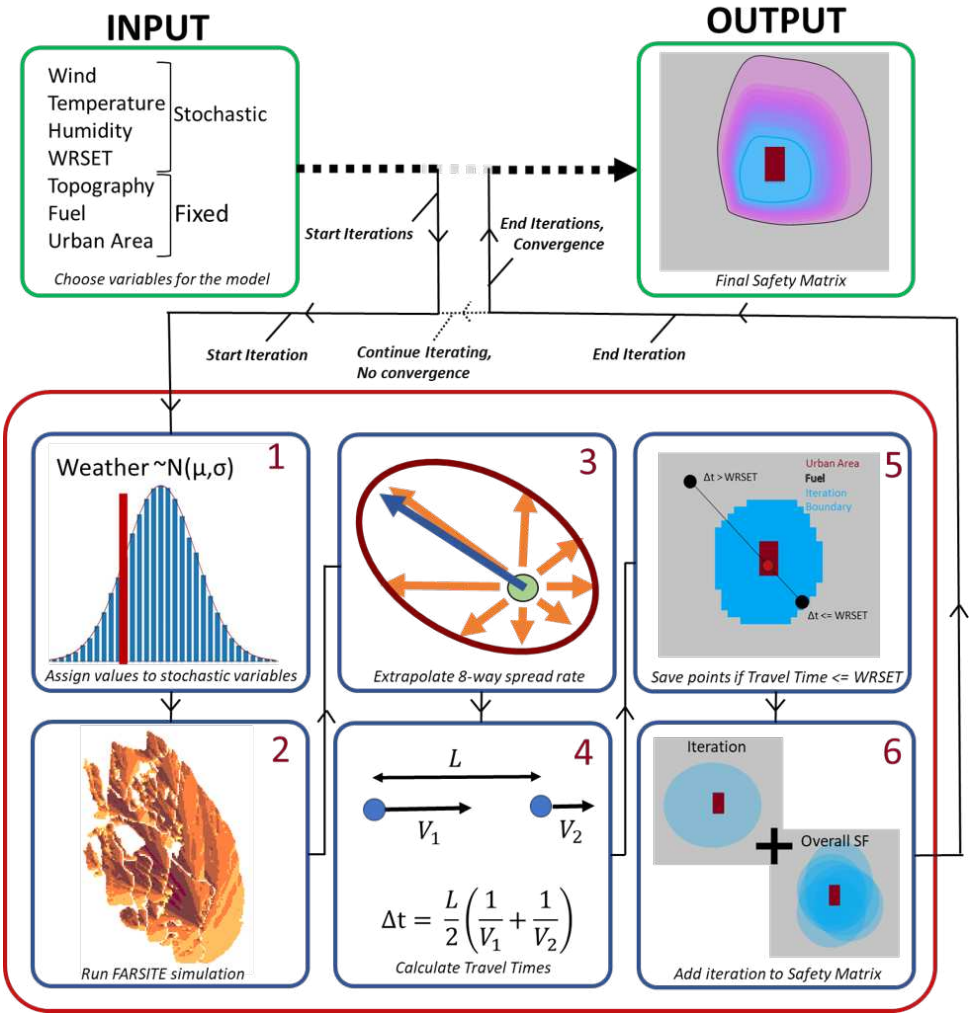


Figure 3.1: Flowchart explaining the k-PERIL algorithm. The input weather variables are stochastic, all others are of fixed value. Iteration steps (1) to (3) find the rate of spread between points in the landscape by first selecting a set of weather conditions from the input distributions (red line). Steps (4) and (5) find the points where the travel time of the fire to the community is equal or lower than WRSET. Step (6) adds the result of the iteration to the overall probabilistic trigger boundary, referred to in the figure as Safety Matrix. This process is repeated until convergence is achieved.

$$ROS(\theta) = [a\sin(\theta)]^2 + [c + b\cos(\theta)]^2 \tag{3.2}$$

$$a = \frac{ROS}{2LB}\left(1 + \frac{1}{HB}\right) \tag{3.3}$$

$$b = \frac{ROS}{2}\left(1 + \frac{1}{HB}\right) \tag{3.4}$$

$$a = \frac{ROS}{2}\left(1 - \frac{1}{HB}\right) \tag{3.5}$$

$$LB = 0.936\exp(0.2566U^*) + 0.461\exp(-0.1548U^*) - 0.397 \tag{3.6}$$

$$HB = \frac{LB + \sqrt{LB^2 - 1}}{LB - \sqrt{LB^2 - 1}} \tag{3.7}$$

Where a, b, and c are characteristic measurements of the ellipse (shown in more detail in [94], LB and HB are Length-to-Breadth and Head-to-Back ratios respectively, and $ROS(\theta)$ is the rate of spread of the fire, in meters per minute, at an angle θ from the main propagation direction. U^* is the effective midflame windspeed, and is a combination of the actual wind and the slope of the ground. In k-PERIL, the effective midflame windspeed is calculated in Equation 3.8 by vector addition of the actual midflame wind vector U_m and the wind-equivalent slope vector S:

$$U^* = \left\| \vec{U_m} + 0.06\vec{S} \right\| \tag{3.8}$$

The 0.06 factor is an empirically derived conversion constant, based on the Rothermel model [95], [96]. In the Rothermel model, the rate of spread is affected by a wind and a slope factor. As a simplification, it is set that the slope factor can be approximated as 0.06 times the slope, based on select results. The exact slope factor depends on the fuel structure and other factors [96]. Also note that the midflame wind, U_m is used in this equation, as opposed to the wind as specified by the historic averages. Those wind measurements are usually taken from weather stations, 10 m above ground level. Various conversion factors can be used to estimate the decrease in wind magnitude due to ground and canopy effects [19]. In this work, the same method as [91].

With the above function, k-PERIL has established the rate of spread of the fire at each cell in the landscape, in relation to each of the neighboring cells. The next step is to convert these rate of spread values to wildfire travel time, from one cell to the other. This will create a network of points, measuring the time required for the fire to travel from each cell to each of its neighbors. Equation 3.9 is used for this conversion, taken from [47], where L is the distance between the cell centers, V_1 and V_2 are the rates of spread of the two cells, along their coaxial spread direction, illustrated in Figure 3.1.

$$\Delta t = \frac{L}{2}\left(\frac{1}{V_1} + \frac{1}{V_2}\right) \tag{3.9}$$

At this point, k-PERIL has established a network of points, each of which is linked to its neighbors by a specific travel time, depending on direction. Since each connection between points (or link) has a wildfire travel time associated with it, also called a "weight", this is referred to as a weighted network.

The weighted network can be used to find the minimum distance of each point to the urban points. That will then be the time taken for the fire to reach the urban area. Many such algorithm exist as this is a popular topic in computer science, commonly referred to as shortest path algorithm. Such algorithms find the distance of all points from a central point. Since the

urban area boundary is comprised of multiple points, this algorithm should be run multiple times, once for each point on the boundary. In k-PERIL, a breadth-first search (BFS) algorithm [97] is implemented. The BFS algorithm calculated the total wildfire travel time from a target urban cell outwards. The advantage of the BFS algorithm is that if finds all points with a total travel time less than WRSET, and stops searching when that time is exceeded.

By retaining all the points with a total fire travel time less than WRSET, a new matrix will be formed with the same size as the original landscape. In this new matrix, the value of every point will equal the time taken for the fire to arrive to the urban point. Since most of the time k-PERIL will be working with an urban area instead of a single point, the process above is repeated for each point in the perimeter of the urban area. After all the urban points have been used, all the new matrices are merged by keeping the minimum value of each point. The result is a matrix where the value of each point is the time for the wildfire to first reach any part of the urban area.

The shortest path algorithm used in k-PERIL sets all the points within the trigger boundary (fire travel time less than or equal to WRSET) equal to a finite, calculated travel time value, while all the points outside the trigger boundary have a travel time value of infinity. To isolate and save all the points inside the trigger boundary, k-PERIL adds them to the probabilistic trigger boundary SF. Using Equation 3.10, the new matrix converts the results of the BFS algorithm to the final trigger boundary of the iteration, with t_t representing the calculated travel time of each point.

$$SF\left(x,y\right) = \begin{cases} SF\left(x,y\right), & t_t(x,y) = \infty. \\ SF\left(x,y\right) + 1, & t_t(x,y) \in \mathbb{N}. \end{cases} \tag{3.10}$$

Once this new matrix has been updated, k-PERIL restarts the process by picking a new set of inputs regarding the wind, weather and WRSET and starting a new iteration, until convergence is achieved. The final output of this model is the probabilistic safety matrix. The final code of the k-PERIL model, as used for this study and the other chapters in this thesis, is given in the Appendix.

As a verification step, a comparison was made between PERIL and k-PERIL. Four separate wildfire simulations were created in Farsite, to compare and contrast the trigger boundary outputs of PERIL and k-PERIL, to ensure they work similarly. k-PERIL in this case only ran one simulation and produced a single boundary to make the comparison feasible. The results are shown in Fig. 3.2. The two models produce similar results, with small differences as a result of the different shortest path algorithms and the trigger boundary visualization algorithms used.

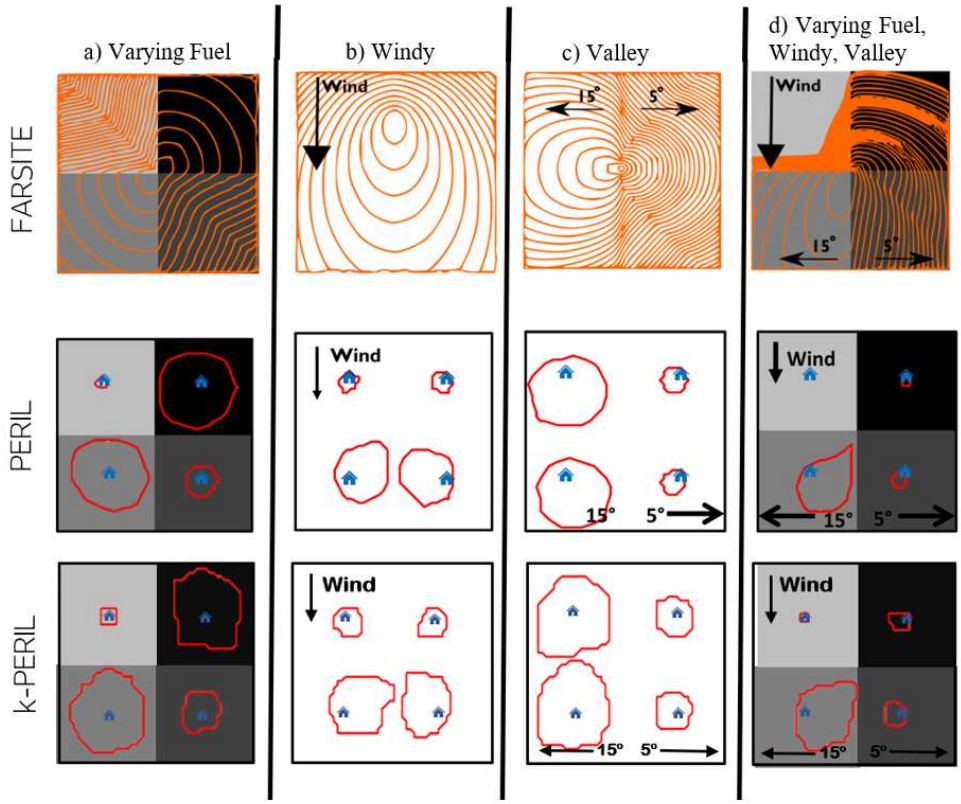


Figure 3.2: A comparison of the trigger boundaries of PERIL and k-PERIL for different wildfire cases and a fixed WRSET time. The houses on each figure denote simulated communities with an arbitrarily chosen WRSET. The wildfire simulations were done with Farsite, with the details of each case described in [40]. Overall the two algorithms produce very similar results, with most of the differences resulting from the different visualisation methods used to draw the boundaries.

3.2 Results applied to Roxborough Park, USA

To show the functionality of probabilistic trigger boundaries and k-PERIL specifically, an urban area was selected and its probabilistic trigger boundaries were calculated. The urban area that has been selected for this study is Roxborough Park, Colorado, United States. Roxborough Park is a small wildland-urban interface area south of Denver, Colorado. According to the 2010 US Census Bureau, Roxborough park is home to $\tilde{1}$0,000 residents, almost double since 2000 [98]. Roxborough Park was also used as a case study for the PERIL algorithm [47].

The Roxborough Park community neighbors the Pike National Forest and the Roxborough State Park on the west, and is surrounded by grasslands on the east, with various farmlands spread throughout. On the 27$^{\text{th}}$ of July 2019 the Roxborough Park community participated in an evacuation drill as part of the FIREWISE program, which aims to teach communities about wildfire resilience and preparation. The community was split in 3 sub-areas, each of which was assigned a specific evacuation route, which would be representative of a real evacuation. This was done so that the population receives prior experience and training in evacuation pre-

paredness and decision making, and for researchers to gather useful data about the evacuating population. The study yielded results about the percentages of the population participating in the evacuation versus deciding to stay and defend, the time at which each household decided to evacuate, and most critically to the current case study, the total time for the entire population to evacuate [37], [42]. That time, which is the WRSET for this case study, was found to be 120 minutes, a graphic representation of which can be found in Fig. 3.3. A map view of Roxborough Park, along with examples of the surrounding vegetation, can be found in Fig. 3.4. This evacuation drill is of great value and has been used extensively in the WUI-NITY project, part of which is k-PERIL.

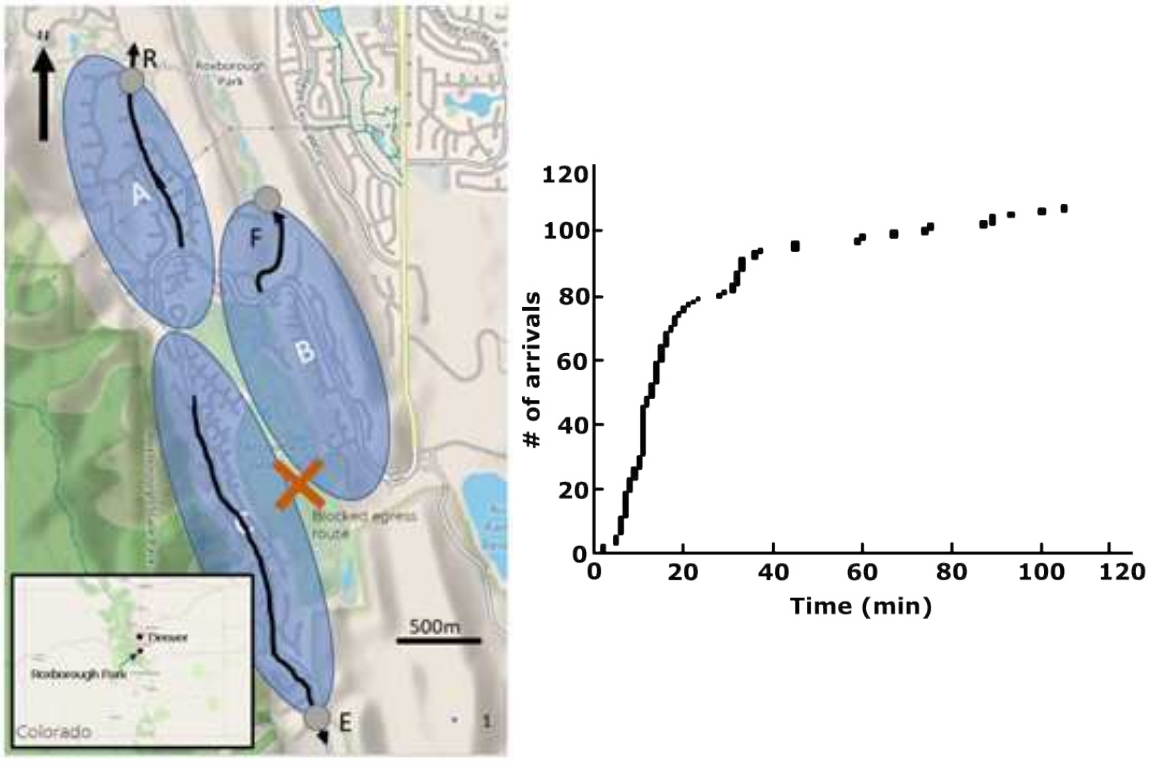


Figure 3.3: [Left] Areas involved in evacuation exercise. Areas A to C show the residential areas involved, and routes E F and R show the suggested evacuation route. [Right] The cumulative arrivals chart as measured at the evacuation route checkpoints (black) versus self-reported from the participants (grey). Data and figures from [42]

For this case study, the evacuation side of the trigger boundary calculation is known, and it is assumed that the fire will not have any impact on it. This assumption is valid for cases where the wildfire does not impact any of the evacuation routes, but would be problematic for cases where the fire makes one or many of the evacuation routes unusable.

In this case study the WRSET has zero standard deviation value as the experiment on which it is based was not repeated. One could estimate the variance of the WRSET, or run this result parametrically. In this instance, to examine one application of probabilistic trigger boundaries, two cases are run. The first has a fixed WRSET of 120 minutes and the second

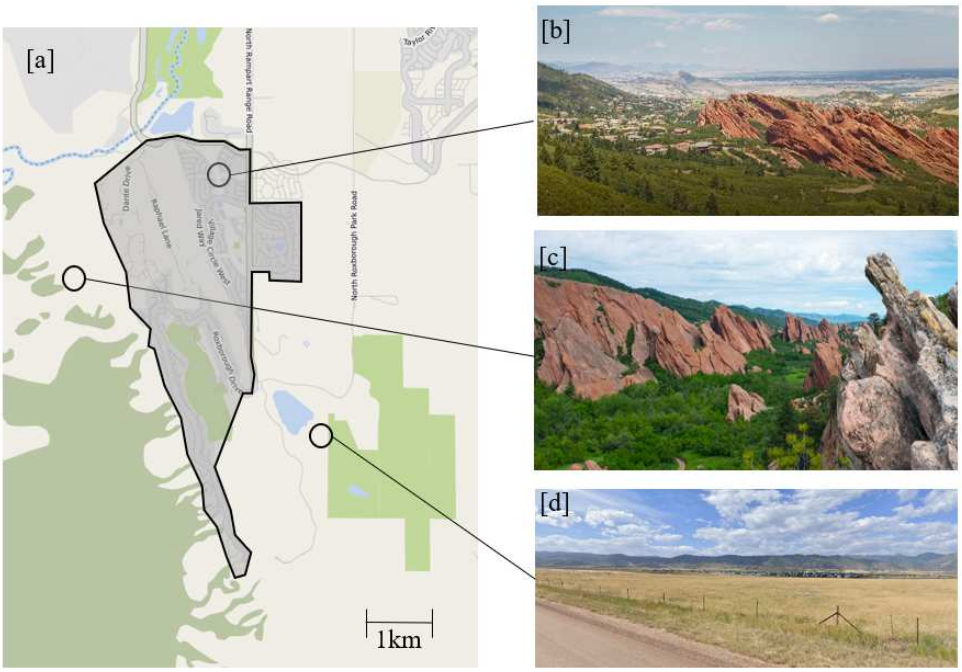


Figure 3.4: A map of Roxborough Park (populated area highlighted with grey) with examples of the surrouding vegetation. [a] OpenStreetMap (OSM) map. [b]: Poendl, 2011 [c]: Shahan, 2013 [d]: Google Street View.

has an increased WRSET to 360 minutes, reflecting a good-case and a worst-case scenario. It then is possible to compare the resulting stochastic trigger buffers and evaluate the effect of such events. The historic weather data was collected from the Lake George Automated Weather Station, the closest discovered automated weather station to Roxborough Park, but still a significant distance away. A table with the input parameters is given in Table 3.1. A table with the fuels used in this simulation, taken from the LANDFIRE database in Scott and Burgan fuel models, is given in Appendix A

With the above input data, the probabilistic trigger boundary for the Roxborough Park area, for both scenarios, is shown in Fig. 3.5 and a sample of the data generated for this simulation is shown in Fig. 3.6. The section on the top follows the same methodology as Fig. 2.5, where each area of the same color marks out an area of equal probability. Some cases, representing 1% of the total, were removed as they were unfeasible, spurious predictions caused by computational errors.

The resulting probabilistic trigger boundary is colored with a Blue-Pink colormap. This colormap is a product of the probabilistic nature of the boundaries, and arises from the multiple stochastic trigger boundaries added together. Each iteration creates a stochastic trigger boundary. To create the probabilistic trigger boundary, a large number of stochastic trigger boundaries are compiled together. Some areas on the landscape will be within a stochastic trigger boundary multiple times. Areas where multiple of the stochastic trigger boundaries coincide are colored in Blue, and areas where a few or a singlular stochastic trigger boundary occur, are colored in

Table 3.1: The simulation parameters for the probabilistic trigger boundaries of Roxborough Park. Values with no standard deviation were kept standard. The wind direction is always set from the selected ignition point to the center of the urban area.

Quantity	**Mean Value**	**Standard Deviation**	**Units**
WRSET	120 or 360	0	min
Maximum Temperature	30	3	C
Minimum Temperature	15	3	C
Maximum Humidity	45	2	%
Minimum Humidity	15	2	%
Time of Maximum Temperature	15	1	Hours
Time of Minimum Temperature	22	1	Hours
Wind Magnitude	15	3	km/h
1-h Fuel Moisture	6	0	%
10-h Fuel Moisture	7	0	%
100-h Fuel Moisture	8	0	%
Live Herbaceous Fuel Moisture	60	0	%
Live Woody Fuel Moisture	90	0	%
Canopy Foliar Moisture Content	100	0	%
Cloud Cover	0	0	%
Precipitation	0	0	mm

Pink. The number of times each part of the landscape is within a stochastic trigger boundary is an important parameter. At the time that this part of the work was done, it was not fully understood, what to call it or what its function is. At this stage, this value is called "Coverage", referring to how many of the iterations, or stochastic trigger boundaries, each point "covers". Areas with high coverage lie within multiple stochastic trigger boundaries, and areas with low coverage lie within few stochastic trigger boundaries. This value will be explored further in Chapters 4 and 6. What is apparent now is that areas with steep color gradient indicate that the wildfire spread through that area does not vary significantly with input conditions. Areas with shallow color gradients indicate uncertain wildfire behavior, which greatly depends on the input weather conditions, and may warrant more attention and resources in case of wildfire. In the case of Roxborough Park, an area of great uncertainty is to the west of the community, where a road splits the trigger boundary. Readers are encouraged to source the online version of this thesis to clearly see the color scale and differences of the figure.

In the case of Roxborough park there are two separate boundaries that formed, one surrounds the urban area and the other surrounds the road to the east of the area. This is an indication that the road to the east of Roxborough park is effective as a fire break in many of the simulated fires, stopping the fire from reaching the urban area. This is an indication that probabilistic boundaries can also be used to assess the statistical effectiveness of fuel- or fire-breaks, but such an analysis has not yet been investigated. Since this study was originally done, an alteration was done in k-PERIL. In wildfire spread models, landscape types such as bodies of water, roads and built-up areas do not allow wildfire to spread through them. Essentially, they all

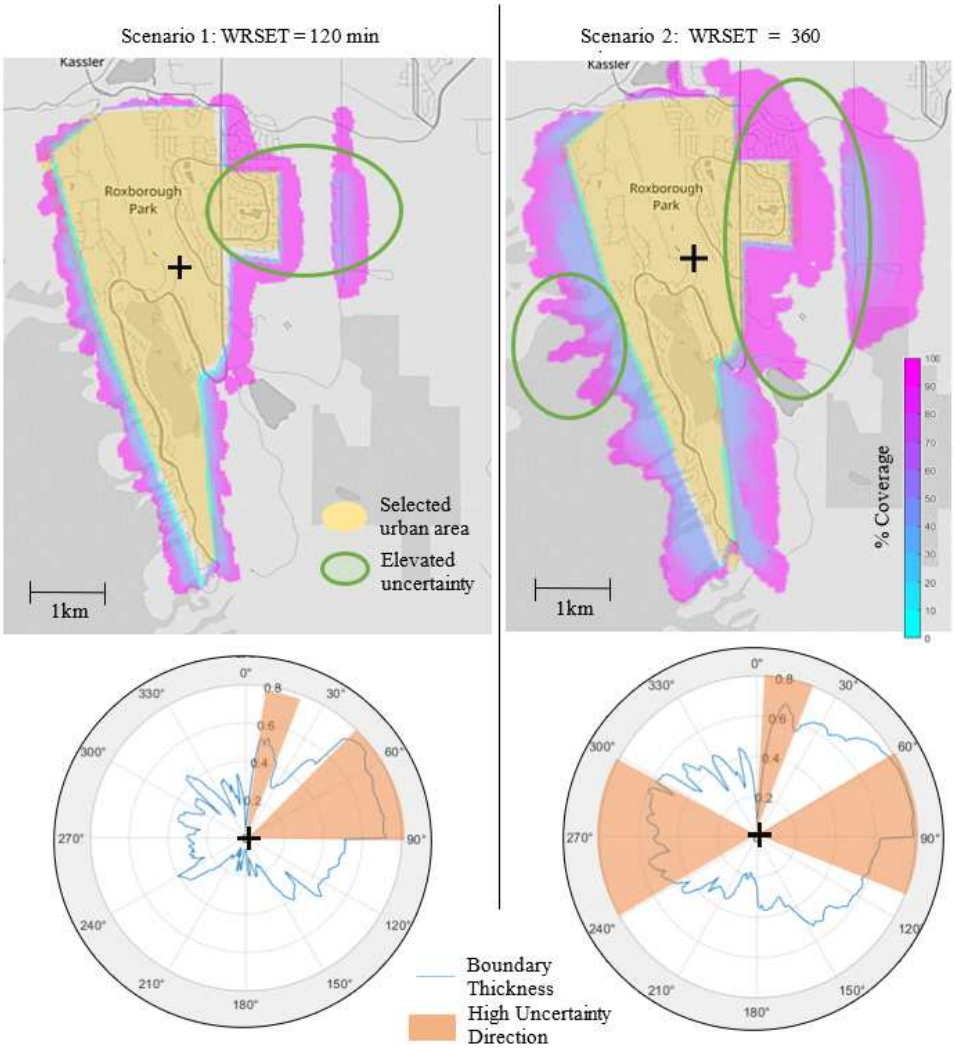


Figure 3.5: The results of the two cases, displayed in map view and uncertainty rosette view. The map sections show the uncertainty for each area based on the color map gradient. The uncertainty rosette identifies the directions of wildfire of most uncertainty, and thus risk, to the community.

have a rate of spread of zero. This caused an issue in the original PERIL algorithm; if the drawn urban area rectangle was surrounded by "built-up" pixels, those would not allow fire spread, and the designated community would never have wildfire reach it, implying that it will be "safe" no matter the conditions, with no trigger boundary created. To solve this issue, the urban rectangle is allowed to automatically shift if it surrounded by "built-up" pixels. The way this shift is done is, for each iteration, by shifting each point within the rectangle to the one closest to them that has a nonzero Rate of Spread. This alleviates the problem that PERIL has, but when unrestricted as was the case in this study, can create unexpected issues, such as the existence of a trigger boundary surrounding a road. This occurred because, for some iterations, the only points with nonzero rate of spread were to the east of the road, as the road prevented further fire spread. Gently shifting the urban area to the closest point that can spread wildfire leads to more accurate results overall but can result in detached boundaries,

like the one in 3.5. After this study, the extent that the urban area can be dynamically shifted has been limited, with k-PERIL stopping the probabilistic calculation if the wildfire simulation stops significantly far from the urban area, for now arbitrarily set as more than 6 cells.

As an initial attempt to understand the use of probabilistic trigger boundaries, the distance of the outermost area of the probabilistic trigger boundary to the urban area edge was highlighted. The larger this distance, here called the "boundary thickness", the higher the uncertainty of the wildfire behavior, and the more dangerous the area with relation to the evacuation response. A thicker boundary denotes a higher uncertainty, because of the implied shallower color gradient, as described above. This boundary thickness is not further researched in subsequent chapters, as the relation to safety was stronger with the current "coverage" metric.

The radar diagrams in Fig. 3.5 are a depiction of the effect of variance on safety. They display the distance between the 0% and the 100% probability lines as a function of direction from the center of the urban area. Higher values indicate higher variability and thus higher danger. From the figure, one can conclude that, for the standard case of WRSET of 120 mins, fires originating from the west of Roxborough Park are most predictable, from the north and south they are very predictable, and from the east they are very variable. This is in line with the vegetation and topography around the area, as Roxborough park is surrounded by forest on the west, grasslands on the east, and lakes, reservoirs and roads on the north and south. For a WRSET of 360 min, the east side of the community is still highlighted as a direction of higher uncertainty. New areas are also highlighted, such as a small sliver to the north, and a significant area to the west. These areas were not highlited in the lower WRSET areas, suggesting that the vegetation in these areas causes a more uncertain fire behavior that their surroundings.This graph is thus a great indication of the most vulnerable directions from where the urban area may be threatened.

By comparing the results of the two test cases, one can see the effects and potential differences of an increased WRSET. The outermost interval line is further away in the second case than the first case, which goes in accordance with the scaled WRSET. The predictability of the western section of the area is gone ins the higher WRSET case, while the unpredictability of the eastern section is especially highlighted in the second case, with the road section once again proving an effective fire break. While most sections of the trigger boundary seem to have scaled linearly with WRSET, there are some sections where this is not the case.

A significant novel addition that k-PERIL provides is a framework of comparing other deterministic trigger boundary algorithms. Different algorithms and models create different trigger boundaries for the same area, wildfire and evacuation scenarios. While such differences can be down to the intricacies of different wildfire or evacuation models, or different chosen weather conditions, there has not been a way to compare them in terms of their effectiveness or accuracy. The results in Fig. 3.5 can be used to compare different chosen or computed trigger boundaries

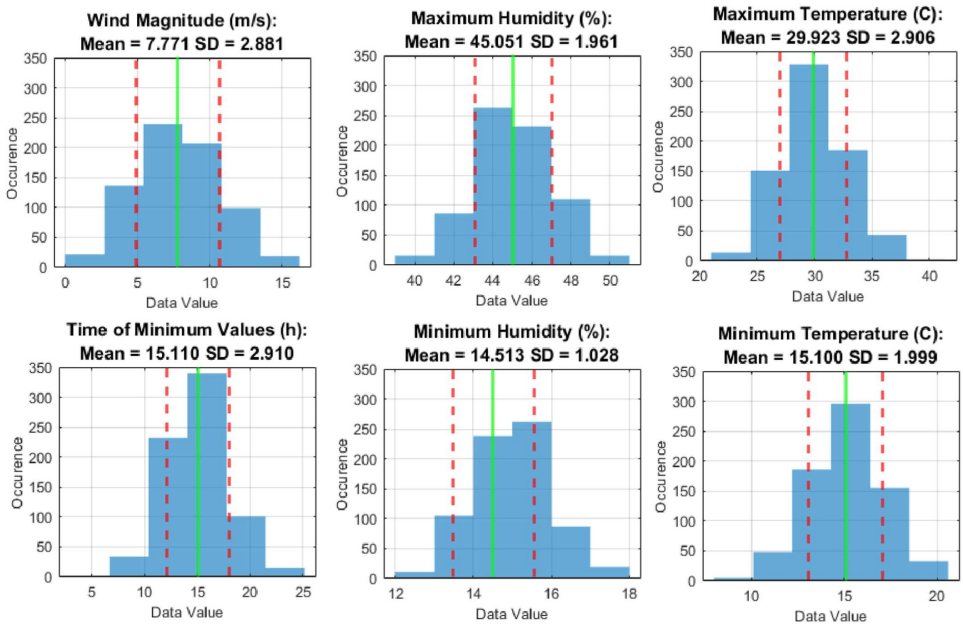


Figure 3.6: All the weather related values are given as normally distributed values. This data is plotted above for the second simulation with a WRSET of 360 min, with a total of 1000 cases. The simulations were run for 8 simulated days, with a total run time of approximately 10 minutes per simulation.

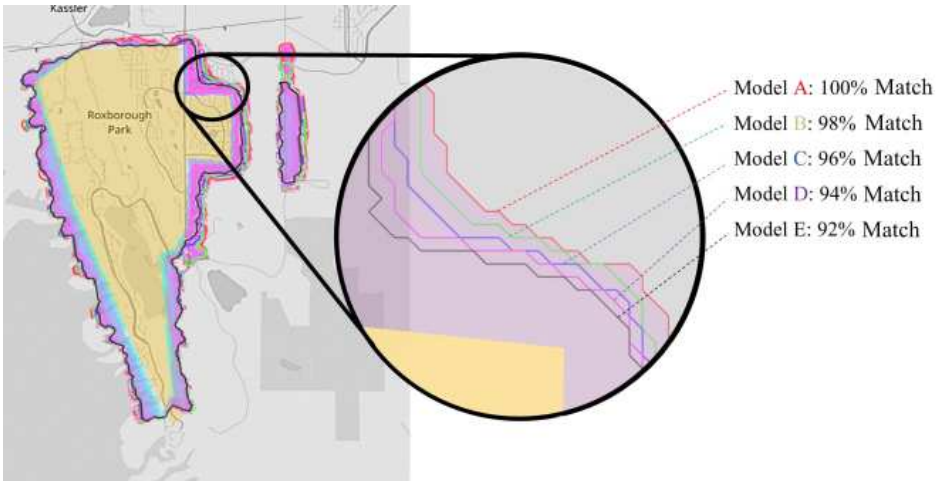


Figure 3.7: An example of boundary match calculation. Five samples, representing five different hypothetical trigger boundary models, have been overlaid with the k-PERIL output. They can then be compared with the uncertainty map to quantify the percent match of each boundary. We refer readers to the online version of the figure for colored boundaries.

based on their match, as calculated by k-PERIL. An example of such an analysis is given in Fig. 3.7. Different trigger boundaries can be placed on the same map as the output of k-PERIL and thus be compared based on their percent match. This would allow for a direct comparison between models, based on whether they are more conservative or broad, and whether they all highlight the same areas of faster fire propagation. It is possible to rate each boundary based on the percent match as calculated by k-PERIL, for a quantitative assessment of its effect and its generated uncertainty.

Though the results generated by this study are actionable, care must be taken when applying trigger boundaries to communities. The accuracy of the trigger boundaries is inherently affected by the limitations of the wildfire spread simulation and the evacuation simulation programs that were used. In this study, phenomena not modelled in Farsite (such as long-range spotting and plume collapse) are not accounted for. Equivalently, evacuation models cannot account for people choosing to initially stay and defend, but changing their minds and evacuating at a time when doing so is dangerous. Such nuances of the fire and evacuation characteristics should be considered carefully before running an equivalent study and applying its results. It is important to note that in this study k-PERIL did not reflect the cases where the fire affects the evacuation routes. In the case study above, there were many simulated cases where the fire first engulfed the main north-wards evacuation route before heading for the urban area, which would significantly change the evacuation dynamics and evacuation time, and the resulting trigger boundaries. Such an effect can only be modelled with a coupled wildfire-evacuation modelling system such as WUI-NITY. The adoption of k-PERIL as blind policy is not recommended because of the many nuances of any one landscape and community that are very difficult to accurately replicate.

3.3 Conclusion

Trigger boundaries are an invaluable tool in calculating the best times to commence the evacuation of a community under threat of an approaching wildfire. This chapter presents k-PERIL, a probabilistic trigger boundary algorithm improving on previous models. k-PERIL couples the evacuation and wildfire dynamics of the area surrounding a community to help inform safer evacuations. The k-PERIL model addresses the issue of how a wildfire may spread due to variations in initial conditions such as weather, by generating probabilistic trigger boundaries based on a range of wildfire scenarios. Probabilistic trigger boundaries were generated for a well-studied community in the US (Roxborough Park) to show the outputs of k-PERIL and the community evacuation requirements, for the average predicted wildfire and evacuation conditions, and for a worse case evacuation.

This chapter show that probabilistic trigger boundaries can improve the safety of community evacuation planning, and can quantify areas of increased uncertainty, where the wildfire progress and the community evacuation response are the most variable. Beyond previous work on trigger boundaries, k-PERIL provides the unique advantage of not only providing a measure of when a community should be evacuated, but also how predictable the evacuation process may be. Due to the time-sensitivity of evacuation planning in the case of an impending wildfire, uncertainty rosettes are introduced as a novel uncertainty mapping technique to identify the most at-risk regions of the community, allowing for prioritization in evacuation planning. k-PERILs

functionality as a framework to compare different trigger boundary models is also discussed, with its ability to categorize and rate different model outputs based on their percent coverage. kPERIL can be valuable to communities globally to inform and prepare safe evacuation plans, ensure evacuation orders are not given too late or too early, and overall help tackle the increasing hazard of wildfires.

Chapter 4

Quantifying dire evacuations and 2018 Mati wildfire in Greece

Currently, there is no method of assessing whether an evacuation is dire or quantifying the likelihood of a dire evacuation occurring. Some studies of wildfire evacuations have analyzed the application of WRSET safety factors in planning evacuations [27], [67], [73], introducing the concept of a late evacuation. While the word dire is not used in these studies, dire evacuations have been brought up in the past as a consequence of missing an evacuation deadline. A widely applicable criterion that can be applied in preparation of any wildfire, instead of specific wildfires and evacuation responses, has not been established yet. A rigorous framework is therefore required to identify dire evacuations and allow planning against them in long term community resilience projects. This chapter presents a rigorous, mathematical definition of dire evacuation using a safety factor, based on the probabilistic nature of WASET and WRSET.[1] Here we show that probabilistic trigger boundaries can be used prior to or after a wildfire to indicate when the last safe moment to begin evacuating is, before an evacuation becomes dire. We study and put forward the concept that dire evacuations occur when WASET is smaller than WRSET, meaning there is not enough time to execute a safe evacuation of the entire population.

The trigger boundary tool used in this study is k-PERIL, a probabilistic trigger boundary tool that requires stochastic inputs regarding the landscape and vegetation of the area, and probabilistic input arguments regarding the weather, wind and WRSET to calculate a map-based hazard visualization system [43]. Using k-PERIL, it is possible to estimate a safety factor indicating the chances of a successful or failed evacuation. In the previous chapter on k-PERIL, the output of probabilistic trigger boundaries was named uncertainty or coverage,

[1]This chapter is based on the following publication: N. Kalogeropoulos, H. Mitchell, E. Kuligowski, *et al.*, "Quantifying dire evacuations in case of wildfire using trigger boundaries and case study of the 2018 Mati wildfire in Greece," *Safety Science*, vol. 181, Jan. 2025, Publisher: Elsevier B.V.. DOI: 10.1016/j.ssci.2024.106691

like in figure 3.5. In this chapter, the probabilistic output is described as an evacuation safety factor, which is more appropriate for planning. Our definition of this safety factor is found in the next section.

4.1 Probabilistic Distributions of WASET and WRSET

For estimating future parameters and future planning, the values of the available and required safe egress times (WASET and WRSET) can be described as statistical variables. The statistical nature of WASET depends on the variations of the wildfire spread rate due to fuel growth, management, moisture content, and wind. WRSET is probabilistic because of the current understanding of human behavior on an individual level, combined with the impact of traffic and the road networks. In examining the literature, no information was found on the statistical distribution that describes WASET and WRSET. Some analyses such as Lovreglio et al. [99] and Purser and Bensilum [100] found that community pre-evacuation times, a component of WRSET, are lognormally distributed. The distribution of the overall WRSET remains unknown.

Should a set of ensemble wildfire or evacuation simulations be done, a methodology employing convergence testing and comparisons to distribution fits can be used to examine the fit of the data to standard distributions. Statistical tests, such as the single-variable Kolmogorov-Smirnov test, can compare any given dataset to another and provide conclusions on the relevance of the two. If one was to generate the second dataset based on a reference distribution, such as a normal or Poisson distribution, they would be examining the fit of the input dataset to that distribution. The degree of fit between the two sets can be used to measure the convergence of the wildfire simulations. Alternative convergence tests have been used in the past in the context of wildfires. For example, a study of pre-evacuation times [99] used an R2 comparison method to find the best fit of the input data, while another study on fire evacuation data [101] used Euclidean Relative Difference and Euclidean Projection Coefficients to compare their datasets. For WASET in particular, examining its distribution can be done via the range of values describing the rate of spread of the wildfire across all the simulations, the results of which are discussed in Section 4.3 The WASET of the wildfire can be approximated as the distance of the current wildfire perimeter to the community D, divided by the average rate of spread of the wildfire ROS, as defined in Eq. 4.1.

$$WASET = \frac{D}{ROS} \tag{4.1}$$

Assuming that the distance of the wildfire from the community at time of detection is a deterministic value with no variance, it follows that the variance of the WASET is directly propor-

tional to the variance of the average rate of spread (ROS) of the fire. Pre-evacuation factors like time of detection and time to make the decision to evacuate can be added to this analysis in the future, by directly adding them to the WRSET value. Consequently, the WASET can be examined first via the average ROS of the wildfire in each simulation. Dividing the distance of the wildfire to the community by the average rate of spread of the fire and its variance would result in the mean and variance of the WASET. As the distance of the wildfire from the community decreases with time, it follows that the variance of the WASET will be continually decreasing as the wildfire approaches the community. The closer the wildfire is to the community, the less distance the fire has to travel, the less the variations in the rate of spread. This analysis was conducted for the case study of this chapter, the results of which can be found in Section 4.2.

4.2 Evacuation safety factor and dire evacuations

Assuming that the WASET and WRSET probabilistic distributions are known, a framework that discusses the two as probabilistic functions that evolve depending on the location of the wildfire perimeter allows for a definition of dire evacuations, as illustrated in Fig. 4.1. The progress of the wildfire is depicted in three distinct stages. In stage (a), the wildfire is away from the community. In stage (b), the wildfire is close enough to the community that the WASET and WRSET curves are close to overlapping. In stage (c), the wildfire is close to the community, and the WASET and WRSET curves have a significant overlap, with the WRSET curve possibly past the WASET curve. This overlap signals that there is a chance of an evacuation not having enough time to be safe. With this framework, dire evacuations are those initiated when there is an overlap between the WASET and WRSET curves. The later an evacuation is initiated, be it by an official signal or spontaneously by a community, the larger the overlap between the two curves, and the greater the chance of entrapments.

The subtraction of the available egress time (WASET) from the required safe egress time (WRSET) is a good indication of the relative safety of the evacuation process, or equivalently, the direness of the evacuation process, first discussed by Cova et al. [30]. With the framework presented in Fig. 4.1, a formalized safety factor can be calculated, to represent the possibility of dire evacuation, as done in the field of reliability engineering [102]. The safety factor can be calculated using Eq. 4.2, 4.3, and 4.4.

$$SF^* = \Phi(\beta) \tag{4.2}$$

Where Φ is the cumulative distribution for the standard normal variable. This analysis applies to the intersection of two normally distributed variables.

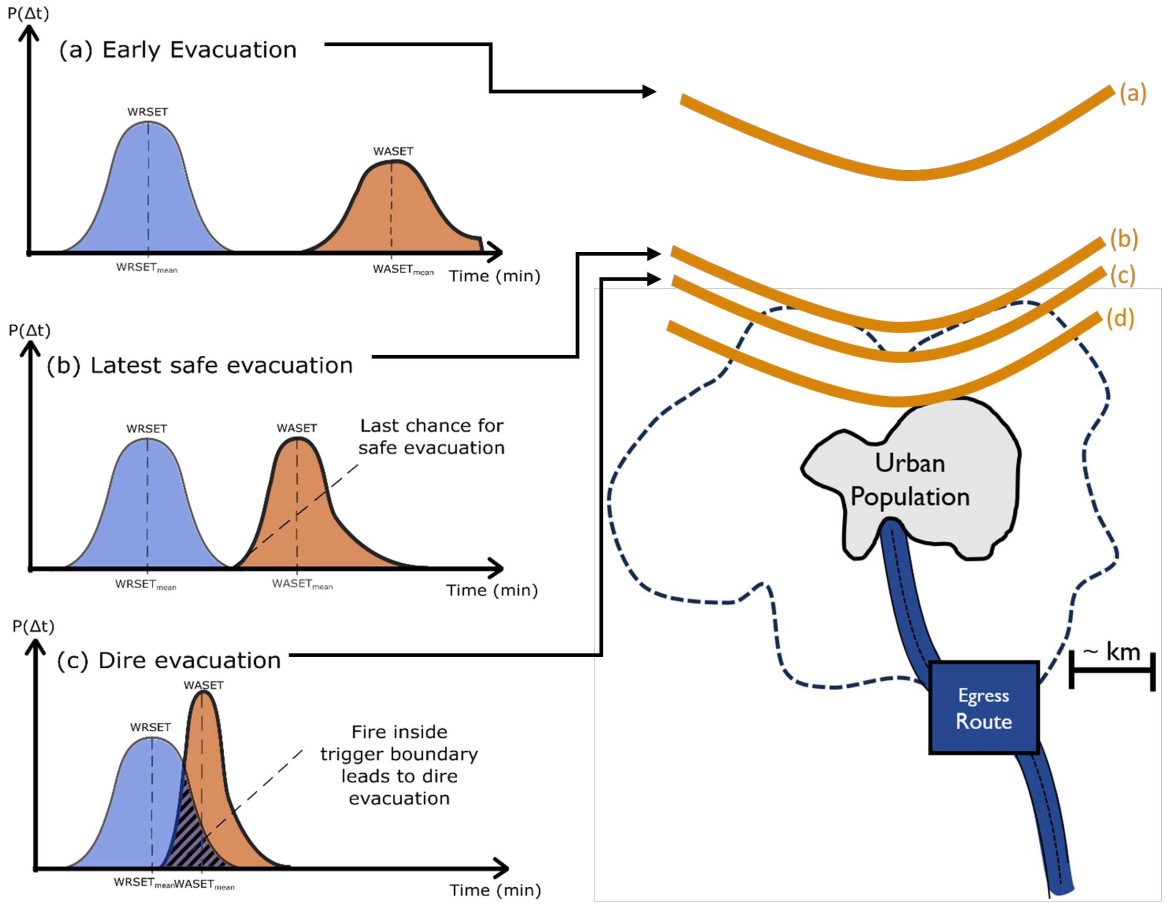


Figure 4.1: A probabilistic illustration of evacuation (WRSET) vs. wildfire (WASET) progress towards a community. Equation 4.5 can be used to estimate a safety factor (SF) of evacuation, with values greater than 1 leading to safe evacuations and values less than 1 leading to dire evacuations. The SF continuously decreases as the evacuation is delayed. At time (a) the wildfire is far enough from the community that there is no chance of a dire evacuation ($SF > 1$). At time (b) the fire is close enough where there is the last instance of $SF \geq 1$, meaning this is the last opportunity to call an evacuation with zero risk of entrapment. At time c) the wildfire is close enough that it is now a possibility that a dire evacuation will occur ($SF < 1$). At time d) the wildfire has reached the boundary of the urban area, making the area compromised.

$$\Phi(\beta) = \frac{1}{\sqrt{2\pi}} \int_{-\infty}^{\beta} e^{-\frac{x^2}{2}} dx \tag{4.3}$$

β is referred to as the reliability index:

$$\beta = \frac{\mu_{WASET} - \mu_{WRSET}}{\sqrt{\sigma_{WASET}^2 + \sigma_{WRSET}^2}} \tag{4.4}$$

Additionally, μ and σ refer to the mean and standard deviation of each curve. The safety factor SF^* is constrained to values between 0 and 1, with values close to 1 reflecting an infinitesimally

small possibility of failure, and values close to 0 representing a high chance of failure.

Even in cases where WASET and WRSET are not normally distributed, since there is no consensus on their distribution, there are methods to approximately transform a number of distributions into normal distributions for the purposes of this analysis [103]. Because the statistical variables are continuous, there will be no point where there is no overlap between WASET and WRSET, and it holds that $SF^* < 1$ at all times. This means that the safety factor will always reflect a possibility of dire evacuations. It would be more beneficial to use safety factors that can range from 0 to ∞, so that $SF = 1$ can be used as a critical value representing the last evacuation opportunity. One way to do so is by using confidence intervals, used to derive Eq. 4.5, which represent the cumulative probability that a target value lies within a specific interval. Common values to select in probabilistic evacuation modelling are confidence intervals of 95 % [104]. The critical value that represents the 95 % confidence interval in the standard normal distribution can then be used as a metric against the reliability index β to yield a safety factor metric, where a result of 1 reflects an evacuation with a 95 % confidence interval of resulting in a safe evacuation, explained in Eq. 4.6.

To satisfy the requirement that SF can approach but not drop below zero, another value needs to be included in the calculation. The reliability index β with a WASET of zero represents the lowest possible value of β, now defined as β_L in Eq. 4.7 for any wildfire scenario, and can be used to ensure that SF can range from infinity to zero and never become negative. The new evacuation safety factor, SF, can be defined by Eq. 4.5, 4.6, and 4.7.

$$SF = \frac{\beta - \beta_L}{\beta_U - \beta_L} \tag{4.5}$$

With β_U defined by:

$$\Phi\left(\beta_U\right) = 0.95 \tag{4.6}$$

And β_L:

$$\beta_L = -\frac{\mu_{WRSET}}{\sqrt{\sigma^2_{WASET} + \sigma^2_{WRSET}}} \tag{4.7}$$

This formulation allows for safety factors greater than 1 for cases where WASET is considerably larger than WRSET, and safety factors approaching 0 for cases where WASET is considerably smaller than WRSET. A graphical representation of the evolution of the safety factor as a function of the elapsed time after wildfire detection can be found in Fig. 4.2. The timesteps highlighted in Fig. 4.1 are identified in Fig. 4.2. The probability of the evacuation becoming dire (P_d) can then be found from the reliability index using Eq. 4.8.

$$P_d = 1 - \Phi\left(\beta\right) \tag{4.8}$$

A link between the safety factor, dire evacuations and the progress of the fire can be formed by using probabilistic trigger boundaries. As shown in Fig. 4.1, a fire at position (a) that will lead to a safe evacuation and has a safety factor greater than 1 will fully be outside the trigger boundary of an area. Position (b) was previously identified as the last safe evacuation opportunity, when the safety factor is equal to one, and is the last opportunity to evacuate with no chance of a dire evacuation. The trigger boundary denotes all the locations where an evacuation initiated when the fire front crosses it will do so with a safety factor of 1. An evacuation starting when the fire is at position (c), and inside the boundary between positions (b) and (d), may result in a dire evacuation with a safety factor less than 1. A probabilistic trigger boundary also depicts the safety factor of the evacuation depending on the position of the fire.

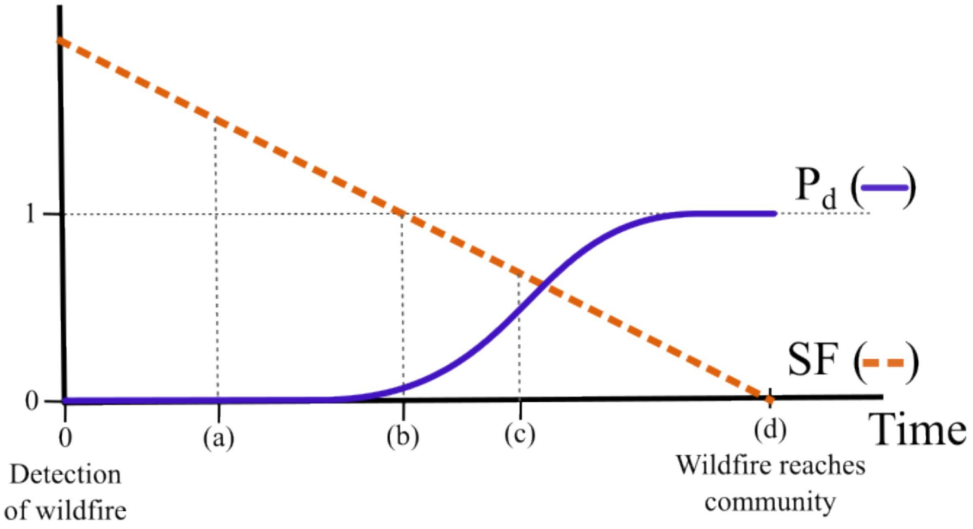


Figure 4.2: Dependence of the safety factor and probability of evacuation becoming dire over time. Assuming a wildfire starts far away from the community, the safety factor starts with a value greater than 1, and gradually declines as it approaches the community. The Safety Factor always start with a discrete value, since upon detection the wildfire will be a set distance and WASET away. The probability of dire evacuation starts at zero and increases up to 1. Time instances (a) (b) (c) and (d) correspond to the highlighted cases in Fig. 4.1 and Fig. 2.5

Trigger boundaries can be used to identify the last opportunities to announce a safe evacuation. Trigger boundaries can be used to run analyses such as the one in Fig. 4.1, and use the results in planning. Trigger boundaries can be calculated for any community, provided the input data is available. As such, trigger boundaries define dire evacuations based on the evacuation safety factor.

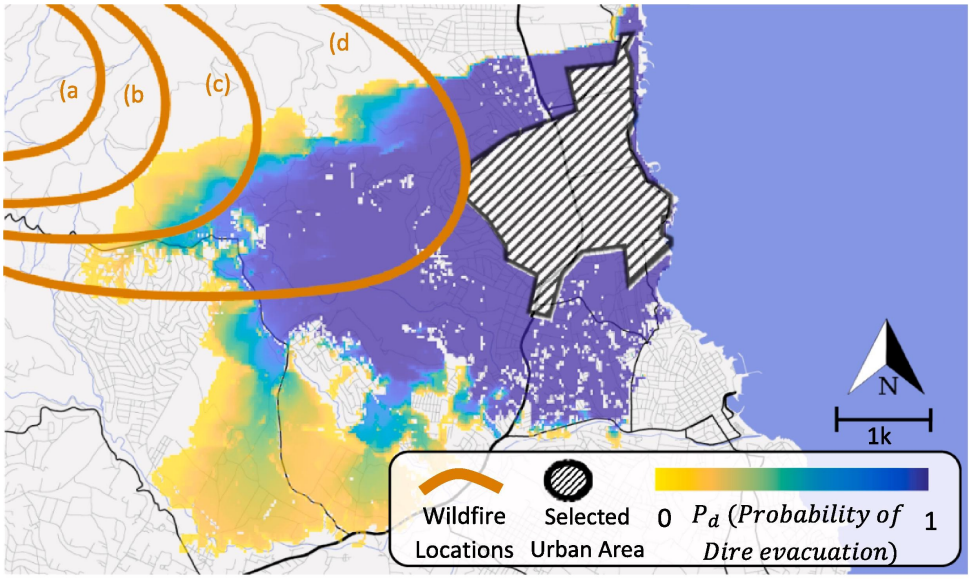


Figure 4.3: (Left): The probabilistic trigger boundary for the 2018 Mati area. The wildfire perimeter locations (a), (b), (c) and (d) correspond to the same timings as in Fig. 4.1

4.3 Application of evacuation safety factor to the 2018 Mati fire

For this study, the wildfire model used was FLAMMAP [105], a different implementation of the Rothermel model, akin in nature to Farsite [23]. It has been applied before to European landscapes [106], and provides instantaneous ROS values for the entire landscape, without needing an ignition location, or temporal weather variation (ignitions were still randomly selected to establish the random wind direction). The landscape data for the Mati area was obtained from the CORINE Land Cover dataset from Copernicus [107], as the only and most reliable vegetation classification dataset available. Each vegetation type was then converted to a classification recognizable by FlamMap, namely the Scott and Burgan models [108] based on their description, the methodology in Giannaros et al. [26], and field observations of the area by the authors. The resulting conversion of one dataset to the other can be seen in Appendix A. As a verification measure, the hourly temperature, relative humidity, and wind data of the day of the fire was collected and a FLAMMAP simulation was run, with the ignition location of the real fire. This was done to compare the rate of spread and arrival time of the wildfire to the real one as recorded by Athanasiou and Xanthopoulos [32], to assess whether the resulting landscape data were accurate. The weather and wind data was obtained from the closest automated weather station [109]. For the subsequent probabilistic analysis, the July and August data for the last 20 years was compiled, the maximum and minimum temperature and relative humidity values were isolated, and the averages and standard deviations of the temperatures and relative humidity were found, as previously described in Chapter 3. the FLAMMAP model was used to estimate the starting fuel moisture conditions for each iteration. The maximum

and minimum temperatures and humidities were used to interpolate a diurnal weather profile, which was used for fuel moisture preconditioning. Most wildfire disasters occur in conditions far worse than the averages. Using a probabilistic approach ensures that the results reflect both the variability of the historic weather conditions and the effect of the worst-case scenario. Some of the iterations will be conducted with a combination of the worst wind, weather, and ignition locations, by the nature of randomness.

Evacuation data was found from the work of other researchers, who studied the evacuation response of Mati. Two research groups ran different models of vehicular and pedestrian evacuation, putting focus on pedestrian evacuations with the shelters set as the nearby beaches [110], [111]. Using a range of input walking speeds and milling time, the researchers found evacuation times ranging from 58 to 89 min. Their simulations assume that an evacuation order was issued, received and followed by all the residents, approximating the real evacuation as a spontaneous evacuation.

Starting with the WRSET, there is very little data available to make an informed decision regarding the mean and standard deviation of the evacuation of Mati. What is available are the results of 4 evacuation simulations, with varying input conditions [111]. The outputs of the simulations range from 57 to 89 min. It was decided that an assumed normal distribution with a mean value of 75 min and a standard deviation of 6 min provides a representative plot that includes the most optimistic and pessimistic simulations as the two extremes. A total of 4 evacuation simulations does not allow for statistical conclusions. The above 4 simulations are the best data found on Mati but we hope that future studies will improve this imbalance. More research would be needed to make a conclusive statement about the probabilistic nature of WRSET for the evacuation of the Mati fire. The discrepancy between the number of wildfire simulations (500) and the evacuation simulations (4) is evident. In this Chapter, a new convergence criterion for k-PERIL has been implemented, which will be discussed in detail in the following section. In Chapter 3, the value of 1000 simulations was arbitrarily chosen. In this chapter, 500 simulations was also arbitrarily chosen but was shown to be sufficient. In subsequent chapters, the convergence of the results is checked dynamically, and thus the number of required simulations will vary. The exact input data used in this study, varied in each iteration, are shown in Table 4.1. The ignition location was varied with each iteration, each time choosing a starting point that allows wildfire spread, far away from the community. No canopy data was found for the area (at this stage of the study), and as such were not included. Later chapters include canopy data as indicated.

Fig. 4.4 presents the real ROS data of a set of ensemble wildfire simulations of Mati, plotting each simulations average rate of spread in a histogram distribution. The set convergence and fit with a lognormal distribution was tested using the single-variable Kolmogorov similarity test. The null hypothesis was rejected with a $D < 0.05$ after 140 simulations, although

Table 4.1: The input conditions for k-PERIL. Fuel moisture values are not given as they were dynamically adjusted on each iteration, for 30 simulated days.

Quantity	**Mean Value**	**Standard Deviation**	**Units**
WRSET	75	10	min
Maximum Temperature	32	1	C
Minimum Temperature	23	1	C
Maximum Humidity	58	6	%
Minimum Humidity	16	3	%
Time of Maximum Temperature	14	1	Hours
Time of Minimum Temperature	5	1	Hours
Wind Magnitude	17	3	km/h
Cloud Cover	0	0	%
Precipitation	0	0	mm

the test was continued since the ensemble test was comprised of 500 simulations. With the full simulation set, the Kolmogorov-Smirnov test stabilizes at statistic test values of 0.05.A lognormal distribution was found to be the most fitting for the generated data. The best fitting lognormal distribution is fitted on the data in Fig. 4.4 along with its mean and standard deviation data. Other tested distributions include normal, Cauchy and Poisson distributions. Using Equation (1), the ROS histogram can be converted to a WASET histogram. The results of this conversion can be found in Fig. 4.4 for two fire locations. The first location is when the fire started, marked by a red cross in Fig. 4.5, 2.3km away from the community edge. The second location is when the evacuation first started, marked in Fig. 4.5, 0.64 km away from the community edge.

With all the input data in place, the simulation ran until convergence is achieved. Convergence is assumed achieved when each subsequent iteration does not change the overall area of the probabilistic trigger boundary by more than 1 % for 20 iterations in a row. The results display a representative probabilistic trigger boundary of the area of Mati. In Fig. 4.3, fire fronts (a), (b) and (c) conceptually represent their counterparts from Fig. 4.1, showing the locations of the fire fronts that would lead to an evacuation with a safety factor greater than, equal to and less than 1 respectively. In Fig. 4.5, the real evacuation of the Mati fire of 2018 is plotted, which occurred when the wildfire front was very close to the community, showing that the real evacuation was completely dire with $P_d = 1$. The ignition location of the wildfire is also indicated on the map which, had an evacuation started immediately, would till result in $P_D = 0.38$. The wildfire started adjacent to houses in the area, so it is assumed that the ignition and detection of the fire coincide in time and space.

Using the results of Fig. 4.4, and the reasoning presented earlier regarding the distribution of WRSET, an analytical calculation of the evacuation safety factor was undertaken, and the results were visualized with the same system as Fig. 4.1. The results are shown in Fig. 4.6. Equation 4.5 was used to calculate the analytical safety factor of the two cases using the

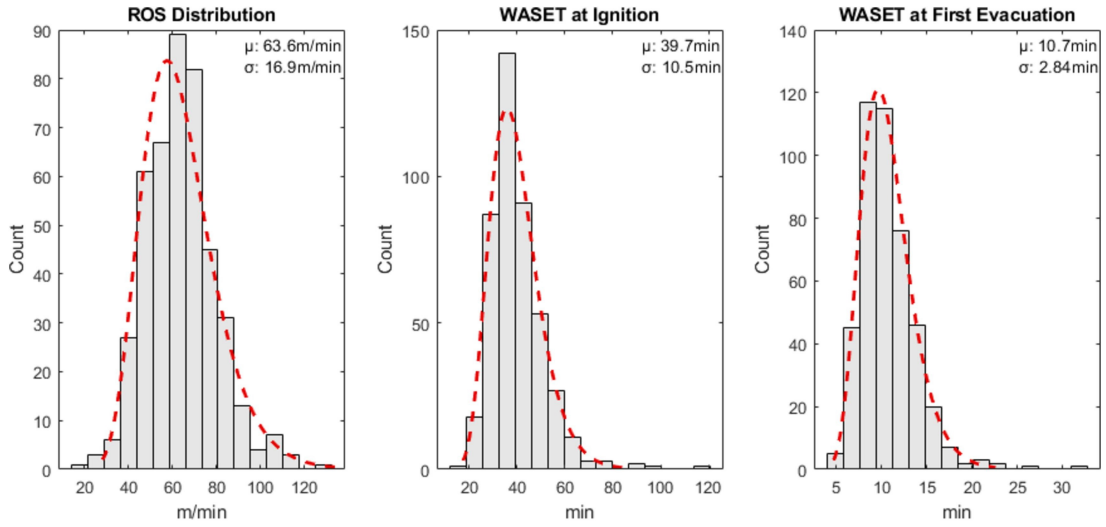


Figure 4.4: The results of 140 wildfire simulations of the Mati area. Right: The total rate of spread distribution among all simulations. Center: The statistical WASET of the fire at the point of ignition, using Equation 4.1. Right: The statistical WASET of the fire when the first evacuations started. The ignition and first evacuations can be seen in Figure 4.5 All curves can be defined as lognormal distributions with a mean and standard deviation values.

analytical values of mean and standard deviation.

4.4 Conclusion

So far in the literature, there has been no definition of dire evacuations. Evacuations have been characterized as successful, failed or late, based on whether there were any casualties or other issues with the evacuation process. A loose framework does not allow for thorough investigations of dire evacuations, the overall probability of dire evacuation, or a deeper insight into the issue.

The method presented in this chapter, where an evacuation safety factor is proposed based on the temporal distance between the WASET and WRSET, provides a definition of dire evacuations. Using this new framework, one can go further from characterizing an evacuation as late or failed, and can understand the degree to which an evacuation was dire. The safety factor can guide when issuing an evacuation notice during the wildfire event. This, coupled with probabilistic trigger boundaries, adds a valuable tool to the collection which communities have available when planning their wildfire strategies.

When a wildfire approaches a community, the position and intensity of the wildfire may alter the evacuation process, most usually by slowing or stopping traffic due to smoke [87] or because of cars that have been abandoned. The wildfire itself affects the evacuation progress, and the two are not independent as treated here. The probabilistic trigger boundary could, for example,

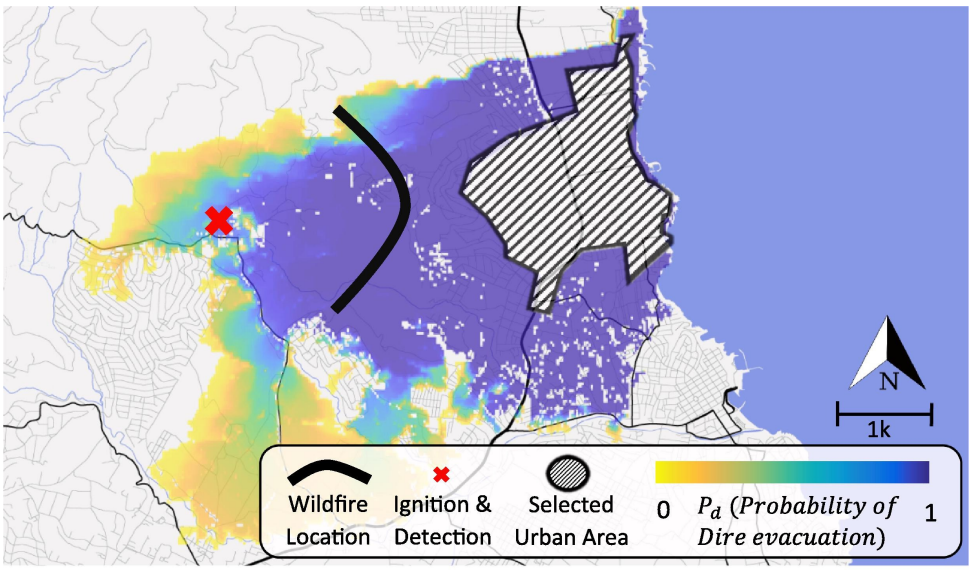


Figure 4.5: (Left): The probabilistic trigger boundary for the 2018 Mati area. The wildfire location denotes the approximate position of the wildfire when spontaneous evacuations of Mati started. The evacuation started with a Safety Factor very close to zero, resulting in a dire evacuation.

achieve this coupling of the wildfire and evacuation, affecting the probabilistic spread of the evacuation time [27], [43]. We ignore the effect of any firefighting action to reflect the worst case scenario of a faster wildfire. We are also aware that the evacuation time may be larger (or infinite) during a dire evacuation because of the presence of smoke [112], traffic congestion or road blockages, which would affect the perceived safety of the population. These effects are difficult to model and are part of the unexplored area of dire evacuations. This framework is created to indicate the probability of a dire evacuation, prompting a study into quantifying its effects.

When considering a wildfire evacuation from a risk-based approach [113], there are two components that require assessment: the likelihood of a dire evacuation, and the severity of a dire evacuation (i.e. number of injuries and fatalities) if it does occur. The methodology of this approach provides a practical method of assessing the likelihood of an evacuation becoming dire based on the comparison of probabilistic WASET and WRSET values. Therefore, to converge upon a fully risk-mitigation-based approach, future work could attempt to quantify the severity of a dire evacuation. When combined with the method of this chapter, this would allow for full characterization of the risk associated with a wildfire evacuation. This chapter provides a definition of dire evacuations. These are the situations when there is not enough time to fully and safely conduct an evacuation, but one is initiated despite that.

Using an evacuation safety factor to illustrate the possibility of a dire evacuation occurring provides both a rigorous definition and a means of analyzing dire evacuations before and after they occur. The lack of a definition of late evacuations has been an obstacle in understanding

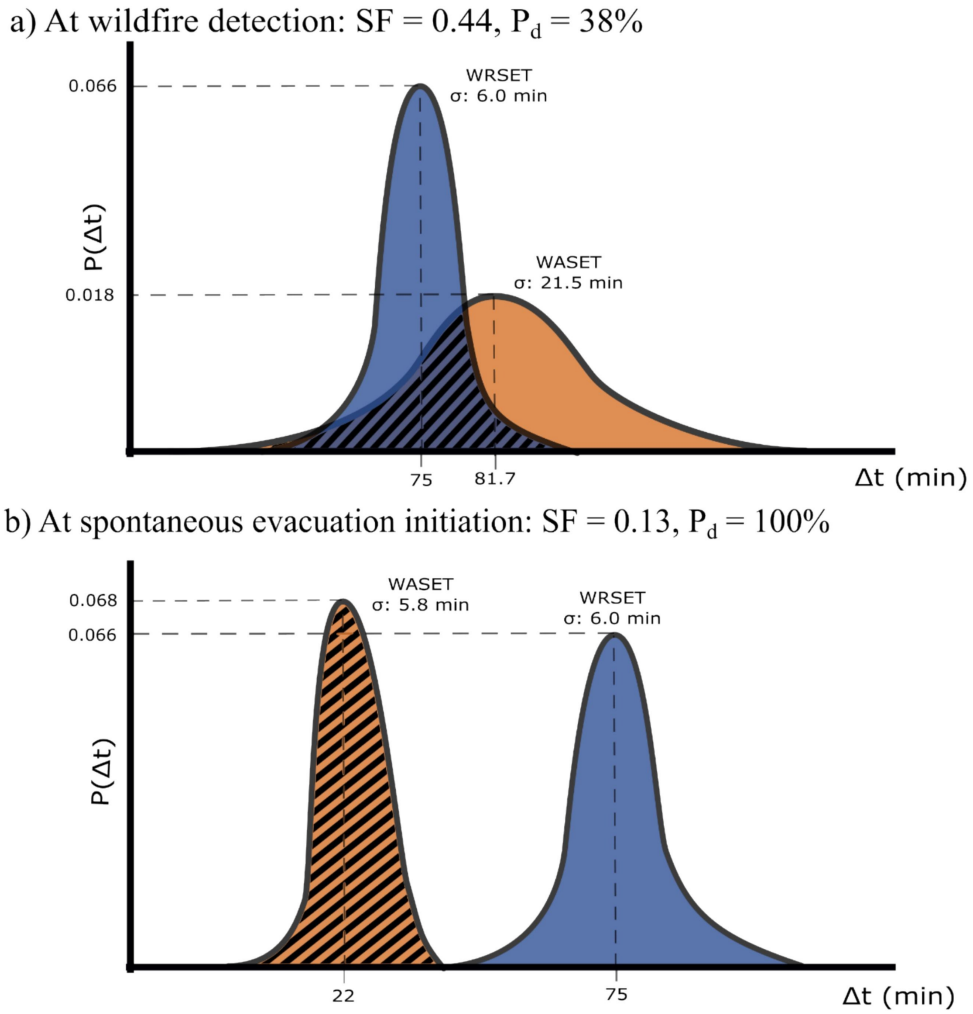


Figure 4.6: The distributions of WASET and WRSET at fire ignition / detection (a) and at the point of the first reported evacuations (b). At fire ignition, the fire is already inside the trigger boundary of Fig. 4.5, which is reflected by a calculated safety factor of 0.44. During the evacuation start, the fire is very close to the community, with a safety factor of 0.13. The safety factor can be calculated analytically or shown qualitatively as the overlap of the two curves, and the color hue of the corresponding trigger boundary location.

and communicating the causes and effects of dire evacuation, which this chapter has addressed by considering the probabilistic nature of evacuations and wildfires. While the evacuation safety factor is a great method for assessing and defining trigger boundaries, probabilistic trigger boundaries are an equivalently great method to predict and prepare for evacuations by relating the potential direness of an evacuation with the position of the fire front at the time of an evacuation initiation. Both methods can be used in both analyzing historic fires, and in preparing community evacuation strategies based on what-if scenarios. The development of an evacuation safety factor is a first step in quantifying the problem of dire evacuations, to encourage the deep and thorough research of the causes and methods to avoid them.

The probabilistic trigger boundary analysis of Mati could have been used before the fire to inform evacuation policy and forest management. The trigger boundary can be used in a

similar manner to Fig. 4.1 to make retroactive conclusions regarding the dire evacuation of the Mati Fire. Analyses like the one conducted for the Mati fire of 2018 can be conducted for other case studies to draw results on the source of any failings of the evacuation process. The firefighting agencies were criticized for the tragedy of the Mati fire of 2018, whereas this analysis shows that, even upon wildfire detection, there was little chance of a successful evacuation. The results of the Mati fire study are horrific, illustrating that the community had no opportunity at which an evacuation would have been completely safe. The example of this methodology used in the Mati fire is an incentive to other communities to use it to plan their evacuation strategies, to identify areas critical to dire evacuations, and plan out long-term fire resilience strategies based on the results.

Chapter 5

Benchmarking of Wildfire Spread Models

Wildfire models are essential tools for understanding fire behaviour, predicting fire spread, and managing wildfire risks. These models integrate complex environmental factors, including vegetation, weather, and topography, to simulate fire dynamics in various ecosystems [113]. These wildfire models use simplified physics to provide a prediction in a short timeframe, to respond to active incidents [81]. Different models employ different assumptions and mathematical formulations. These differences cause diverging and sometimes contradictory results of wildfire behaviour, making the choice of model as important to the results as the input parameters. Employing a wildfire model without understanding its assumptions and consequences may result in inaccurate or unrealistic expectations of wildfire speed.

The majority of operational wildfire models are 2D spread models, operating on a top-down map representation of the landscape, with some accounting for the wind field and the wildfire-atmosphere feedback. These models first calculate the maximum 1D rate of spread of the fire at each point in the landscape, depending on the wind, topography, fuel structure and fuel moisture. The models then employ an algorithm to interpolate the 2D spread of the wildfire based on its 1D maximum rate of spread, and subsequently track a developing fire front along the landscape. Wildfire models employ different algorithms for each part of the process, thus raising the possibility that their results may vary. While higher-fidelity and complexity models are expected to provide more accurate results, the data requirements to run them may be unfeasible even for high-risk areas.

In tandem with the issue of model assumptions and model selection, the calibration range of the model also needs to be considered. Wildfire spread models are developed for specific parts of the world, commonly because they employ empirical correlations that are parameterized for specific vegetation types [95]. Whether an extrapolation will yield accurate results, and

whether generalization of wildfire models beyond their original design areas is appropriate has not been studiedeven if it is a frequent occurence.

A benchmarking of different models allows for a thorough examination of fire behaviour [114]. Existing comparison studies only compare the assumptions of the model only and do not compare their outputs. Benchmarking models to real wildfires that occur in areas for which the models were not developed will also show whether such an extrapolation can yield accurate results.

This chapter compares seven wildfire spread models, five of which are state-of-the-art models currently used to plan against and study wildfires, and two machine-learning surrogate models developed by Google.[1] We benchmark the outputs of the model to three simple scenarios and to the 2018 Mati wildfire, in an area where no model was designed for. We prove that, for a complete analysis of wildfire behaviour, multiple models need to be used through ensemble modelling. We show that each model can produce accurate results when used beyond their design range, and then show that while each individual model produces contradictory results, their combination provides an accurate estimate of wildfire spread.

5.1 Operational Wildfire Spread Modelling

Wildfires spread through heat transfer to adjacent fuel, drying, pyrolyzing and igniting vegetation along the direction of fire spread. Attempting to model these processes is computationally expensive [78]. Wildfire spread models use simplified physics, using bulk values to represent the average properties of the area, and then yield a rate of spread of the fire for that area, assumed homogeneous. The most renowned model that simplified wildfire physics and was used to calculate wildfire spread is the Rothermel model developed by the US Forest Service [95], [96]. It states that the rate of fire spread of wildfires is a relationship between the released energy of the fuel, and the required energy of ignition.

Once the rate of spread has been obtained, another model is needed to propagate the fire along the landscape temporally. The most common way to do is by employing the Huygens propagation principle, discretizing the fire front [91], and expanding it based on a set shape describing fire spread from a point source [116], as shown in Fig. 5.1. Another method to spread wildfire through a landscape is the level set method [117], [118], which described fire spread as a differential equation, and solving it as a temporal mathematical problem. Both methods require the use of assumptions on the spread of a fire from a point source, most commonly an ellipse.

[1] This chapter is based on the following submitted publication: N. Kalogeropoulos and G. Rein, *Benchmarking of Semi-Empirical and Machine Learning Models of Wildfire Spread Outside their Calibration Region*, Oral Presentation, Corfu, Greece, Jun. 2025

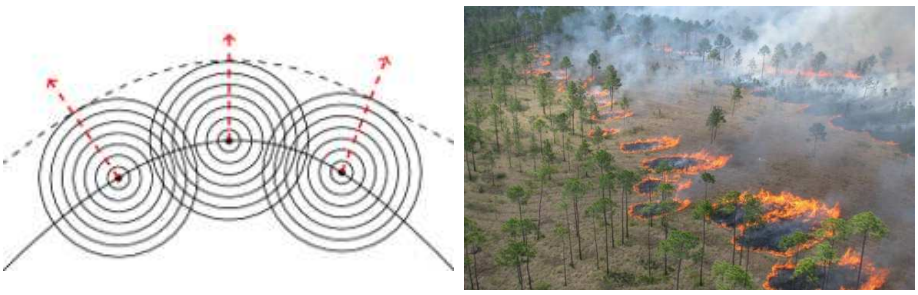


Figure 5.1: Left: An example of the Huygen's propagation principle, using circles as the point spread shape. Figure from [115] Right: Example of fire spread from a point source, in this case helicopter drip ignition. The resulting spot fire shapes can be described in a variety of methods, most commonly ellipses. Photo from U.S. Fish and Wildlife Service, 2013.

5.2 Selected Models

Sullivan [78]–[80] classifies wildfire modes into a spectrum ranging from empirical to physical. Empirical models solely depend on experimental regressions, and physical models solely use physical laws. In the middle are semi-empirical models, ones that are based on physical principles but use experimental regression for calibration. The selected models represent a range of methodologies, shown in Fig 5.2, and are all considered state of the art and validated, are in open access and are used for wildfire research. The total number of selected models is seven, including Farsite (run in FLAMMAP version 6.2), Prometheus (Version 2021.12.03), ELMFIRE (Version 2024.0831), FDS (Fire Dynamics Simulator) Level Set Mode 1 (LS1), FDS Level Set Mode 4 (LS4) (both version 6.9.1), EPD (Encoder-Processor-Decoder) and LSTM (Long-Short-Term-Memory) (no version number)

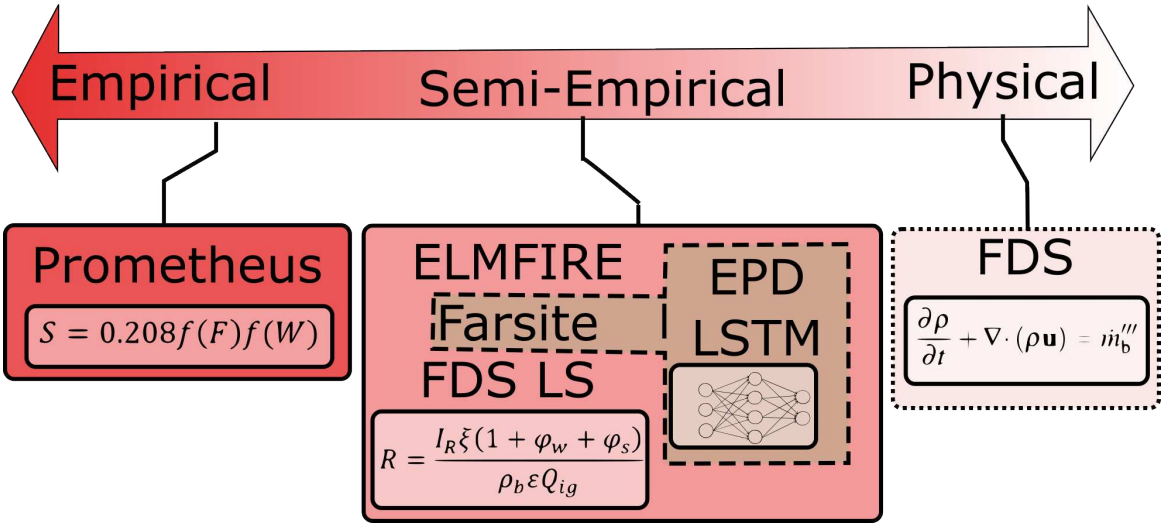


Figure 5.2: The model spectrum as outlined by Sullivan, and the chosen models placed on this spectrum

In the empirical category is Prometheus, developed by Natural Resources Canada [81], for the Canadian forests, but also employed in equivalent latitudes such as the UK. Its physical and

mathematical layers are based on the Canadian Forest Fire Danger Rating System (CFFDRS), and specifically on the Fire Weather Index (FWI) component. The FWI completely relies on field measurements and correlations, originating from lookup tables and later evolving to parameterized equations. Prometheus has been validated for wildfires in Canada [81], while the underlying Fire Behavior Prediction (FBP) system it uses, based on the FWI, has been independently validated [119].

In the semi-empirical category is Farsite, ELMFIRE, EPD and EPD-ConvLSTM. Farsite was developed by the US Forest Service [91], and is used operationally for planning prescribed burns or responding to active incidents, and has been extensively used outside the US [43], [47]. ELMFIRE [82], is a popular, open-source model that has been used by researchers to expand the capabilities of wildland fire spread modelling, and has been included in an online platform that tracks existing wildfires in the continental US and probabilistically predicts their future spread. Both employ the Rothermel physical and mathematical models to predict the maximum spread rate of the fire at each point of the landscape. Farsite then uses the Huygens propagation principle as part of the computational layer to calculate the 2D spread of the wildfire across the landscape, while ELMFIRE uses the level set method. Both models have been validated with wildfires in the US. EPD and EPD-ConvLSTM (LSTM) are both Machine-Learning surrogates of Farsite developed by Google [83]. They were developed to prove that AI wildfire models can model wildfire spread per timestep, not just the final extent of the fire. They were trained on fabricated weather data and real, randomly sampled California landscapes. While they were trained on the already validated Farsite model, they themselves were not validated against real wildfire data.

In the physical category is FDS, developed by the National Institute of Standards and Technology, currently the most often used model for fire simulations at the scale of a room or a building[24]. It uses Large-Eddy Simulations (LES) to calculate fire and smoke behavior in 3D space. To simulate wildfires, the vegetation can either be modelled explicitly, which is computationally expensive and requires granular vegetation data, or it can be modelled explicitly via fuel models. When fuel models are specified, FDS uses the Rothermel model and the level set method (LS) to estimate the fire spread through a landscape (Mallet et al., 2009). FDS models the effects of wildfire and landscape on wind, that may accelerate or hinder the wildfire. FDS allows for selection of the atmospheric coupling to the wildfire, ranging from no coupling (Level Set Mode 1, LS1) to full coupling (Level Set Mode 4, LS4). It thus can be used with a semi-empirical wildfire spread model and a fully physical atmospheric model. LS1 can be considered semi-empirical only, while LS4 has a semi-empirical wildfire model, and a physical atmospheric model. LS4 models the smoke buoyancy and resulting air entrainment, changing the value of the wind and either hindering or accelerating the simulated wildfire. FDS LS1 and LS4 have been validated by the developers [120]

These models use a mixture of mathematical and computational layers, fuel classification schemes and required computational resources. A synopsis of their characteristics is given in Table 1. To make wildfire modelling operationally feasible, standard fuel categories have been developed to standardize how vegetated areas are represented in wildfire spread models. Such wildland fuel classification schemes are the 13 Andersen fuels made for the US, A13 [121]; the 40 Scott and Burgan fuels made for the US, SB40 [108]; and the 16 fuel types of the CFFDRS for Canada [22]. The fuel classification scheme each model uses is shown in Table 5.1.

Table 5.1: The Mathematical and Spread Layer of each model, along with the design region and fuel classification scheme they use.

Model	**Source**	**Mathematical Basis**	**Spread Model**	**Design Region**	**Fuel Scheme**
Prometheus	[81]	FWI	Huygens	Canada	CFFDRS
Farsite	[23]	Rothermel	Huygens	USA	A13, SB40
ELMFIRE	[82]	Rothermel	Level Set	USA	SB40
EPD	[83]	N/A	N/A	USA	SB40
LSTM	[83]	N/A	N/A	USA	SB40
FDS LS1	[122]	Rothermel	Level Set	USA	A13
FDS LS4	[122]	Rothermel	Level Set	USA	A13

5.3 Methodology

The comparison of the models will be conducted in two steps. First, a set of verification cases are used in accordance with a proposed wildfire model verification guide [47]. This guide outlines five test scenarios, starting from a simulation with no wind, flat terrain and uniform fuel as a base case, and sequentially varying the wind, topography and fuel models. Each scenario varies one of these at a time to show their isolated effect on the predicted fire spread. The fuel maps were first created using the US classification models by Scott and Burgan (SB40) and converted to Anderson's 13 (A13) and Canadian (CFFDRS) based on the description of each fuel model, using the official guides of each fuel classification scheme [22], [108], [121]. While some of the models can work with simple matrix data (specifically Farsite, EPD, LSTM and FDS), ELMFIRE and Prometheus require geolocated files, with specific projection information and coordinates. The landscape data used in this chapter are the same as Chapter 4, with the fuel converted as shown in Appendix A. The conversion from SB40 to CFFDRS fuels was done using the two visual selection guides [108], [123], selecting the most appropriate models based on description and accompanying photos. Chapter 6 uses a more mathematical methodology for this conversion.

Table 5.1 shows that all the models were developed and calibrated for the US and Canada. The fuel models they use, their calibration and validation were all done with US and Canadian data. To provide insight of each models generalizability to areas beyond their calibration range, the Mati fire of 2018 was selected as a case study [32], [34]. The 2018 Mati fire happened near Athens in Greece, outside the range of all selected models. The weather station data of the day of the fire were obtained from the weather station closest to the wildfire (in the port of Rafina), and a fuel map was made based on the available vegetation digitization of the Copernicus CLC+ dataset [107]. Since the CLC+ dataset uses a unique vegetation classification scheme, care was taken to translate the dataset from vegetation models to fuel models. The CLC+ dataset was first converted to A13 fuels, for use with Farsite and FDS, using the Andersen fuel classification scheme guide [121], satellite images of the areas, and using comparative photos taken near the affected area, like the one in Fig. 5.3. For Prometheus, the CFFDRS guide was used to select fuels based on their descriptions and image examples [22]. For ELMFIRE and the Google models, the SB40 fuel classification scheme guide was used similarly to the A13 one [108]. A comparison in Farsite of the SB40 and A13 fuel model maps was conducted as validation, using the real wildfire ignition, wind and weather parameters. The A13 fuel models, despite using the guide conversion chart, produce faster ROS values and a 28% greater burn scar extent. Despite the difference, it will be used as is since the map was made using the provided conversion map.



Figure 5.3: Left: The extent of the Mati wildfire overlayed over an aerial photo. The fire started on the point marked x and was driven by east winds. Right: Vegetation reference used for developing fuel maps in the wildfire-prone area, illustrating the plant types and density critical for fire behaviour modelling. This site was classified as SB 165 - Very High Load, Dry Climate Timber-Shrub (even if the description itself is different than pictured).

A limitation of the Google models is that they were only trained on Californian landscapes, and not on fuel models absent from their training dataset. The list of fuel types that the Google models were well trained on, or the list of fuel types that they did not encounter does not exist. To create these lists, to then choose fuel types that the Google models can accurately make predictions with, the LANDFIRE dataset of California was downloaded, and the presence of each SB40 fuel model was measured. This created a list of the most frequent fuel models

present in California. These frequently present models are the ones that the Google models have been extensively trained on and can provide accurate results for. The landscape data were also resized to fit the model landscape size. While the landscape for the other models was 274 x 274 pixels, the Google models can only work on 126 x 126 pixel landscapes, and only simulate fixed timesteps of 15 min, assuming the landscape pixel size is 30 m. The landscape had to be down sampled, and the timesteps had to be modified accordingly to 32 min per timestep to account for the change in landscape size. Fuel moisture content values were left default for each model, as there is no literature on the fuel moisture conditions on the day. The Google models include fuel moisture as an input, but do not have a standard value. Spotting was not included in any models. All simulations were run on a Core i7-11850H processor with 16 logical processors.

5.4 Results

5.4.1 Verification

A total of five scenarios were conducted. The results are given analytically for two of them and are then presented together for the five scenarios. The two scenarios that are shown analytically are the ones where the wind and the slope are varied. The analytical results in Fig. 5.4 and Fig. 5.5 show the spread of the simulated wildfires through the landscape, with contours every simulated hour. The complete results in Fig. 5.6 show the outputs of all the models for a set wildfire simulation time. The wildfire was allowed to spread for the same time in each scenario, for a simulated 48h timespan.

The results of the point ignition in Figure 5.6 show how all models treat no wind and no slope conditions. For all the models it is expected that the fire will spread uniformly and radially away from the central ignition. Indeed, this happens for all models. The EPD and LSTM cases create skewed isochrones, which is a result of such a case being beyond their training set. Machine Learning models trained on real cases struggle with idealized cases but preform respectably in real cases.

The Windy cases in Fig. 5.4 all conform to the expectation of fire spread being faster along the wind direction. The difference between Farsite and ELMFIRE shows the difference between the Huygens and the Level Set methods of fire spread. Examining the first isochrone of the two models, the rate of spread of the head fire is identical, which is expected considering they both use the Rothermel model. The flank- and backfire of ELMFIRE compared to Farsite are both 40% slower, while a similar trend occurs for Prometheus. The difference between Farsite and FDS is significant, with 36% higher spread rates in all directions, and cannot be immediately

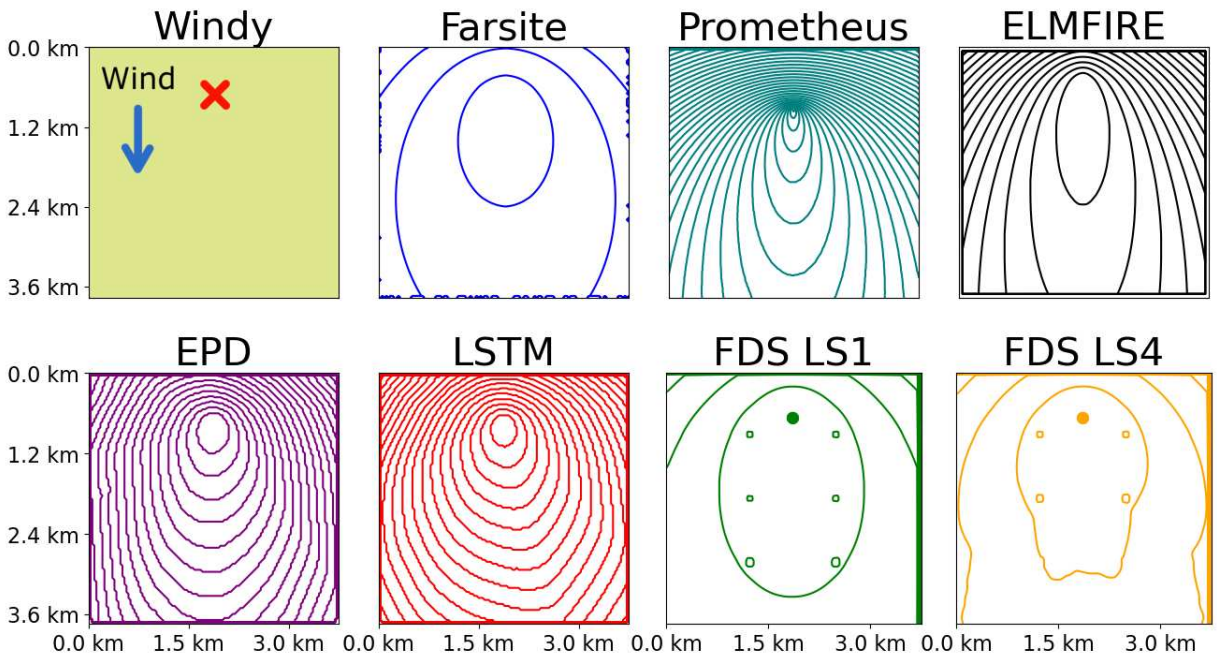


Figure 5.4: The scenario with uniform fuel, constant wind and flat terrain, with ignition north of the centre. Hourly wildfire isochrones are shown.

explained. One factor is the difference in the preset fuel moisture of each model (in the case of 1-hour fuels, 6% for Farsite and 3% for FDS). These values were not changed from the default values; Since they are difficult values to quantify, many users may deem the default values acceptable and will use them as is. Repeating simulations with identical fuel moisture values was not enough to explain the discrepancy. The ML models once again produce irregular shapes, since such simplified cases are not within their training sets. The FDS LS1 and LS4 cases both show dots and bumps in the domain in all test cases. These occur at mesh boundaries, as each case was split into 12 meshes to accelerate computation time. Since these results use the Level Set model of FDS, they do not have grid dependence issues. The LS4 results are significantly faster than LS1, because of the inclusion of wildfire-caused air entrainment.

The Valley case in Fig. 5.5 shows how elevation changes the wind behaviour. The ML models provide unrealistic results since such cases were not in their training sets. Other effects they saw in their training may be influencing the results. The Farsite and FDS LS1 cases are incredibly close, while LS4 shows the effect of modelled atmosphere in a very pronounced manner. The difference between Farsite, ELMFIRE and Prometheus shows the effect of the different computational layers, very similarly to the effects seen in the Windy case, with differences in head fire spread rate of 10% over and under respectively.

The quadrant case in Fig. 5.6 varies the fuel model in each landscape quadrant, while the complex scenario adds all the other scenarios together, with varying wind, slope and fuels. The results show how each model can accommodate different fuel types and varies the speed of the head fire based on the selected fuel model. The complex case shows how the models compile

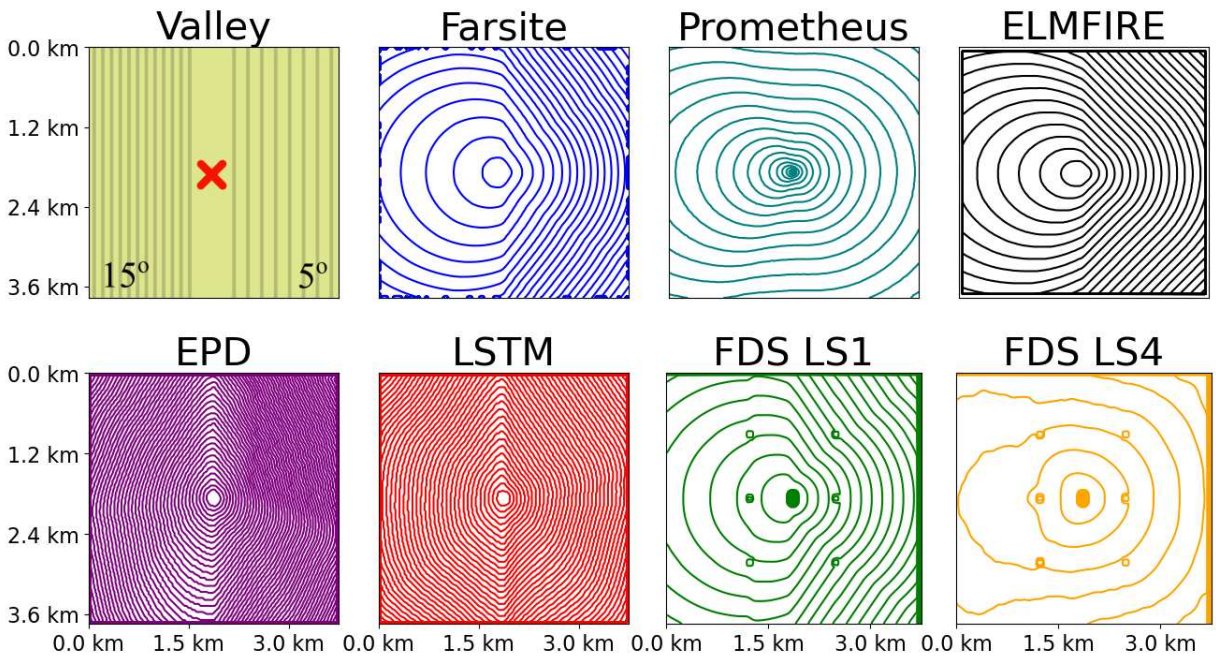


Figure 5.5: The scenario with uniform fuel, no wind and an upwards elevation of 5 degrees eastwards and 15 degrees westwards. Hourly wildfires isochrones shown.

the results of each individual case to achieve results. Overall, all models follow the same trend, with faster head-fires for some models and slower for others.

Fig. 5.6 shows how the models can have contradictory results for the same input parameters. Some of the models may overpredict the fire spread, while other underpredict. It is impossible to say whether one model is better or more accurate than the rest. This is a first indication that ensemble modelling is a step forward in wildfire modelling, as while each individual model may give unique and uncertain results, ensemble modelling allows for the comparative study of the predicted wildfire speed and total spread. With the results of several models, areas of agreement and disagreement are highlighted, allowing for a more conclusive result regarding the fire behaviour of an area.

In terms of model timings and resources, most models behaved similarly. Farsite, ELMFIRE and Prometheus took approximately 5 seconds each to reach 72 simulated hours. EPD and LSTM took about 2 and 16 minutes respectively, with a very consistent time of 0.5 seconds and 4 seconds per simulation timestep respectively. FDS LS1 needed approximately 3 hours (single-core) to finish simulating, and LS4 needed more than 3 days (with 12-core discretization) for the Valley scenario. The landscape was 126 by 126 pixels, with a pixel size of 30m. The EPD and LSTM models were trained on this size of landscapes and can exclusively model landscapes of this size.

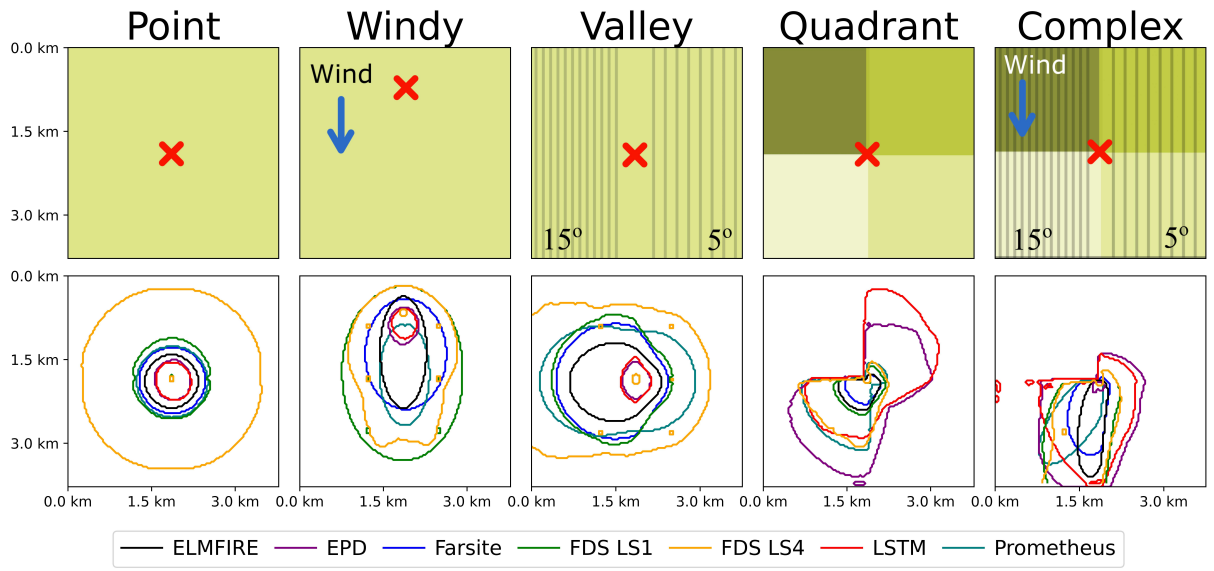


Figure 5.6: The five scenario results, all overlayed on the same plot. All the contours are plotted for the same contour time.

5.4.2 The 2018 Mati Wildfire

With the verification results in hand, the model estimates of the Mati fire can be examined in Fig. 5.7. Each model was given the same weather data, the same topographic data, and the same fuel map (converted to each models fuel classification scheme, as in Appendix A.1), and the fire was simulated from the real ignition point for 9 hours (from 14:00 to 23:00, the same as the real Mati fire). The real wildfires final scar is also included in the figure. A quantitative comparison of the simulated and the real fire scar is performed using the Jaccard similarity coefficient, shown in Eq. 5.1, where X and Y are the two wildfire scars expressed as sets. The Jaccard similarity coefficient is used when comparing wildfire prediction and real data and is defined as the ratio of the intersection of the two areas, over their union. Jaccard values closer to 100% indicate a complete match between predicted and actual wildfire scar. A comparison of these results, with each models computation time, is given in Fig. 5.8.

$$J(X,Y) = \frac{X \cap Y}{X \cup Y} \tag{5.1}$$

In simulating this fire, the EPD model was the fastest, requiring only 18 timesteps and 9 s, followed by ELMFIRE at approximately 1 min, then Prometheus, Farsite and LSTM taking approximately 5 min due to the complex fire front shape requiring more detailed discretization and thus more computational resources. Finally, FDS LS1 took approximately 30 min to complete, and FDS LS4 took approximately 1 day. The total time of each model, along with a measure of their output similarity to the real fire scar explained below, can be found in Fig. 5.8.

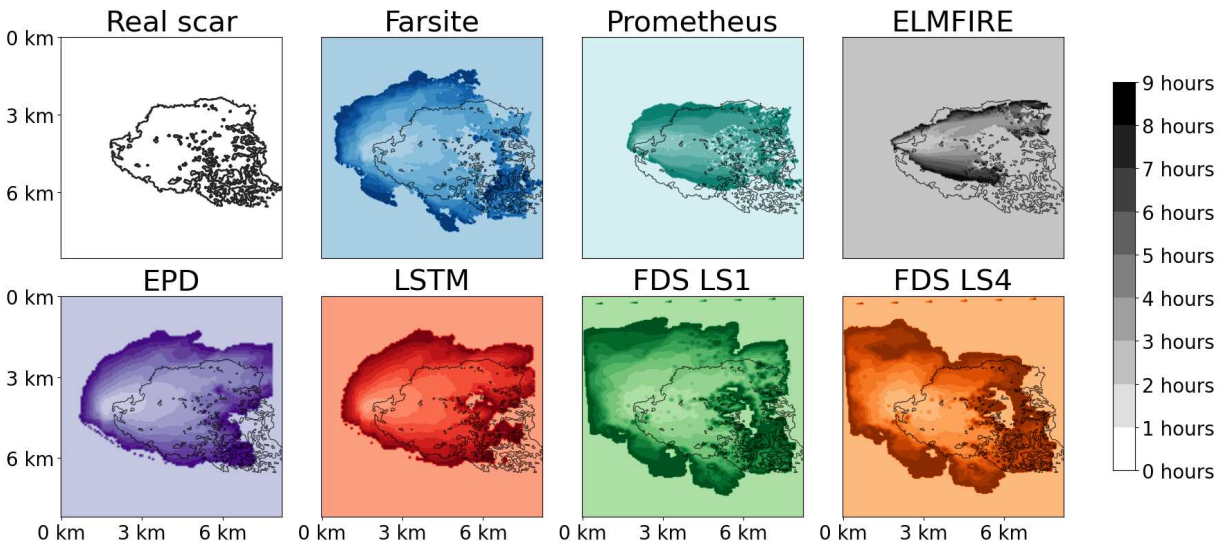


Figure 5.7: The results of the Mati fire model results, along with the real fire scar by the Copernicus Mapping Service. Shaded areas in each plot delineate hourly isochrone areas.

The elementary behaviours of the models based on the five verification cases can be reflected in their outputs of a real case like Mati, the results of which are shown in Fig. 5.7. Starting with Farsite, the results overestimate the backfire and flank fire spread, and underpredict the spread of the fire towards the built-up community. This is a common issue with wildfire spread models, which treat built-up areas as nonburnable. As such fire cannot spread through built up communities. The fire spread stops in built up area and can only go around them, resulting in a low overall similarity score of 39%. Note that the real fire had very little suppression, so the simulated results should not be significantly different from the real scar. The overestimate of the back fire could also be attributed to small-scale influences of the real fire that cannot be depicted in a 30 x 30 m cell size scale, such as small dirt roads to the west and north of the ignition point, stopping fire spread early. Farsite also models the effects of the weather on the dead fuel moisture dynamically through the simulation which influences the result, but the short duration of the simulation along with its heterogeneity makes it hard to see its effects. Prometheus has the best similarity of all the models, with a score of 59%. It underestimates the flankfire to the south but predicts the head and backfires well. The core reason for this high score is Prometheus ability to model wildfires going through fire breaks. While this feature was originally meant to model wildfires crossing over rivers and roads, it still applies for fire going through communities. As such the fire scar of Prometheus includes more of the community that Farsite and the other models show as unburned. Prometheus also dynamically adjusts the fuel moisture over time.

ELMFIRE also underpredicts the flankfire spread but correctly predicts the backfire spread, similarly to Prometheus. It is hindered by its inability to model community wildfire spread, similarly to Farsite, which is why it receives an overall similarity score of 45%. It was one of the fastest non-AI models, showcasing the advantages of the level set method since it does not

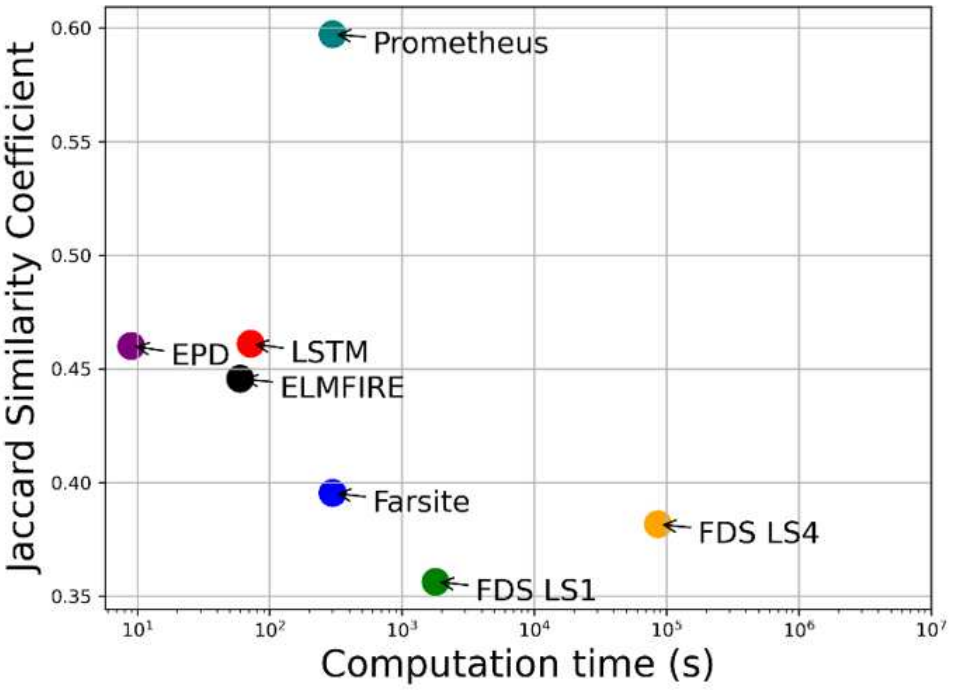


Figure 5.8: The Jaccard similarity coefficient results of each model, comparing the real wildfire scar to the simulated scar. The results are for a Core i7-11850H processor system.

require the same degree of discretisation as the Huygens propagation. The two Google models performed very similarly to Farsite, as was expected of them. The downscaling and retiming of the simulation steps meant that the EPD model was the fastest model with a respectable similarity of 46%, identical to LSTM. The downscaling of the area allowed the wildfire to reach further into the built up area than Farsite, which is why their similarity scores are higher. The two FDS settings overestimate the flank- and backfire spread considerably. The inclusion of fire-atmosphere interactions of LS4 compared to LS1 do change the results but not to a considerable extent. Overall, the FDS models has the lowest similarities of 36% for LS1 and 38% for LS4. While LS4 does provide benefits like smoke visualisation, the computational cost and the inaccuracy of the result require further research.

Another important point of comparison for the models is the rate of spread, which is generally consistent among the models. The majority of models use the Rothermel model to calculate the maximum rate of spread along the wind-slope combined vector. It is important to investigate the rates of spread that the models predict. This paper examines two methods of comparing rates of spread. The first method is a comparison of all the rate of spread values of the rasters. Such a comparison displays the rate of spread distribution of the simulated wildfires along all spread directions. Figure 5.9 shows a histogram of the rate of spreads of each model. Most model follow the same distribution, with can be explained by them all using the Rothermel model (or equivalently be trained on Rothermel-based models), similar 2D spread algorithms, and similar simulated burn scars. FDS LS1 and LS4 were expected to have larger ROS values

due to their expanded burn scars, but seem to fall in line with the majority of the models. This may be an artifact of the interpolation required to calculate ROS values from arrival time data, the only data FDS can currently output. Prometheus and ELMFIRE output differing ROS values, which can be explained by Prometheus using a unique system to calculate rates of spread, and ELMFIRE having the smallest burn scars with limited flank-and back fire spread.

The maximum rates of spread of all the models are also compared in Figure 5.9. To estimate the maximum rate of spread of each simulated fire along the wind, the average of the highest 10% of rates of spread in the raster is calculated and plotted for each models. ELMFIRE has the significantly highest rates of spread of all the models. This occurs due to some parts of the landscape with particularly high rates of spread ($> 200 m/min$) in tandem with the high winds of the simulation. While other models such as Farsite employ a limit to the ratio of the headfire and flank and backfires, ELMFIRE may not employ such a limitation and allows the headfire to rise to incomparable levels. Of the other models, the machine learning models generally predict higher maximum rates of spread, but again this may be an inaccuracy due to the interpolation required from arrival time to rate of spread. All the rest of the models have comparable windward rates of spread.

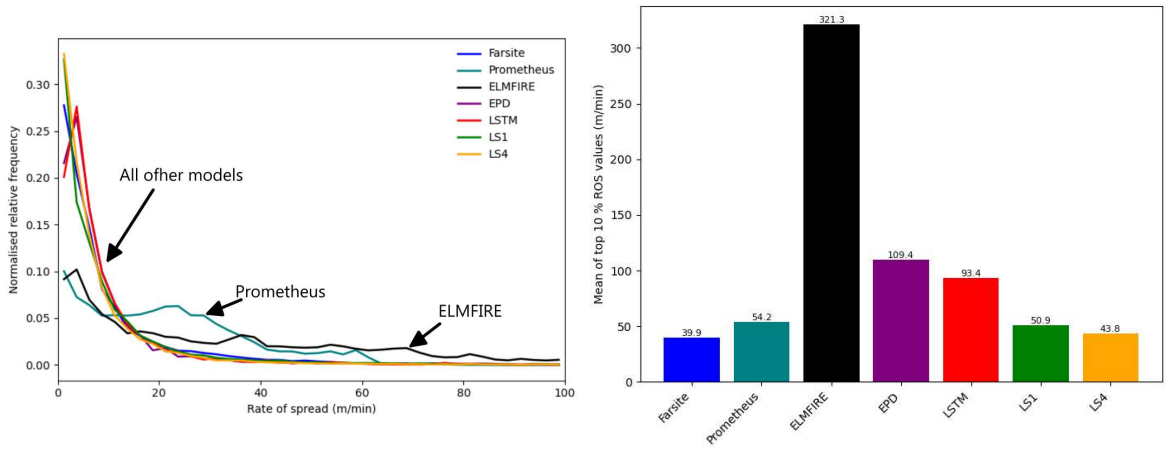


Figure 5.9: Left: A histogram of the rates of spread of the entire simulated burn scar of each models. Almost all the Rothermel-based models follow the same ROS distribution. Prometheus and ELMFIRE follow different distributions with higher average rates of spread, primarily because of their limited flank- and backfire spread. Right: The average windward ROS of each model, defined as the average of the 10% highest ROS values of each raster. ELMFIRE has the highest maximum rates of spread by a large margin.

5.4.3 Ensemble modelling

Ensemble modelling is used extensively in fields such as weather forecasting, where it originated [124], and has expanded to other wildfire related fields, such as transportation and evacuation modelling [125]. Ensemble modelling relies on the use of multiple data sources and forecasting

models, with the goal of removing the reliance of each individual model to a set of assumptions and parameterisation. It is a critical methodology in fields where complex phenomena must be modelled using simplification and bulk quantities.

Using any one model to simulate the Mati fire yields different results, either in the burn scar of the fire or the rate of spread. Using a multitude of models shows both these hazards better than using any single model. An ensemble model analysis of the Mati fire based on the seven models is shown in Fig. 5.10 by adding the fire scars predicted by each model together. The probability of the fire reaching each area is dictated by the number of models that include that area within the burn scar. This gives an accurate overall estimate of the 9 h fire propagation. This shows the importance of ensemble modelling when working on community safety, along with understanding the elementary behaviour of each model to explain the simulated fire spread.

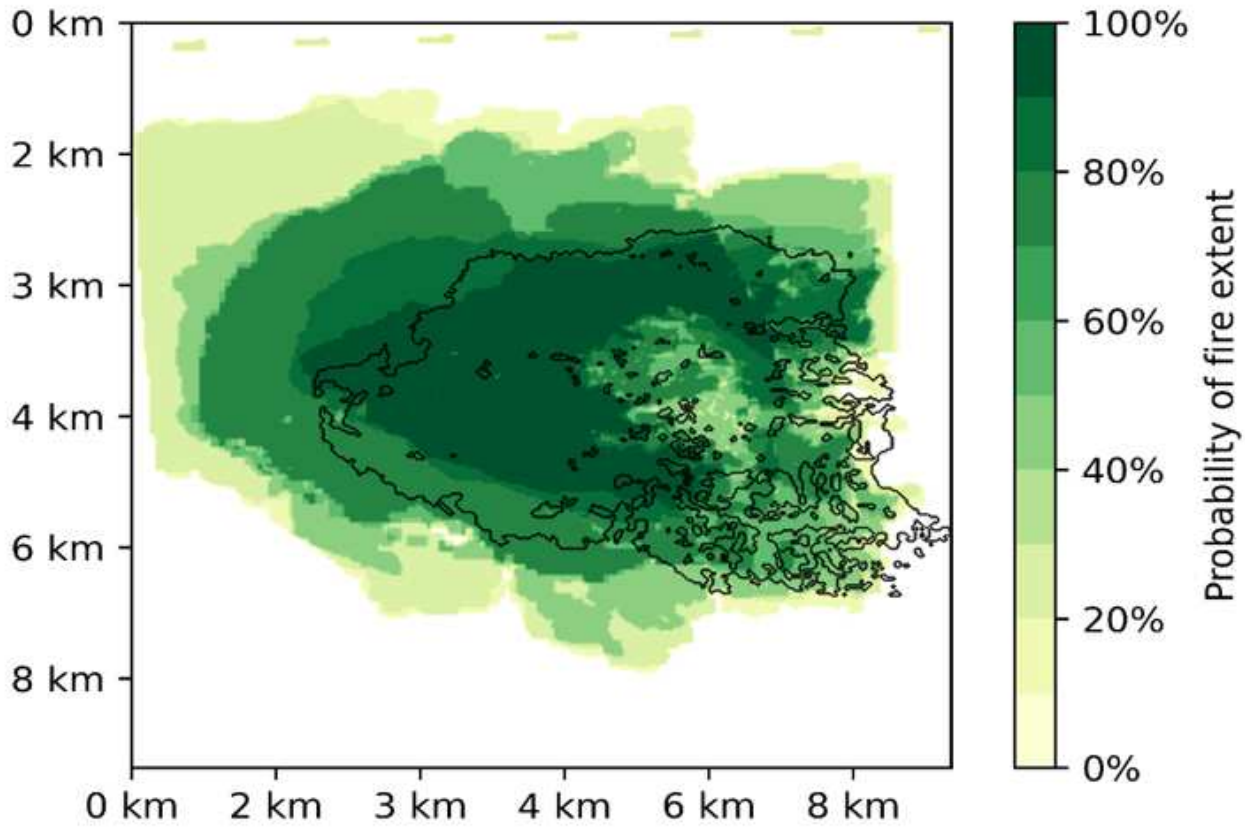


Figure 5.10: The probabilistic burn scar result of the Mati fire, based on the ensemble modelling using all examined models.

Using ensemble modelling alows for a more complete assessment of the fire spread through an area. The results show areas of high agreement between the models, where the wildfire is predicted to go through. Other areas of the landscape have lower agreement between the models, showing areas where models may over- or underpredict. This allows for a more certain conclusion on the fire behaviour prediction, no longer relying on the assumptions and limitations of a single model, but leveraging the strengths of all the models and allowing a comparison of

the limitations and differences of the results.

5.5 Conclusion

While many wildfire spread models exist, there have been no benchmarking studies directly comparing them. This chapter shows that ensemble modelling is an improvement for wildfire prediction, taking advantage of the different assumptions and strengths of all models. While each individual model has a different agreement between predicted and real wildfire scar (ranging from 35% for FDS Level Set Mode 1 to 60% for Prometheus), a combined ensemble modelling result provides a probabilistic result. The verification scenarios highlighted the consequences of the model assumptions and parameterisation on the result and allowed the explanation of the model disparities on the real fire results. Considering Farsite as a basis, ELMFIRE and Prometheus yield 50% slower flank- and backfire with the same head fire, resulting in smaller burn scars. FDS overestimates the effect of the wind by 50% in all directions, resulting in larger fire scars. EPD and LSTM struggled in the verification scenarios but performed very similarly to Farsite in the Mati case, with 82% agreement between the three, requiring 300 times less time to finish simulating. This is probably because their training range only included heterogeneous, realistic landscapes and no idealised one. The selection of fuel types and the conversion to each model has a direct impact on the results. It can be argued that the effect of choosing a specific fuel type over another is limited comparable to the intrinsic error of the assumptions that come with each model. This effect is not explored in this chapter but can be explored in the future, in an attempt to quantify the sources of error of wildfire spread models. Arguing that each of the models chosen is part of the state-of-the-art, the differences between each model need to be highlighted, benchmarked and studied, while the best way to prepare for future wildfires is by using a multitude of models, to reach a conclusive and certain result.

Chapter 6

Ensemble Probabilistic Trigger Boundaries

6.1 Introduction

Trigger boundaries have been calculated using a single wildfire model in the past [43], [45], [47]. As different wildfire models predict different wildfire behavior, the choice of model is bound to have an influence in the generated trigger boundaries, and the perceived safety of a community. This influence of model choice on trigger boundaries has not been studied or quantified. Previous work comparing wildfire models has recommended that an ensemble approach, where all available models are used collectively, is necessary for accurate risk assessment [46]. This chapter aims to generate probabilistic trigger boundaries for a community, using an ensemble of state-of-the-art wildfire spread models. The generated trigger boundaries will be compared, and will be compiled to provide and ensemble-probabilistic trigger boundary. The ensemble trigger boundary methodology is applied to the Fort McMurray community in Canada, which underwent a monumental dire evacuation during a wildfire in 2016. The results show that ensemble wildfire modelling is required to adequately assess the fire behavior of an area, and the long term safety of a community. Some conclusions are also made on the use of trigger boundaries in high-risk communities like Fort McMurray, where the required evacuation is large and the available evacuation time is small.

6.2 Modelling Background

A number of wildfire spread models were chosen for this study, taken from the state-of-the-art, already explored in Chapter 5 [46]. These models range from purely empirical to semi-empirical

and semi-physical [78], [79]. On the empirical side of the spectrum is Prometheus/WISE [81], which is developed by the Canadian Forest Service, originally released as Prometheus but currently re-released as WISE. On the semi-empirical side are Farsite, ELMFIRE, and FDS LS (Fire Dynamics Simulator, Level Set). Farsite is developed by the US Forest service [23], ELMFIRE is developed by Lautenberger et al [82], and FDS has been developed by the US National Institute of Standards and Technology [24]. FDS is a fire modelling tool with a semi-empirical component of wildfire spread, either on its own (LS1) or with atmospheric coupling (LS4). Lastly, a pair of Machine Learning models developed by Google, named EPD and EPD-ConvLSTM [83] have been developed as surrogate models to Farsite, aiming to produce comparable results with much less computational time.

Each of the models above predicts different wildfire spread for the same input conditions, as shown in Chapter 5. [46]. The models were first verified, using ideal cases to test the effects of topography, wind and fuel on the simulated fire behavior. The first verification case was of uniform fuel in flat terrain with no wind, and subsequent verification cases added topography changes, wind and fuel changes sequentially. The models were then compared against the burn scar of the 2018 Mati fire in Greece. All the models had different predictions of fire spread in the verification and validation cases, with the ultimate conclusion that ensemble modelling, taking into account all the models, is an improvement in quantifying wildfire risk of communities.

6.3 The Fort McMurray Case Study

The selected community for this study is the Fort McMurray area in Alberta, Canada. In 2016, Fort McMurray underwent the largest evacuation in Alberta's history, due to a wildfire that became the costliest natural disaster in Canadian history, with overall damage of US$7.61 billion. The Fort McMurray community has a permanent population of around 90.000 and a shadow population of about 30.000 [126], with the surrounding area consisting of boreal forests, lakes and oil sand mines, as shown in Fig. 6.1. The real wildfire started from the southwest of the community, and spread for months afterwards towards the east, enveloping most of the west and south parts of the community.

Several data sources were used to generate the trigger boundaries of the Fort McMurray community. The historic wind and weather data for the region from 1999 to 2024 was retrieved from the Environment and Climate Change Canada National Climate Archive's Hourly Weather Data, specifically from the Fort McMurray Airport weather station. The collected data include the hourly temperature, humidity, and wind magnitude and direction. The fuel type and digital elevation data for the area were retrieved from the Canadian Wildland Fire Information System. The fuel map was provided in the Canadian fuel classification scheme (FBP). The elevation data was used to derive the slope and aspect of the landscape. The canopy cover

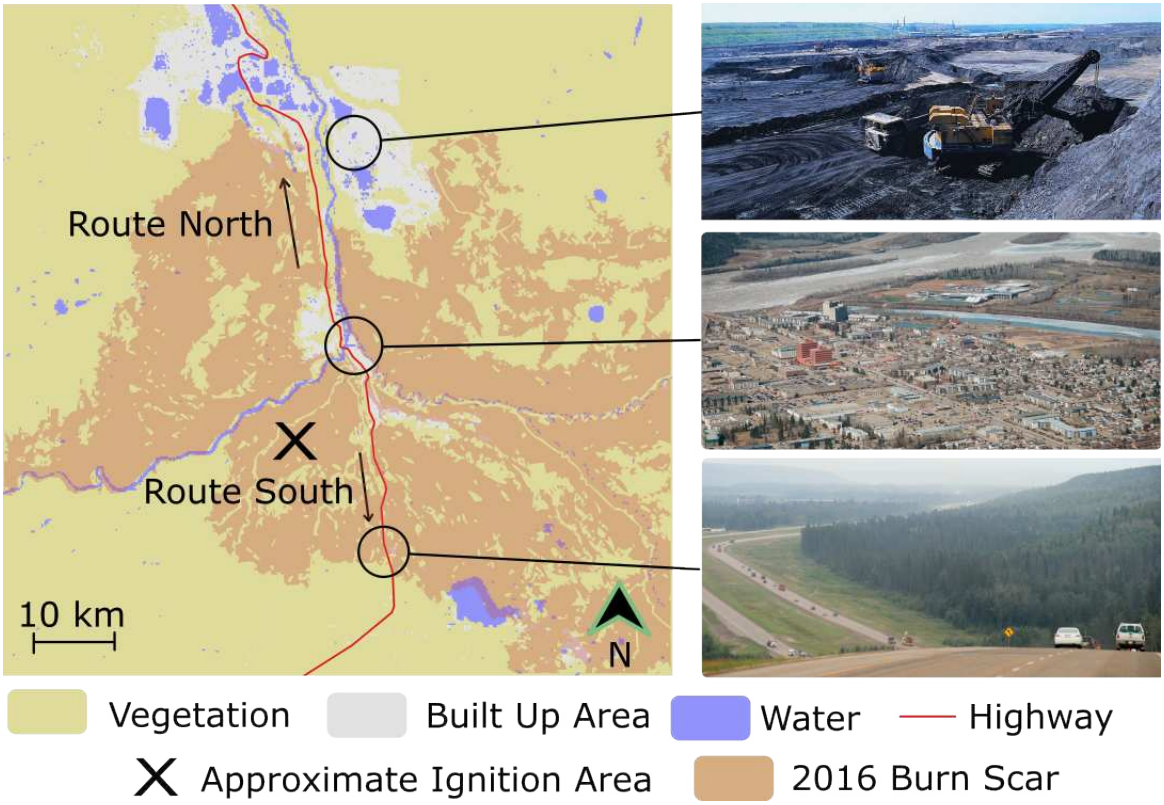


Figure 6.1: A map view of the Fort McMurray area, with indicative photos of the surrounding vegetation. To the north of Fort McMurray there are large areas of surface mines and oil sand fields. The main evacuation routes of the Fort McMurray community is the main road, to the North and the South. The oil sands fields to the north of the community act as natural inhibitors to wildfire spread. An example of the vegetation around the Fort McMurray area is shown in the bottom photo. Credit top to bottom: Suncor Energy, Jason Woodhead 2016, Andrew Bates 2013.

data was retrieved from [127]. The canopy characteristics (canopy height, canopy base height, and canopy bulk density) were taken from a survey of forests south of the Fort McMurray area [128]. All the geodata collected were of different sizes, scales and proportions. They were all reprojected to have matching cell sizes of 200 x 200 m. While this size is coarse compared to the usual 30 x 30 m cell size used in wildfire spread models such as Farsite, not all datasets were of such a high fidelity. A suitable size of area was then cropped for the simulations. The landscape data used for the simulation were required to be square to be used in the Google EPD and LSTM models.

The process of collecting and collating the wind and weather data is the same as in Chapters 3 and 4. The results are shown in Table 6.1 From the historic weather information, the maximum temperature of each year was first found, along with the minimum temperature of the same day. The minimum and maximum humidities were identified at the same hours as the maximum and minimum temperatures respectively. This resulted in a distribution of maximum yearly temperatures, minimum temperatures of that day, and corresponding humidities. This

Table 6.1: The kPERIL parameters for the Fort McMurray Case. These parameters were applied to all the models. For models where fuel moisture content is a direct input, Flammap was used to interpolate it based on a repeating diurnal weather profile with the above conditions.

Quantity	**Mean Value**	**Standard Deviation**	**Units**
WRSET	900 or 1300	90 or 130	min
Maximum Temperature	31	6	C
Minimum Temperature	10	4	C
Maximum Humidity	78	10	%
Minimum Humidity	27	20	%
Time of Maximum Temperature	15	1	Hours
Time of Minimum Temperature	5	1	Hours
Wind Magnitude	20	11	km/h
Cloud Cover	0	0	%
Precipitation	0	0	mm

distribution reflects the most severe conditions of each year. The wind magnitude was collected irrespective of time of year and used to find a wind distribution. The historic wind direction was not used, as the wind direction will be set in each iteration to drive each wildfire towards the community. This reflects a worst-case scenario and excludes wildfires that do not pose the community in immediate danger.

The fuel map of the area was provided in the Canadian fuel classification scheme [22], and needed to be converted to the Scott and Burgan (US) fuel classification scheme [108], for use in all the other models. While this remapping was done based on matching fuel classification descriptions in the past [44], a more rigorous approach was required. The fuel models of the two classification systems, while similar, do not reflect the same properties and thus cannot be directly substituted. In the previous chapter, the fuel types were directly converted from one to another empirically, through guide photos and other conversion charts. A more mathematical and objective method was researched for a better conversion method. In doing so it was discovered that the American and Canadian fuel models operate differently, in how the wind and slope affect the rate of spread. The US scheme uses fuel models as substitutes for a collection of physical variables such as fuel loading, fuel bed depth, etc. The Canadian scheme, on the other hand, uses fuel types to set three empirical constants, used in Eq. 6.1, 6.2 to directly calculate the effect of wind on rate of spread. Eq. 6.1, 6.2 are used for the majority of fuel types, although some use modified equations.

$$R = a\left[1 - exp(-b \cdot ISI)\right]^c \tag{6.1}$$

$$ISI = 0.208 \cdot 91.9 \left[1 + \frac{(5.31M)}{4.93 \cdot 10^7}\right] \exp\left(-0.1386M + 0.05039U\right) \tag{6.2}$$

Where R is the Rate of Spread in m/min, ISI is the Initial Spread Index, part of the Canadian Fire Weather Index, M is the fine fuel moisture content in percent, U is the wind speed in km/h, and a, b, and c are empirical constants. The three empirical constants are set for each fuel type [81].

The goal of this process would be to find a corresponding US fuel type for each Canadian fuel type present in the Fort McMurray area. An initial attempt was made by comparing fuel maps of Alaska, since the Landfire database contains fuel maps in both the Canadian and US classification scheme. Using the same methodology as [44], a map was created, mapping which US fuel models were used in place of each Canadian model, and in what frequency. To examine the accuracy of this conversion, a single wildfire was simulated with WISE using the Canadian fuel map, and ELMFIRE using the derived US fuel map. The results showed a drastic mismatch between the predicted wildfire speeds. ELMFIRE predicted 60% to 80% slower fire spread than WISE for the same weather conditions. The conclusion was that this conversion strategy did not yield accurate results.

A second attempt was made, this time with a direct comparison of the rates of spread of each fuel. To do this, Eq. 6.2 and 6.1 were solved directly for varying wind and a set fine fuel moisture content, to find each fuel's rate of spread over wind curves. For the US fuel models, the Rothermel model was used directly through the *SFM_metric* R package, to calculate the no slope, varying wind rate of spread of each SB40 fuel model with varying wind and the same fine fuel moisture content. This yields the rate of spread over wind magnitude curves for the Canadian and US fuels. Each graph of the Canadian system was then compared with each of the US fuels, and their similarity was quantified using a normalised root mean squared error metric, in Eq. 6.3.

$$RMSE = \sqrt{\left[\sum_{U=0}^{U_{max}} \left(\frac{R_{US}(U) - R_{FBP}(U)}{R_{FBP}(U)}\right)^2 \frac{1}{n}\right]} \tag{6.3}$$

Where U_{max} is set to 40 km/h, representing a typical maximum wind during wildfires, and n is the number of samples in each plot. U_{max} has been set to 40 km/h as an estimate for strong winds, even though wildfires are known to spread under worse conditions. For winds more than 40 km/h, the two fuel types significantly diverge, not changing the results significantly. The divergence can be already seen in Fig. 6.2This metric compares the overall match of each curve between the two models. In the case of Fort McMurray, the historic average wind is 11 km/h with a standard deviation of 6 km/h. The conversion process could have used a U_{max} value of 20 km/h to optimize for the Fort McMurray area. Such a specific value would be restrictive and not generalizable to other Canadian communities, and was not chosen. The proposed process is to be applied to all Canadian communities and landscapes, and not optimised based on local

wind magnitudes.

Ultimately, no two curves were identical in the comparison between the two fuel classification systems, primarily because the no-wind rate of spread in the Canadian system is much greater than the no-wind rate of spread in the US system. This would not change with different spread models, since they all use the same equations and parameters to estimate the 1D rate of spread before advancing the flame front. An example of this comparison, with the two best-matching plots for Canadian fuel model o1b "Grass" is given in Fig. 6.2. This comparison metric is best to create a map of fuel types that best translate the dependence of rate of spread and wind. A single wildfire simulation was used to compare the newly converted fuel map, using WISE and ELMFIRE, and the difference was reduced to approximately 8%, a result deemed acceptable. The above methodology was done twice, once with all the SB models present, and again only with US models that can be used in the Google models, since the training set of the "california" models used in this study did not include all the US fuel models. The results of this comparison are given in Table 6.2, with each CFFDRS fuel given a corresponding best-matching SB fuel type. The complete root mean square error per fuel pairing table is given in Appendix B

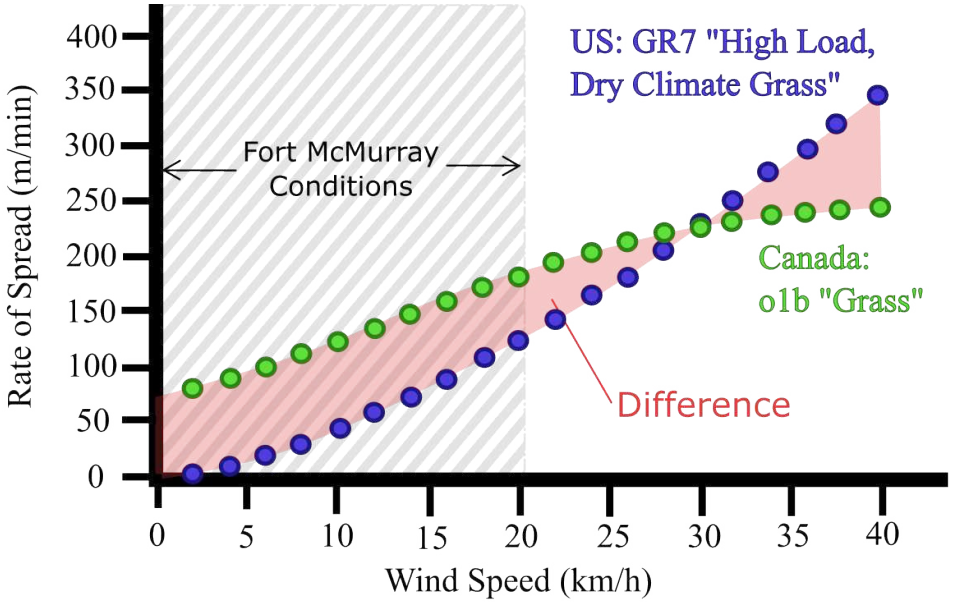


Figure 6.2: The best-fit equivalent between Canadian model 01b "Grass" is the US model GR7 "High Load, Dry Climate Grass", with the minimum RMSE error from Equation 6.3. The RMSE is calculated in a typical ambient wind range of 0 to 40 kph.The ROS values were only calculated in 1D manually, solving the American and Canadian models directly, without any of the spread models used here. The Fort McMurray historic wind ranges from 0 to 20 kph. In this range, the Canadian fuel model predicts 3 times higher spread rates than the US model. This happens for all best-fit equivalents, as Canadian models routinely have higher zero-wind rates of spread, and US models' rate of spread increases faster with wind. For low wind values, there is a near 80-fold difference between the two models, a significant difference and consequence of how the two models treat low-wind effects.

Once all the input data was collected, and converted to formats acceptable by all models, iter-

Table 6.2: The conversion chart from CFFDRS to SB40 fuel models. The root mean square error is also displayed for each model. All the values are concerningly high, primarily because of the different ways the two fuel model systems scale with wind.

Model	**Most Similar**	**RMSE**	**2nd Most Similar**	**RMSE**
C-1	GR3	3.0	SH9	3.0
C-2	SH5	2.8	SH9	2.8
C-3	SH5	3.0	SH9	3.0
C-4	SH5	2.8	SH9	2.8
C-5	SH6	2.8	SH8	2.9
C-6	SH7	2.7	GS4	2.8
C-7	SH6	2.8	SH8	2.9
D-1	TU2	2.9	TL9	3.0
S-1	SH5	2.7	SH9	2.7
S-2	SH7	2.7	GS4	2.8
S-3	SH5	2.7	SH9	2.7
O-1a	GR8	2.8	GR7	2.9
O-1b	GR9	2.9	GR7	3.0
M1	SH7	2.7	GR3	2.9
M2	SH5	2.8	SH9	2.8

ating could start. Each iteration, the ignition location, maximum and minimum temperatures and humidities, times at which those occur, and wind magnitude, are selected randomly based on the normally distributed input ranges. The ignition location is prevented from being on a fuel model that prevents fire spread (such as water or built-up areas), and has to be at least 3/4 a domain size away from the center. It was important to set projection information to the randomly generated ignition point, for compatibility with all the models, so the use of a geographic-related data library, GDAL (Geospatial Data Abstraction Library), was necessary.

The overall process for a single iteration is shown in Fig. 6.3. One critical issue was identified when operating different models. Models like Farsite, ELMFIRE, the Google models and FDS require the fuel moisture content as a direct input. WISE does not allow fuel moisture as an input, and instead estimates it from the weather conditions during and before the wildfire. Farsite does dynamically adjust the fuel moisture during the simulation, using the fuel moisture inputs as starting conditions. This means that, for a consistent comparison, the fuel moisture used in one set of models should correspond to the fuel moisture interpolated by the weather in the other set. To bridge this gap, before simulations start, a simulation in FLAMMAP is done, with the purpose of estimating the fuel moisture content for fine and coarse fuels, based on the weather. It uses the Nelson model to estimate fuel moisture, given some initial conditions and information regarding the weather, canopy cover, and landscape aspect, among others [129]. The weather input is a diurnal, sine-based interpolated hourly weather profile based on the selected maximum and minimum temperatures, humidities, and times thereof. This weather profile is repeated for 30 days to ensure the coarse fuels had time to adjust their moisture

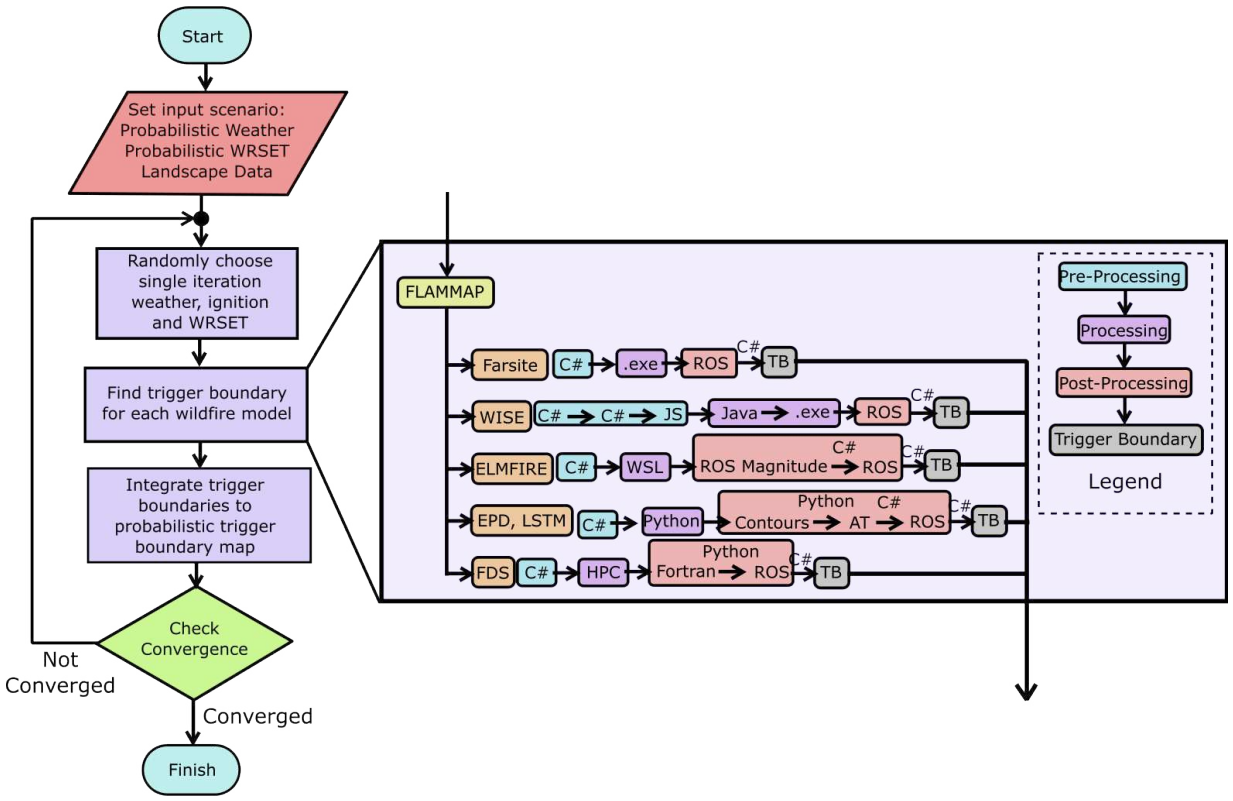


Figure 6.3: A flowchart of the process of creating probabilistic trigger boundaries (TB) via ensemble modelling. The process of running each model is highlighted. Before all models, FLAMMAP is used to estimate the fuel moisture.

content. The simulation ends at 16:00 of the last day, to ensure that the fine fuel moisture is reflective of dry daytime conditions and avoid situations where the simulation ends at night, where the fine fuel moisture is highest.

The result of FLAMMAP is a spatially heterogeneous map of 1-hour, 10-hour and 100-hour dead fuel moisture. ELMFIRE can use this heterogeneous map without modifications, but the other models require an average fuel moisture per fuel model. The results from FLAMMAP are thus averaged per size class and per fuel to be used in the other models. At this stage, the fuel moisture input is reflective of the simulated weather, and simulations of each model can begin. The simulations intially run for 500 simulated hours, which is enough time for any simulated wildfire to spread through the entire landscape. A wildfire lasting 500 hours is extreme or unrealistic, however this is a purely computational necessity to allow the simulated fire to spread through the entire landscape, to have ROS data for the trigger boundaries to be calculated. The simulation durations for each model were then adjusted based on predicted wildfire spread rates, to minimize computational time. When the wildfire spread models are used, the weather is a constant as maximum temperature and minimum humidity, with constant wind, to ensure that the wildfire spreads with the worst conditions of each day across the entire landscape.

Compared to previous work on ensemble modelling [45], where the models were only used for one scenario, models need to be used dynamically for repeated scenarios, with changing ignition location, wind and weather conditions and fuel moisture content. As such, command-line versions of all models were sourced and used for this study. Each of these models required different setups and procedures to automatically run simulations. The program governing these iterations is written in C#, as it is an expansion of the WUINITY project [27], [37], [38], wholly written in C#. The details and intricacies of using each model are shown in the Appendix

With each iteration, a new set of maximum and minimum temperatures and humidities are chosen, along with the times at which those occur. A diurnal wind and temperature profile is interpolated and used to calculate the new starting fuel moisture. The wind magnitude is chosen based on the input parameters, and the direction is set from the ignition point to blow towards the center of the community, to mirror the worst case scenario. The ignition location is chosen randomly. as long as it is in a point that is vegetated and can allow wildfire spread, significantly far away from the community. Once all the trigger boundaries are calculated and the simulations are finished, each model's boundary is added to the total, probabilistic trigger boundary. The iteration is complete, and a new one may start. The iterations continue until a convergence criterion, discussed in [45], is achieved. In this study, 350 iterations were sufficient for convergence.

6.4 Results

Two evacuation scenarios have been considered to develop trigger boundaries in this study. As seen in Figure 6.1, the Fort McMurray community has two egress routes, a northern and southern road. Ideally, both egress routes would be used in an evacuation. However, situations arise that deem one of the two egress routes unusable. For example, in the real evacuation of the Fort McMurray area in 2016 the south egress route was unusable due to the arrival of wildfire smoke and flames. Ideally, the effect of wildfire impingement on evacuation routes would be reflected in the trigger boundaries dynamically through a coupling of wildfire, smoke, and evacuation modelling. Without this coupling, the effect of road closures will be shown here as two scenarios. The first one has a WRSET of 900 min and standard deviation of 90 min, representing the use of both the north and south road, with contraflow conditions, where both road directions are used for the evacuation. The second one has a WRSET of 1300 min and standard deviation of 180 min, representing the use of only one road, with contraflow conditions. In the real wildfire of 2016, the conditions were extreme and not represented by average values used here. The purpose of the probabilistic analysis executed here is to reflect both the variability of the wildfire due to weather conditions, and to include the most extreme conditions realistically possible. These worst case conditions are reflected in the analysis because

of the randomness of the process, with some of the iterations being conducted under conditions where wildfire speed is extreme.

Following the analysis from above, a computational landscape of size 80 x 80 km was chosen for this study, with 200 m cell size (total raster size of 400 x 400). This is based on the maximum WRSET and the expected wildfire rate of spread. This is considerably larger than most wildfire simulations, which use landscapes with sizes in the order of 10 x 10 km [23], [46], [82]. The computation time per iteration for each model is shown in Fig. 6.4. A distribution of all the rates of spread estimated by each model is shown in Fig. 6.5.

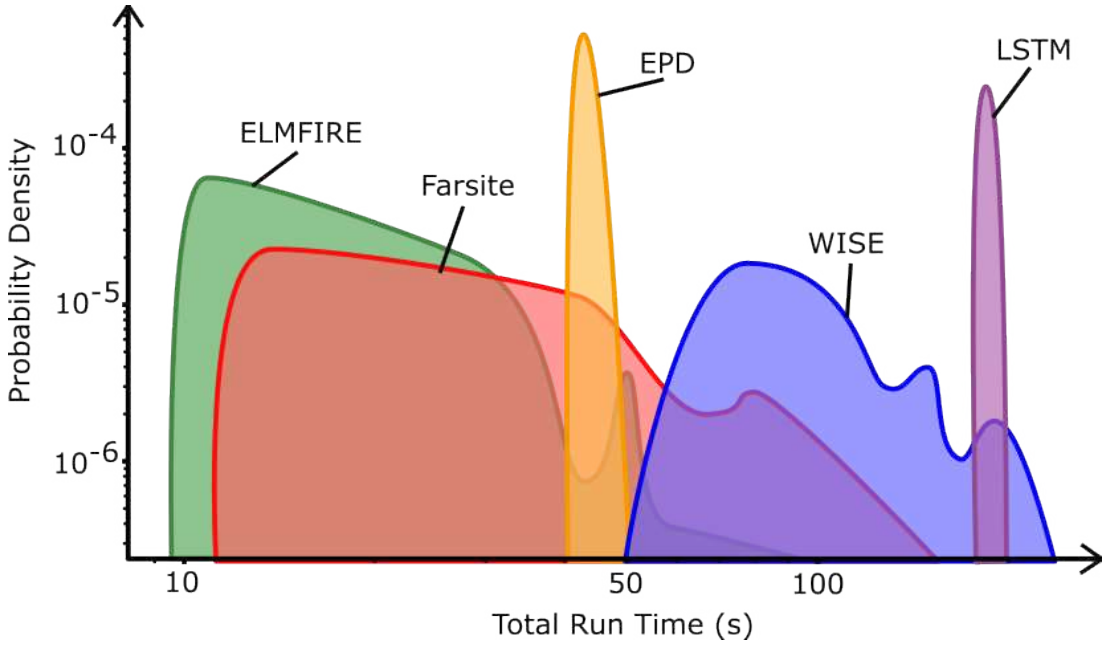


Figure 6.4: The distribution of times taken per iteration for each model to compute the fire spread through the Fort McMurray area. Each model was ran for enough time for the simulated wildfire to reach the Fort McMurray area from the boundaries of the landscape. The Machine Learning models (EPD and LSTM) are very consistent in the time taken for computation, while Farsite, WISE and ELMFIRE are very variable as their calculations directly relate to the size and complexity of the predicted wildfire fronts. FDS is not included in this plot, as all simulations were run in a separate HPC system, and ran for 30 minutes consistently. The PC used for the simulations is a Core i7-11850H system, with no GPU acceleration used.

The total time taken for the models to finish computing shows how the Machine Learning models are less variable than the others. Farsite and WISE require discretizations of the wildfire front to calculate propagation. As such, their total runtime depends on the simulation duration, and the size and complexity of the wildfire front. They also have a wide range of options to make the simulations coarser, decreasing run times. ELMFIRE and FDS does not require extensive discretizations based on the fire front, since they models propagation by solving a differential equation. FDS still requires discretisation in 3D. This means ELMFIRE can be very fast irrespective of the extent of the fire front, and with limited effect from the simulation duration. EPD and LSTM do not rely on the extent of the wildfire, but model the fire spread in discrete

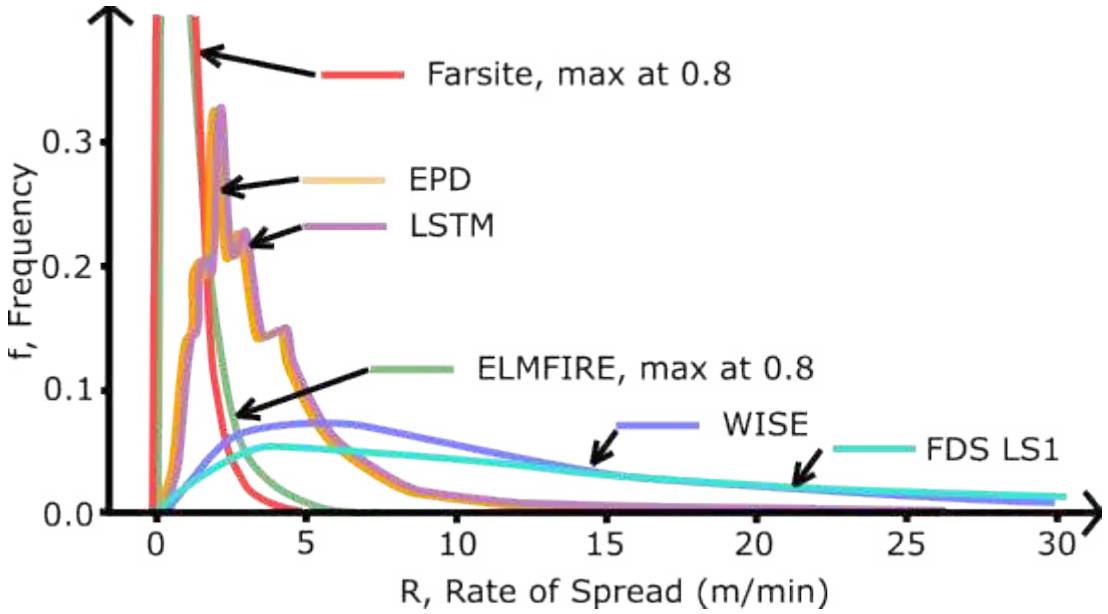


Figure 6.5: A distribution of the rates of spread of the wildfire through the Fort McMurray area, as predicted by each model. Some of the models, like ELMFIRE and Farsite predict drastically slower fire spread, while models like WISE predict faster and more uncertain wildfire spread. FDS predicts very variable rates of spread. In the real wildfire, at its fastest phase, the wildfire spread with a 3-hour average of 29 m/min [130]. The same report highlights how the Canadian FBP system predicted wildfire spread and speeds comparable to the ones that occurred.

time steps. As such, EPD and LSTM are almost linearly related to the simulation time. At the same time, the total extent of the domain has an effect on all the model run times. Larger landscapes will require more resources and more time to compute for Farsite, WISE, FDS and ELMFIRE. For EPD and LSTM, larger landscapes require downsizing in space and up-sizing in time, meaning that larger landscapes result in faster computation. The above analysis explains why, unexpectedly in this case, the LSTM machine learning model is on average the slowest model in this study. In cases with low wind, the generated fire fronts are small and simple, and are solved quickly in Farsite, ELMFIRE and WISE. The machine learning models are linearly related to the simulation time, while the other models have much more complex relationships between run time and simulation parameters. It is expected that, in other simulation setups with different simulation durations, landscape sizes and resolution parameters, the computation rumtime results will vary.

Starting with Farsite, as shown in Fig. 6.5, the simulated wildfires were of very low rates of spread, with an average value of 1.04 m/min. This is primarily because of the existence of the canopy impacting the local wind velocity estimation, therefore on average decreasing rates of spread in canopied areas. Farsite downscales the wind, taken from the weather input data, first to account for the atmospheric boundary layer, and then to account for the canopy. This two-fold reduction drastically reduces the mid-flame wind speed, and thus the fire rate of spread. The wildfire duration was set to 500 h, to allow enough time for the wildfire to spread to the

community. The resolution of the simulated wildfire front had to be increased to 400 m, to ensure the simulations are finished in an acceptable time of approximately 3 min per iteration, compared to 15 minutes per iteration with a 200 m resolution. The resolution increase did not affect the predicted rate of spread. Additionally, with the finer resolution the simulation would never finish, possibly due to a computational bug, forever readjusting the discretisation of the fire front. The bug has been reported to the developers.

WISE, a model primarily implemented in Canadian regions, was expected to be the most easily applicable model, since the case study in question is a Canadian region, and the original data was formatted for the Canadian fire behavior prediction system. WISE predicted faster wildfire spread compared to Farsite, because it did not scale the wind down twice. The majority of the vegetation around the Fort McMurray area is Boreal Forests, so this effect is significantly pronounced. The faster wildfire spread, with an average value of 12.3 m/min, resulted in a reduced required simulation time of 50 h. The faster average rate of spread is also influenced significantly by the difference in the Canadian fuel classification system and the US fuel systems. In comparing fuels of the two systems, like in Figure 6.2, it is apparent that the Canadian system has significantly higher rates of spread at low midflame windspeeds. With an average wind magnitude of 11 km/h, the Canadian system is predicted to yield faster wildfire spread. The reduced simulation time was offset by the slow overall running time of WISE. It required significant time to complete an iteration, placing a strain on the computational system.

ELMFIRE predicted similar rates of spread to Farsite, with an average of 1.2 m/min. It is unknown whether ELMFIRE also scales the wind down based on the canopy characteristics, although the results do seem to suggest this. ELMFIRE was also ran for 500 simulated hours, although it finished each iteration much faster than Farsite, due to it using the level set method requiring little discretisation.

The Google models, EPD and LSTM, have the fundamental limitation that they can only output wildfire isochrones. The location of the fire front at specific time intervals can only be known, and interpolation is needed to get rate of spread. This limits the accuracy of the rate of spread data derived from the machine learning models, but they can nonetheless be used to calculate trigger boundaries. Their average rate of spread was 4.8 m/min for the two models, much higher than Farsite even if they were trained from it. This large discrepancy cannot be explained immediately, but it is possible that during training one of the wind scaling factors was not used, most likely the tree canopy scaling. The increased rate of spread means that simulations run for a simulated time of 200 hours.

FDS can only output the arrival time of the fire, which has to be converted to rate of spread with the method discussed in the Fort McMurray Case Study section. The resulting rate of spread of the fire is very variable, as can be seen in Figure 6.5. This variability means that a large number of simulations are required to generate a converged probabilistic trigger boundary. A total of

288 iterations were solved in an HPC system, which was enough for the rest of the models to converge. This number proved insufficient for FDS, with a final convergence of 10%, much higher than the set criterion of 1%. It is estimated that more than 600 simulations would be needed for convergence. This is why FDS does not appear in the final trigger boundary results in Figures 6.7 and 6.8, but does appear in Figure 6.5. Since FDS cannot be used dynamically like the other models, as it must be used in an HPC system to make its long run times viable, approximately 1000 to 2000 FDS simulations must be pre-generated and solved.

Ultimately, the models that predict slower wildfires are expected to produce smaller and possibly sparser trigger boundaries, and WISE, FDS LS1 and FDS LS4 are predicted to create the widest trigger boundaries. The isolated boundaries of each model are shown in Fig. 6.7 for the 1300 min WRSET case and in figure 6.8 for the 900 min WRSET case, with spurious cases excluded [45]. Each probabilistic trigger boundary on its own could be used with the justification that it was made with a state-of-the-art wildfire model and input data from governmental sources or peer reviewed literature. Comparing the trigger boundaries shows the importance of choosing which wildfire spread model to apply, as different models with the same inputs can yield different results.

In past work on probabilistic trigger boundaries [45], the wildfire spread models used would yield rate of spread results for the entire landscape. Instead of modeling wildfire spread from a point source, these models predict the wildfire rate of spread for the entire landscape, for a specific set of weather conditions [105]. This meant that every generated trigger boundary, that made up the probabilistic trigger boundary, contained the entire community within it. As such, the evacuation safety factor could be directly related to the probabilistic trigger boundary.

In this paper, wildfire spread models are used, simulating fire spread from a point source. The transient simulated wildfire spreads from a point source towards the community, and the simulation may stop when the wildfire has arrived to, but not engulfed, the community. The resulting trigger boundary will cover a part of the community, but not surround it, similar to the results for the UK case study of [47]. The overall probabilistic trigger boundary cannot be directly used to quantify the evacuation safety factor. A series of mathematical conversions and adjustments can be used to make the probabilistic trigger boundaries equivalent to the evacuation safety factor. An illustration of the adjustment process is shown in Figure 6.6. This is not a new methodology, but a small conversion process that does not alter the results but converts them to an analogue of evacuation safety factor, similar to previous work [45].

Let T_k represent the probabilistic trigger boundary generated by model k. Then we propose that the set of nonzero t_{ij} values, representing all the points within the trigger boundary for a model k, L_k, can be fitted to a lognormal distribution, as in Equation 6.4. Experimentation supports this proposal.

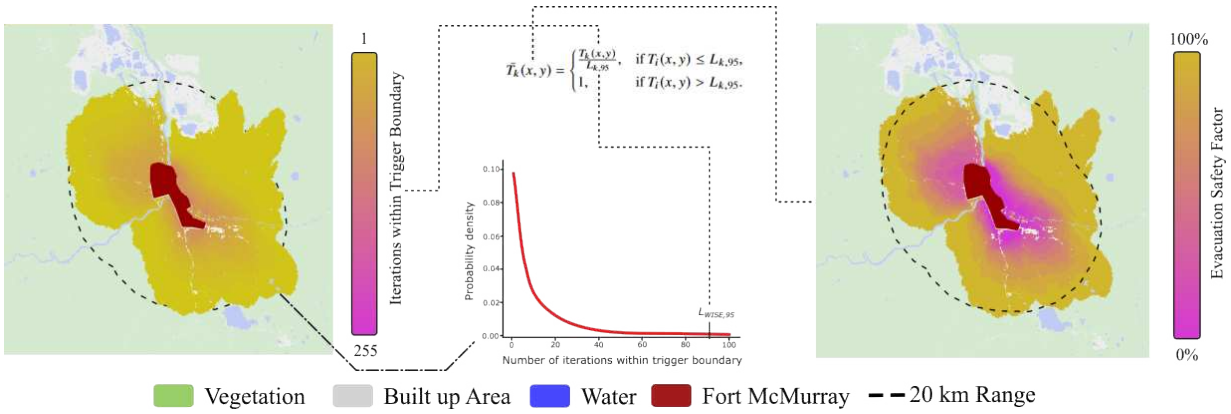


Figure 6.6: A graphical representation of the normalisation process of a trigger boundary. In this example, the WISE model is used with an WRSET of 900 min. The trigger boundary, as calculated by k-PERIL, is shown on the right. The lognormal distribution of the values within the trigger boundary is then plotted in the middle to find the 95th percentile. The normalised result is shown in the right.

$$
\begin{aligned}
&T_k \in {\mathbb{R}_+}^{m \times n}, \\
&L_k = \{\, t_{ij} \in T_k \mid t_{ij} \neq 0 \}, \\
&t_{ij} \approx \mathrm{Log}\,\mathcal{N}(\mu, \sigma^2) \quad \text{for each } t_{ij} \in L_k
\end{aligned}
\tag{6.4}
$$

Thus, we estimate the parameters μ_i and σ_i from L_k to obtain the lognormal fit. L_i can be used to find the new value representing an evacuation safety factor of 1, by finding the 95th percentile of L_n, $L_{n,95}$, as shown in Equation 6.5. Here, 1.645 corresponds to the zeta value of the 95% percentile of a normal distribution.

$$
L_{k,95} = \exp(\mu_k + 1.645\sigma_k) \tag{6.5}
$$

Then $L_{k,95}$ can be used to normalize the probabilistic trigger boundary, as in Equation 6.6, and enable it to be a proxy of the evacuation safety factor.

$$
\bar{T_k}(x,y) = \begin{cases} \frac{T_k(x,y)}{L_{k,95}}, & \text{if } T_i(x,y) \leq L_{k,95}, \\ 1, & \text{if } T_i(x,y) > L_{k,95}. \end{cases} \tag{6.6}
$$

By the end of this process, $T_{k,95}$ has regained the functionality of the evacuation safety factor, with values of 1 representing a near certain chance of dire evacuation.

The results for the 1300 min WRSET are shown in Figure 6.7 and the 900 min results are shown in Figure 6.8.

Finally, the separate trigger boundaries of each model can be combined to an overall proba-

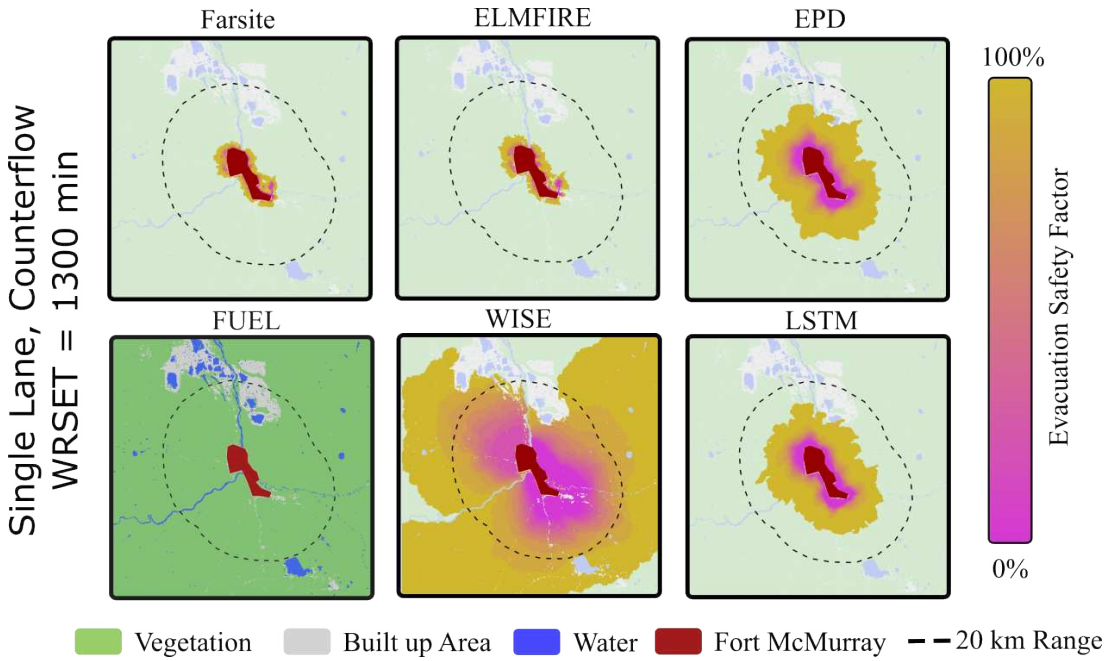


Figure 6.7: The probabilistic trigger boundaries of the Fort McMurray area, generated by each model, for an average WRSET of 1300 min (single route evacuation). Also plotted is the 20km distance from the community line in black. The different models create significantly different trigger boundary and have a critical effect on the perceived safety of the area. WISE calculates a trigger boundary that goes beyond the 50 x 50 km range of the simulated landscape.

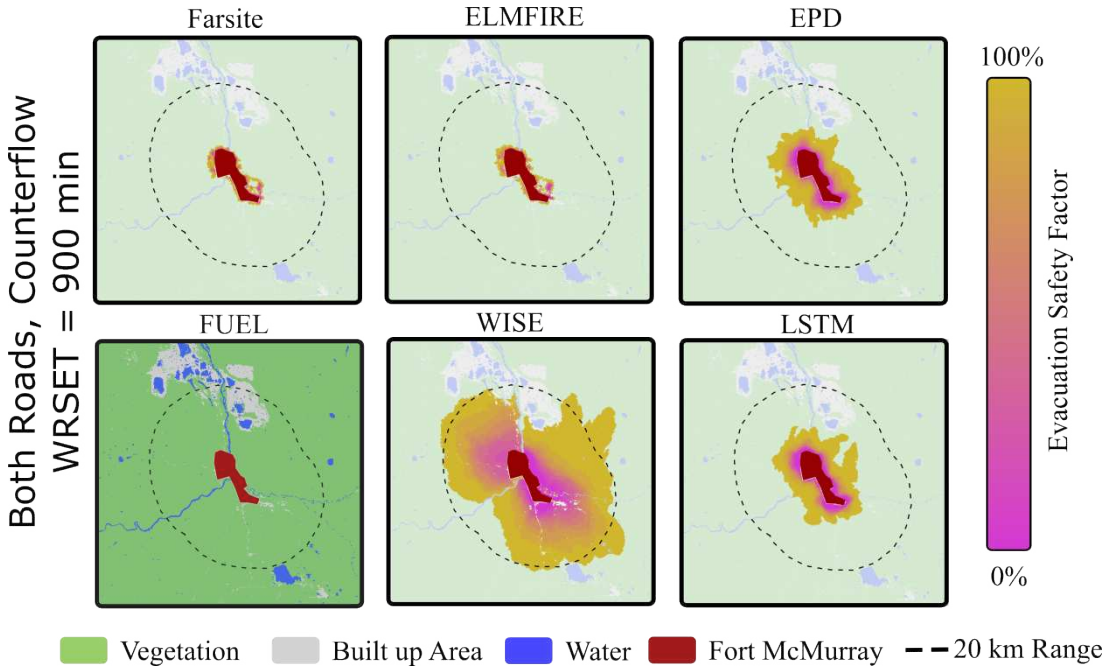


Figure 6.8: The probabilistic trigger boundaries of the Fort McMurray area, generated by each model, for an average WRSET of 900 min (north and south route evacuation). Also plotted is the 20km distance from the community line in black. The different models create significantly different trigger boundary and have a critical effect on the perceived safety of the area. WISE is the only model that suggests that the Fort McMurray area is a high risk community.

bilistic trigger boundary, T, taking into account the results of all the models. The probabilistic trigger boundaries are summed up, in Equation 6.7, and then taken through the conversion process in Equations 6.5, 6.6. This ensures that the ensemble probabilistic trigger boundary retains its ability to function as an estimate of evacuation safety factor. The resulting trigger boundaries are shown in Figure 6.9 and Figure 6.10.

$$T = \sum_{k=1}^{k} \bar{T}_k \tag{6.7}$$

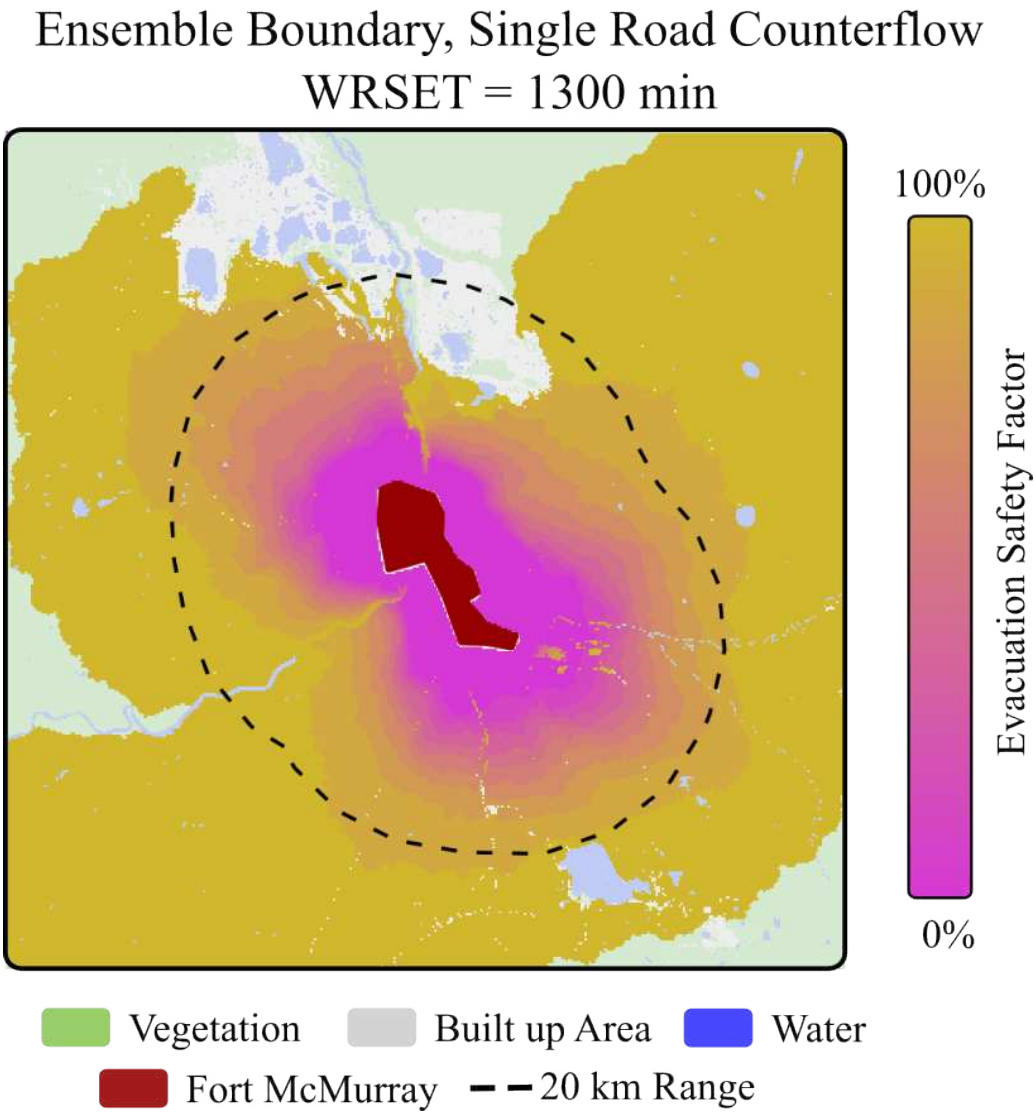


Figure 6.9: The final probabilistic trigger boundary for the WRSET of 1324 min case, generated via ensemble modelling. All models contribute to this final boundary, providing a thorough assessment of the safety of the community.

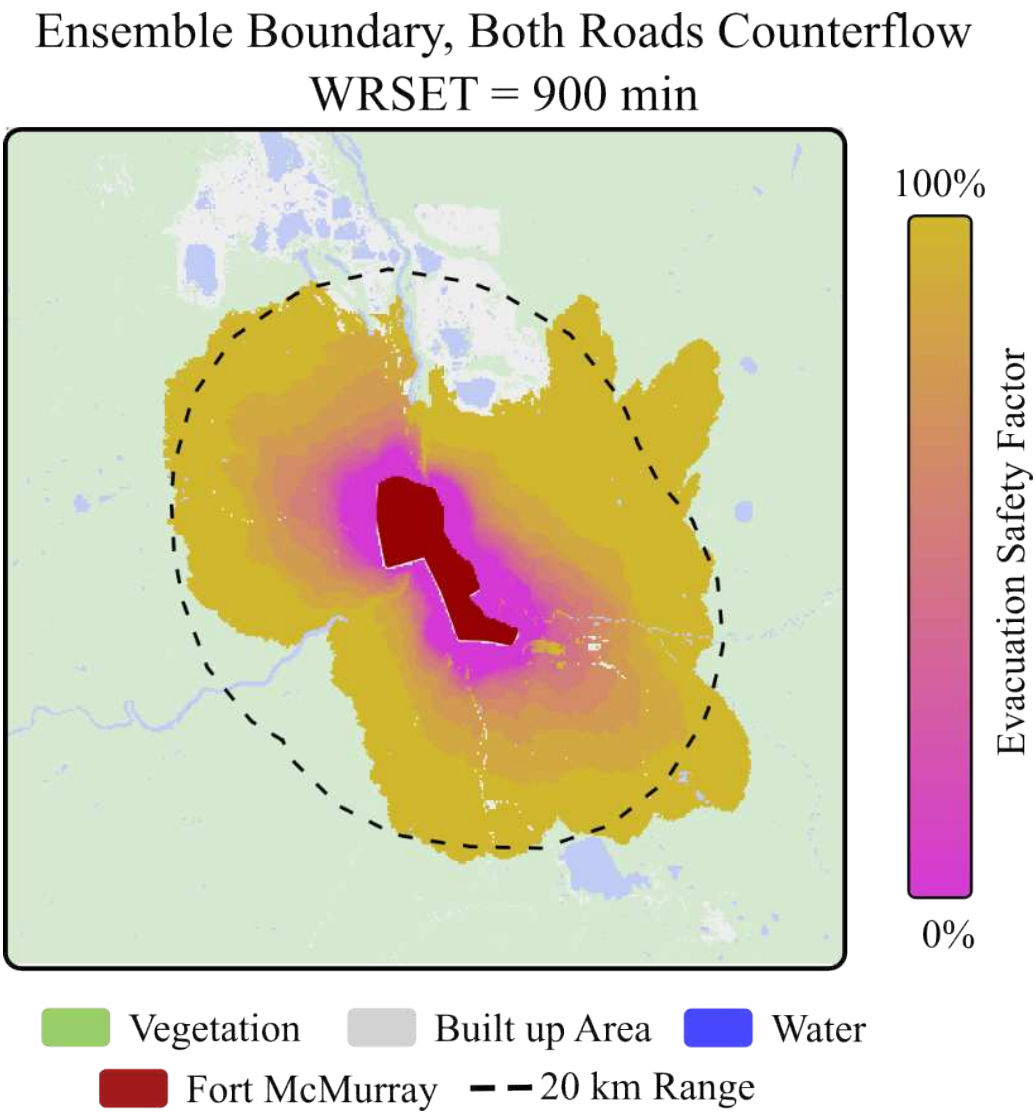


Figure 6.10: The final probabilistic trigger boundary for the WRSET of 900 min case, generated via ensemble modelling. All models contribute to this final boundary, providing a thorough assessment of the safety of the community.

6.5 Discussion

The 20km range in Figures 6.7, 6.8, 6.9 and 6.10 was added to illustrate the maximum range that the smoke plume's location can be observed visually. Typical fire lookout tower effective detection distances range from 10 to 20 km, depending on the ambient conditions and surrounding environment [131], [132]. Taking the 20 km range as a guideline, it can be expected that any given community will be able to detect a wildfire and initiate an appropriate response, when the wildfire is within 20km. This applies whether there are fire lookout towers surrounding the community, or whether the community itself acts as a lookout.

Simulating probabilistic trigger boundaries that extend more than 20km in radius require extensive landscapes for their simulation, and equally extensive simulation times. We argue that

such trigger boundaries are of limited use, as they will extend beyond a community's immediate detection range. While detection methods may exist that extend beyond the community, their availability cannot be guaranteed and cannot be taken as a certainty. We pose that communities whose trigger boundaries extend outside the 20km range are considered high-risk communities. If the trigger boundary is more than 20km away from the community, its value is greatly diminished. Such large trigger boundaries indicate that the evacuation is so slow compared to the relative rate of spread of the wildfire (High WRSET / Low WASET) that it is a high risk community and trigger boundaries are not going to help. In such cases, any wildfire that is detected by the community must immediately lead to an evacuation. The emphasis of such communities, like Fort McMurray, must be in decreasing their WRSET.

Fort McMurray requires extensive works to improve their wildfire resilience regarding their evacuation capabilities in case of wildfire. As is right now, any wildfire spotted by the Fort McMurray community, with wind driving the fire towards it, will immediately be inside its trigger boundaries, and any evacuation attempt will be dire, as was the case in the real wildfire of 2016. This can be achieved either by increasing the potential WASET, controlled by the average rate of spread of the wildfire, and by decreasing the potential WRSET, controlled by the evacuation process. The Fort McMurray community and its greater area should adopt schemes to decrease the potential speed of the wildfire, by implementing fuel control measures such as prescribed burning or manual forest thinning. The opening of fire breaks, either specifically to stop wildfires or as a bonus effect in trail-making and road-building works are imperative to limit the potential egress routes and speeds of any potential wildfire.

The Fort McMurray community should also improve upon its evacuation capabilities to decrease its overall required evacuation time. The most direct yet costly way to do so would be by opening new roads into and out of the community. The current community has a northward and a southward road, with the northward road ending in the nearby oil sand fields. An additional road would improve the road network capacity and the redundancy of existing evacuation routes. The remoteness of the Fort McMurray community makes such a measure unfeasible due to cost, and due to the lack of potential destinations to make such road building works fiscally responsible. Alternative, yet equally effective and important, measures to reduce the WRSET of the community is to design and institute wildfire shelter locations within the community. Popular areas like schools, community centres, gyms and pools can be designed as wildfire shelters, allowing part of the population to reach a safe place without requiring to fully exit the community. Such shelters require careful planning and design against wildfire damage, extensive maintenance works of both the building itself and the provisions within, and advertising to the local community to raise awareness of the capability of such institutions to provide shelter. The ideal solution, along with measures to increase WASET and make incident wildfires manageable, is to ensure that homes are designed with external wildfire attacks in mind. While fire safety of homes currently account for internal fires and compartment-based fire growth, it should be

expanded to external flaming damage, from convection, radiation, and firebrands. Designing wildfire-resistant homes would allow some part of the population to safely shelter in place (as long as relevant provisions are also procured), reducing the load on the road network for people that decide to evacuate. Ultimately, Fort McMurray should adopt a multifaceted approach to their wildfire safety, employing both WASET and WRSET oriented measures, to reduce their danger to wildfires and stop them from becoming high-risk communities. The Fort McMurray should equally increase its detection range to allow for more time for an evacuation to occur. This would make the effective trigger boundary radius larger, though should be used as a fast-acting temporary solution rather than a permanent fix.

In the case of high-risk communities, detailed probabilistic trigger boundaries may be unnecessary compared to a simple and robust trigger boundary calculation. A trigger boundary may be too vast for the finer details of a computed probabilistic trigger boundary to be discernible, especially if they fall outside the 20km range from the community. At the same time, a large trigger boundary calls for a large computational domain, increasing the total computation time exponentially.

The perceived safety of the community of Fort McMurray can be interpreted differently depending on the wildfire model used. In the case that only a single road is used for the evacuation, the ensemble trigger boundary is so large that it extends beyond the 50 x 50 km landscape that was used in the simulations. Rerunning the trigger boundary calculation for a larger area would be computationally intensive, and the conclusion (that the Fort McMurray community is high-risk) would not change.

This raises the question of whether a criterion exists, for high risk communities, to dictate if computed probabilistic trigger boundaries are appropriate, or if the covered distance is too great to be applicable. This criterion relies on the typical distance that a wildfire can be spotted from, and an actionable order can be issued. As such, the criterion in Equation 6.8 can be used to select between using a simplified trigger boundary or a computed probabilistic trigger boundary, where $WRSET_{80}$ is the 80th percentile WRSET value, ROS_{80} is the 80th percentile ROS value, and R_{TB} is the estimated radius of the theoretical trigger boundary. The calculation, following from experimentation using the results of the trigger boundaries of Fort McMurray, is based on the 80th worst WASET and ROS values, based on a statistical evacuation study and a small number of wildfire spread studies. The probabilistic ROS can be obtained by considering the overall ROS across the community. The 80th percentile was chosen based on experimental observations of this case of Fort McMurray, matching the outermost areas of the probabilistic trigger boundaries with little over- or underestimation.

$$WRSET_{80} \cdot ROS_{80} = R_{TB} \tag{6.8}$$

The 20 km range from the center of Fort McMurray has been overlayed in Figures 6.7,6.8,6.9 and 6.10. Following Equation 6.8, Farsite, Prometheus, EPD and LSTM suggest a computer probabilistic trigger boundary for both evacuation scenarios. WISE and FDS suggest that Fort McMurray is a high-risk community, with theoretical trigger boundaries most appropriate.

The impact of model choice on perceived community safety is most evident when comparing the generated trigger boundaries. Some of the models suggest that a probabilistic trigger boundary is an effective and actionable tool for the Fort McMurray area. Other models suggest that the trigger boundaries are so far away from the community that any detected wildfire may result in a dire evacuation. On their own, Farsite and ELMFIRE generate a compact trigger boundary, reflective of their slow and consistent predicted rate of spread. EPD and LSTM predict more extensive and variable trigger boundaries, while WISE predicts extensive trigger boundaries. Combining the results of all models through ensemble modelling, the overall probabilistic trigger boundary combines the aspects of all the models, spanning the largest trigger boundary while showing the variability of the perceived wildfire behavior.

This is a clear illustration why ensemble modeling is critical in wildfire safety quantification. With different models yielding drastically different interpretations of the safety of the area, a multitude of models needs to be consulted for a confident outcome to arise. Understanding the differences in each model, and why those differences may come about, is required to understand the potential fire behavior of an area.

6.6 Conclusion

This chapter shows the effect of wildfire spread model choice on the calculated probabilistic trigger boundaries. The different models yielded significantly different times to start an evacuation for Fort McMurray, the case study selected for this paper. Models like Farsite and ELMFIRE predict slow wildfire spreads of 2 to 3 m/min. The EPD and LSTM machine learning models predict rates of spread of 4.8 m/min. All the predictions of rate of spread, except for WISE and FDS, are much slower than the real value of 29 m/min, though it should be noted that this speed occured in extreme conditions. WISE predicts very fast wildfire spread in the order of 20 m/min. FDS estimates very variable rate of spread values, and requires a large number of simulations for convergence. The differences in expected wildfire spreads and estimated trigger boundary extents show the critical importance of the wildfire model selected to estimate the danger a wildfire may pose to a community. While each model individually would give one set of results, an ensemble methodology shows that the potential wildfire dynamics require further study.

Ensemble modelling, combining different wildfire models and probabilistic trigger boundaries, is

a critical step in producing robust and reliable evacuation plans. The ensemble trigger boundaries of the Fort McMurray area take into account the results of all the models and all the simulation results, thus removing the limitations of the individual models, in terms of their assumptions and constraints. The increased computation time is a result of the increased complexity, but advances in computation, such as parallelisation and simultaneous model execution, can eliminate this added computational time.

Considering the vast extent of the trigger boundaries created by FDS and WISE, a criterion was created to estimate when a detailed, computed probabilistic trigger boundary is necessary, and when a simple estimated trigger boundary is appropriate. With larger trigger boundary diameters, their direct computation becomes exponentially more difficult, while their applicability diminishes. Ultimately more work is needed on ensemble wildfire modelling to estimate the wildfire safety in a community, before any trigger boundaries and evacuation plans can be made reliable and actionable.

Chapter 7

Model of Gaussian Smoke Dispersion near the Ground

One of the mechanisms that leads to complications in the evacuation process, ranging from delays to fatalities, is smoke transport. Wildfires produce large amount of gaseous products such as CO_2, CO, and various Particulate Matter (PM) particles [133]. While much of this smoke is thermally buoyant and rises up the atmosphere and away from the path of the evacuees, some of the smoke stays close to the ground and affects the people on the path of the fire. The difference between the buoyant, "hot" smoke and the lingering "cold" smoke comes from the different phases of a wildfire front. The wildfire front will first burn a part of the vegetation in a flaming process, where visible flames can be seen, and will then burn the rest of the vegetation in residual burning, producing more toxic products of incomplete combustion [19]. The total concentration of these products near the terrain surface will then influence residents in communities downwind of the wildfire, either by reducing the evacuees' visibility and forcing them to reduce their evacuation speed, making evacuation impossible for people with respiratory issues, or forcing the evacuation of communities at no risk of wildfire impingement but overwhelmed with smoke. An example of low-lingering smoke and the effect it has on evacuees is shown in Fig. 7.1. Ultimately the concentration of the smoke may be so severe that it has an incapacitative effect on evacuees.

In a wildfire, the flaming and smoldering parts create a buoyant plume of smoke, where the hot gases are driven upwards and then along the wind. Depending on the strength of this buoyant plume, the strength of the wind, and the mixing of the smoke in the atmosphere, the smoke will impact people and communities far away from the wildfire, as was seen in New York during the 2023 Canadian wildfires [134]. The smoke can also impact communities near the wildfire, placing evacuees in great danger. Smoke can impact the speed of the evacuation, and possibly make evacuation unattainable, placing people at great risk of wildfire entrapment [112].

Computational models exist that can calculate the movement of smoke generated by a wildfire along a landscape. Such models, coupled with the wind and atmosphere, are used to study smoke far away from the source, and help emergency responders issue relevant guidance for sensitive groups [135]. Depending on the available data, timeframes and computational resources, these models can be of varying accuracy and fidelity. To simulate the effect of smoke near the fire, for the purposes of quantifying the effects of smoke on communities downwind of the fire, no wildfire smoke model exists that can run in a time scale comparable to that of operational wildfire models, and is maintained to this day.

This chapter presents a novel smoke spread model, Galini, based on the Gaussian smoke dispersion model.[1] Galini can model the effects of terrain downwind from the fire source, for a spatially and temporally evolving wildfire. The model has been designed in such a way that the required inputs of the model are either required or generated by wildfire spread models, meaning Galini can be directly integrated to models such as Farsite, Prometheus, or ELMFIRE. The following sections of the chapter will describe the existing literature on smoke modelling, and all the aspects of Galini. A series of test cases will then be presented to illustrate the capabilities of Galini.

7.1 Smoke Modelling

Various methods exist to estimate the spatial and temporal propagation of smoke from a wildfire. All of these models achieve a balance between complexity and computational requirements [135], and are shown graphically in Fig. 7.2. Box models assume that all the fire products, in steady state, are distributed evenly inside a box, representing a specific volume of air. Inside this box, the products of combustion of the wildfire are assumed to be perfectly mixed [9].

[1]This chapter is based on the following submitted publication: N. Kalogeropoulos, A. Castagna, and G. Rein, "A Gaussian Dispersion Model for Haze Spread with Downwind Terrain Effects," in *Submitted to the International Symposium of Fire and Explosion Hazards (ISFEH 11)*, Rome, Italy, 2025



Figure 7.1: Left: Example of wildfire smoke staying close to the ground, potentially causing issues for downwind evacuees. Photograph Copyright Mark Thiessen, Nat Geo Image Collection. Right: Vehicles driving through a wildfire-stricken area. Photograph Liny Lamberink, CBC

Gaussian dispersion models originate in the study of industrial smoke-stacks, to estimate the flow of products downstream of their accompanying factories. Their mathematical formulation is based on a solution of the Navier-Stokes equations, where the resulting diffusion terms are solved using the assumptions that the smoke products spread via a normal (or Gaussian) distribution [136]. Langrangian or Puff Particles, represent smoke generation through the injection of small parcels of smoke in the landscape. These parcels of smoke are then free to move in the flow-field of the landscape, and diffuse or expand along this path. Computational fluid dynamics solvers, that can implicitly solve the wildfire plume and atmospheric boundary layer, and model the terrain effects on the wind. They are the most accurate smoke models, with some able to also model the evolving chemistry of the smoke particles [137].

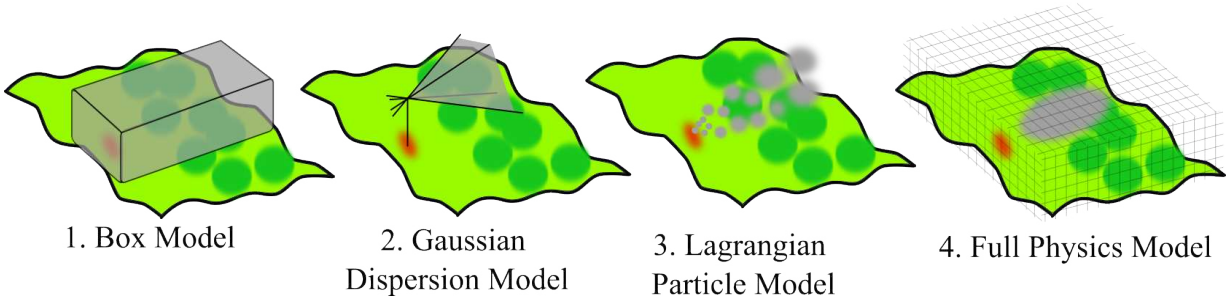


Figure 7.2: An illustration of the four main types of wildland fire smoke models, with increasing accuracy and computational cost.

One consideration of smoke movement is the difference between flaming and smouldering combustion. As a fire front propagates, each point in the landscape progresses through a simplified timeline of drying, ignition, flaming combustion, smouldering combustion, and extinction. Smoke and haze, both describing products of combustion, are generated during the flaming and smouldering phases respectively. In general, smoke refers to the buoyant products of combustion, and haze refers to low-hanging, widely dispersed particulate matter [138]. Smouldering combustion products are most associated with haze, create a low-altitude plume, cause the most harm and are produced for much longer than flaming combustion products [19]. We want to incorporate the differences between these two kinds of smoke. Another important factor is the effect of atmospheric stability. "Unstable" atmospheres promoting atmospheric mixing and "stable atmospheres" restricting mixing. Stable atmospheres result in a smaller plume with higher concentrations, and unstable atmospheres result in wider, more dilute plumes [9].

7.2 The Gaussian Dispersion Model

Galini is based on the Gaussian dispersion model. It originates as a solution to the Navier-Stokes time-averaged mass transport equation. Additional terms can be included in the formulation to account for various effects. One such critical effect, important when estimating ground level

concentration, is the reflectance of the smoke that would be modelled below the ground. The Gaussian dispersion model, as a direct solution to the Navier Stokes Equations, cannot account for smoke reaching the ground and increasing the ground smoke concentration. A reflectance term is thus added to model the smoke being "reflected" off the ground, assuming the fire and smoke spread occur on a flat plane [135]. Other effects can be included, such as an equivalent "reflection" because of the atmospheric inversion layer, important for complex landscapes with peaks and valleys, but these effects do not take effect for low-altitude solutions. The complete Gaussian dispersion model with ground reflectance is given in Eq. 7.1 [135].

$$\overline{c}\,(x,y,z) = \frac{\dot{m}}{2\pi\overline{u}\sigma_y\sigma_z}\exp\left(-\frac{y^2}{2\sigma_y^2}\right)\left[\exp\left(-\frac{(z-z_0)^2}{2\sigma_z^2}\right)+\exp\left(-\frac{(z+z_0)^2}{2\sigma_z^2}\right)\right] \tag{7.1}$$

Here, x_0, y_0, and z_0 are the coordinates of the origin of the plume, $\dot{m}$ is the mass flowrate of the smoke being injected into the domain, $\overline{c}$ is the species concentration, $\overline{u}$ the velocity vector field, and σ_y and σ_z are the Pasquil-Gifford (or dispersion) coefficients (which have been thoroughly defined in literature) [135], and are functions of the downwind distance x. A graphical representation of the results is shown in Fig. 7.3. This solution applies to point sources with no thermal buoyancy, meaning the smoke lift from the ground is not calculated. It is instead modelled by calculating a steady-state smoke height far from the smoke source, and then injecting the smoke from that height. This is referred to as the injection height z_0, and is a critical value when estimating the ground-level smoke concentration.

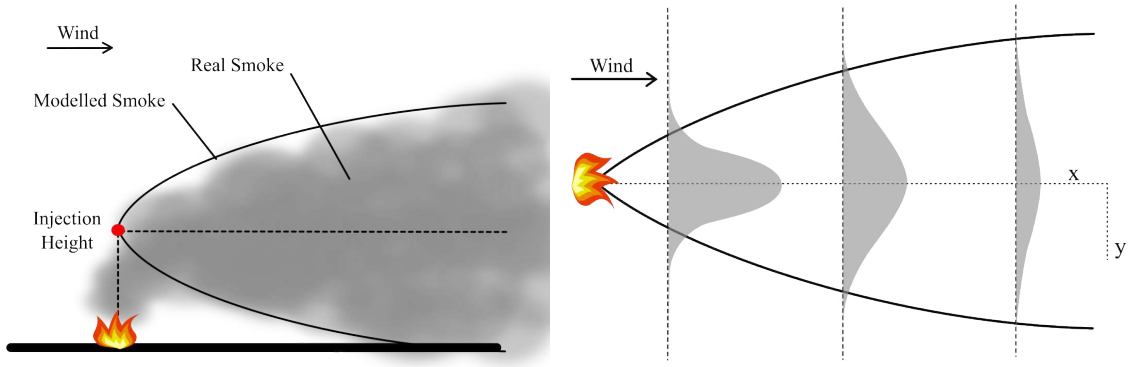


Figure 7.3: Left: A side-on schematic of the Gaussian Dispersion plume, with the steady state height of the real smoke and the corresponding injection height of the modelled smoke illustrated. Right: A top-down illustration of the Gaussian Dispersion plume. At each point downwind of a fire, the concentration of the smoke plume can be described as the superposition of a normal / Gaussian distribution in the y and z planes.

7.3 Galini Model

The smoke model developed in this chapter is the Galini model, named after one of the streets that was impacted by the 2018 Mati fire. Galini is made to model the ground-level concentration of smoke over a landscape. It models the injection of smoke from the fire as a collection of point-sources of the landscape, to model the width and spread of the wildfire front (both flaming and smouldering). Galini is based on the Gaussian Dispersion modelling methodology and employs several sub-models to calculate the relevant required parameters. These sub-models will be discussed in the following sections.

As Galini is designed to be used when communities are in the path of a wildfire, an important property to have is easy interoperability with wildfire models. Ideally all the data required by Galini are available as inputs or outputs of a wildfire model. While some parameters need to be set (see following sections), all the input parameters required by the model are based on the input and output parameters of the Farsite wildfire model. Farsite was chosen as it is the main model used in the WUI-NITY project, which this work is a part of [27], [38].

7.3.1 The Source Term

The most common species in wildfire smoke are CO_2, CO, H_2O, unburned hydrocarbons $PM10$ and $PM2.5$ [9]. The last two species are families of combustion products, each representing complex carbon-based pyrolysates, particles of characteristic diameter less than $10\mu m$ and $2.5\mu m$ respectively. They are very relevant to the smoke's health and visibility effects. As such, Galini solves for the smoke visibility via the $PM10$ and $PM2.5$ concentration downwind from the flame source.

The mass flow rate of the injected species is then found via a submodel that calculates the total emissions of different species per acre of different vegetation types, and their total smouldering and flaming times. The model used is SpatialFOFEM, a spatially-inhomogeneous variant of FOFEM, the First Order Fire Effects Model [139]. It uses the FCCS (Fuel Characteristics Classification Scheme) fuel modelling system [140] to classify and quantify different vegetation types into standard fuel models. SpatialFOFEM provides the total flaming and smoldering time, and the total emissions for the duration of the fire in both phases, so the mass flow rate can be found by assuming that the emissions are emitted at a steady rate, and dividing the two values.

While fuel maps made with FCCS fuels do exist alongside fuel maps used in wildfire modelling (most commonly the 40 standard Scott and Burgan fuels), for example in the LANDFIRE database, it might not be the case that the FCCS fuel map will be available for use in this

model. This is especially the case when this model is used in areas outside the US, where vegetation maps relating to wildfire modelling have to be derived from other geographical vegetation mapping products [45]. As such a method to infer a FCCS fuel map from Scott-Burgan (SB) fuel maps was needed to ensure the interoperability of Galini with wildfire models. In a process similar to the process of finding a conversion between the CFFDRS and SB models in Chapter 6, a study was conducted comparing all the points in the LANDFIRE database, on the two classification schemes. The result was a map connecting each SB fuel model to the FCCS fuel model most frequently associated with it. While some fuel models had near-direct replacements, some SB fuel models would coincide with a variety of FCCS fuel models. While this signals that the conversion between the two fuel classification schemes requires additional information, it was deemed sufficient for this model. As such, to use SpatialFOFEM in Galini, the SB fuel map used in the wildfire model is converted to an FCCS fuel map based on a one-to-one mapping scheme. The complete conversion map can be found in Appendix C

7.3.2 Downstream terrain effects

The Gaussian dispersion model cannot account for smoke compaction due to a heterogeneous terrain. The original "reflectance" term can only work in flat terrains, which could be a valid assumption for country-scale simulations but invalid for community-level, near fire simulations. We use the same concept of a virtual source term symmetrically opposite to the elevation and at the same projected location as the original source, shown in Fig. 7.4. The last term of Eq. 7.1 is modified to include the $-2H$ term. The function and origin of the $-2H$ term is derived very similarly to the original formulation of the ground reflectance term. A virtual source is introduced, mirrored about the height H. Any smoke modelled below the ground at height H is thusly re-introduced through the inclusion of the $-2H$ term. This term only applies for the downwind location where the height H is found, any subsequent elevation changes will have a different value for H. The resulting formulation takes the form of Eq. 7.2.

$$\overline{c}\,(x,y,z) = \frac{\dot{m}}{2\pi\overline{u}\sigma_y\sigma_z}\exp\left(-\frac{y^2}{2\sigma_y^2}\right)\left[\exp\left(-\frac{(z-z_0)^2}{2\sigma_z^2}\right)+\exp\left(-\frac{(z+z_0-2H)^2}{2\sigma_z^2}\right)\right] \tag{7.2}$$

where H is the terrain height at the location where the haze concentration is calculated.

For $H > z_0$ the virtual source will be placed at a height larger than the real source, thus leading to a wider distribution of the concentration along the z direction with a maximum occurring above the ground, and at a height closer to the virtual source. Whilst this would still conserve mass, as proven before for any terrain height H and injection height z_0, the results would be unrealistic, especially when compared to visual data. It is hence assumed that for $H \geq z_0$ the

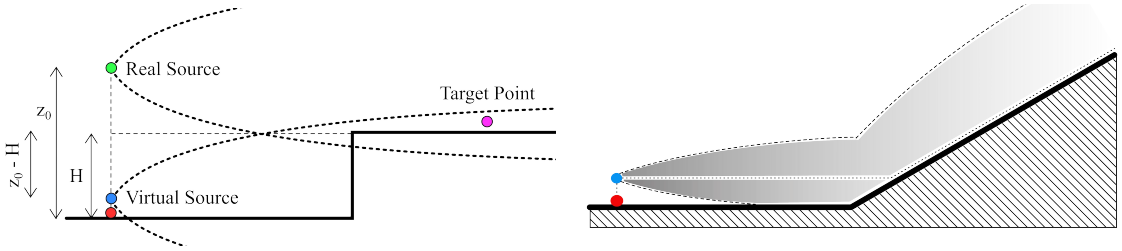


Figure 7.4: Left: The virtual source is modelled as a reflection from the height difference between the source and the target. Right: The effect of an elevation change significantly higher than the injection height and diffusion of the smoke. The centreline of the smoke plume with the virtual source effects is assumed to represent the smoke being pushed up by the terrain.

concentration follows the distribution shown in Fig. 7.4. This assumption is reasonable if one expects the wind to be parallel to the terrain.

7.3.3 Injection Height

Injection height is the most important parameter when calculating the ground-level smoke concentration. It is also one of the most difficult parameters to quantify. The injection height attempts to model the plume rise of the hot gases without solving the physical processes of heat transfer and buoyancy. Various atmospheric phenomena influence the rate of smoke elevation and maximum possible elevation height.

The injection height is an important quantity, and the state of the art is not matured enough to empirically estimate it. Multiple models exist to estimate it, with significantly different results. Galini has tested three models, specifically the Holland Equation [135], [141], the Andersen Energy Balance Equation [142], [143] and the Briggs Plume Rise equation [144]. The Holland equation is a simplified empirical model mainly based on the smoke initial temperature and upward velocity of industrial smoke stacks. The Andersen model is a physical model, considering a parcel of rising hot air, but neglecting turbulent mixing. The Briggs equations are a set of empirically derived regressions that associate the steady state plume heights of real measured wildfires. A comparison of the three models was conducted, to study their predicted injection heights for a flaming frontusing arbitrarily chosen yet typical values for smoke temperature, initial upward velocity, and fireline intensity, among others. The results are shown in Figure 7.5 and are compared with wildfire plume height data from [145]. Of the three equations, the Briggs equations were found to be the best to use in terms of their ease of implementation and their realistic outputs. The Holland equation has a strong correlation to simulation cell size, making it unsuitable for use with coarser meshes. The Andersen equation yields unrealistically high injection height values, beyond the experimental observation range. The Briggs Plume Rise equations was found to be less influenced by the simulation cell size and yields realistic injection height values, consistent with experimental and empirical observations

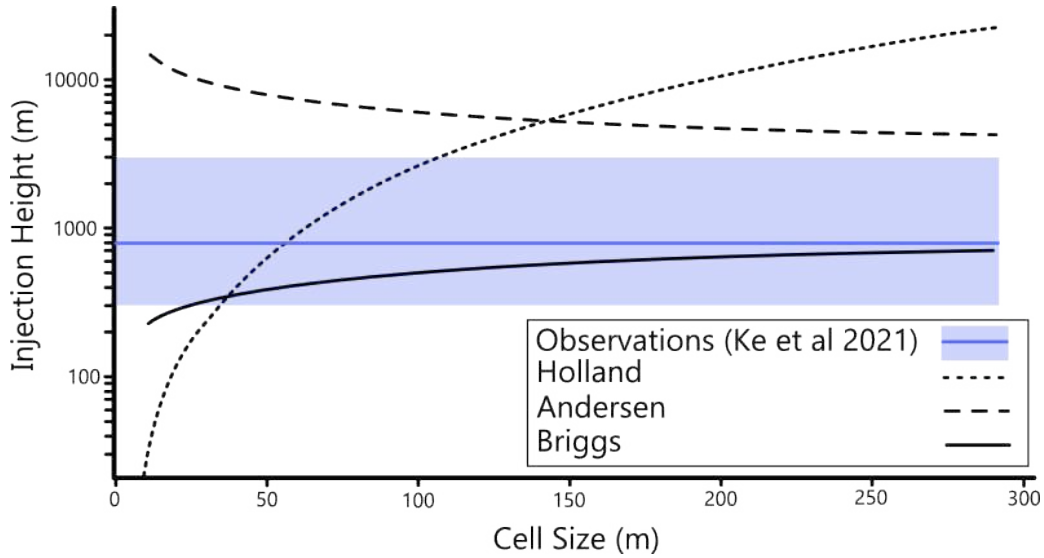


Figure 7.5: A comparison of the predicted injection heights of each model for the flaming front of a wildfire of fireline intensity 10 MW/m^2. Also plotted is the range of observed plume height rise from [145]. The Holland model is strongly influenced by cell size and is thus not suitable for use in Galini. The Andersen and Briggs models both have little change with increasing cell size. The Briggs model predictions lie within the measured plume heights, and has been chosen as the most suitable model.

[9]. The results for a smouldering fire front are also shown in 7.6. The Briggs equation depends on the stability of the atmosphere, the fireline intensity, the ambient temperature, the wind magnitude and a characteristic fire diameter, in this case set equal to the simulation cell size.

The observation by Lavdas is also used [146], whereby 60% of the generated smoke is injected at the injection height, and 40% of the smoke is injected from ground level, to be more accurate compared to experimental measurements. One limitation of the Briggs model is that it requires estimations of the fireline intensity of the flaming and smouldering phases. While it is possible to find this value for the flaming front via the Rothermel model, there is no straightforward method of estimating the smouldering fireline intensity. For now, it is assumed that the smouldering front has 30% of the power of the flaming front, although this value requires more research.

One additional considered effect is the change of wind velocity with height because of the atmospheric boundary layer. Due to the ground roughness and the boundary layer, the wind speed rises with height up to a pseudo-steady state value. The rate of this increase is related to the surface roughness and the atmospheric stability. While the atmospheric stability is calculated in the model, the surface roughness is assumed to be characteristic of a dense forest or built-up area, considering Galini is expected to be used in fires near built up areas. The wind profile equation used in Galini is the Hellmann wind equation [147], recreated in Eq. 7.3, where U_{10} is the 10-m wind speed recorded by a weather station, z is the height above the ground, and α is the Hellmann exponent, which depends on the atmospheric stability (0.27 for unstable atmosphere, 0.34 for neutral and 0.60 for stable).

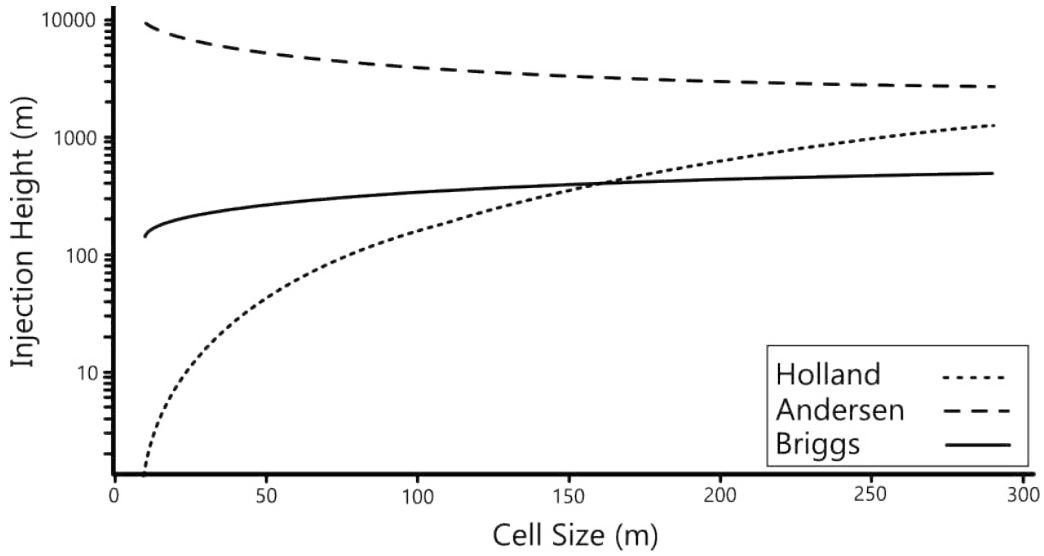


Figure 7.6: A comparison of the predicted injection heights of each model for the smoldering front of a wildfire of fireline intensity 3 MW/m^2 (30% of the flaming front). No data can be found for smouldering fire plume heights. It is a limitation of this decision that only one measurement of steady state plume height could be found. The Briggs model predicts reasonable and consistent values, the Holland model is variable depending on the cell size, and the Andersen model predicts plume heights comparable to the flaming plume values.

$$\overline{u}(z) = U_{10}\left(\frac{H+z}{H+10}\right)^{\alpha} \tag{7.3}$$

This wind speed dependency on elevation requires an iterative solution, as the injection height z_0 changes with the wind speed $\overline{u}$. Such an iterative solution is employed in Galini, by sequentially calculating the injection height, Hellmann-adjusted wind, and the injection height again in a cycle.

7.3.4 Flaming and Smouldering Fronts

Most wildfire smoke models treat wildfires as a point source for smoke, combining the flaming and smouldering products. A single value is assigned for the plume height and injection rates of the wildfires. Some models do spatially resolve the wildfire spread, but still do not differentiate between the flaming and smoldering phases. Galini models flaming and smouldering as two independent wildfire fronts, each with their own plumes, steady state heights, and smoke mass flow rates, and assumes that there is no interaction between the two plumes. An illustration of these two plumes and how they are modelled in Galini is shown in Figure 7.7.

This assumption comes from a fundamental limitation of the literature. The interaction of the flaming and smouldering plumes has not been studied, and no modelling method or accepted convention exists for modelling the two phases separately and simultaneously. The two plumes

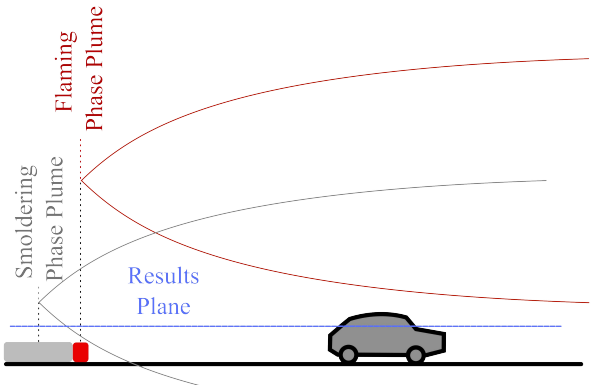


Figure 7.7: An illustration of the smoke simulation of the flaming and smouldering fronts. The smouldering front has a greater effect of ground-level concentration near the fire due to its weaker plume. Also shown is the results of Galini, that display ground-level concentration 1 m off the ground.

are expected to interact to some degree, with some of the smouldering products mixing with the flaming products and rising up the atmosphere. As this interaction has not been studied, and has never been empirically modelled, this assumption required further study.

7.3.5 Atmospheric Stability and Subgrid Modelling

Unstable atmosphere promotes diffusion and mixing of the air, which in the case of wildfire smoke results in a more diffused smoke plume, affecting a wider area with lower concentration. A stable atmosphere restricts mixing and results in a concentrated, denser plume. Quantifying the atmospheric stability can be done in many ways depending on the application [135]. In Galini, the Pasquill Stability index is used, which uses cloud cover, solar radiation and wind speed to calculate a discretised stability index, ranging from A (extremely unstable) to F (extremely stable). The index is then used to calculate σ_y and σ_z, the Pasquil-Gifford coefficients, based on tabulated relations [9], [135].

Galini considers the temporal spread of the wildfire, the flaming phase and the smouldering phase. The injection of the smoke in the flaming and smouldering phase, following from the point source definition of the Gaussian plume, takes effect by discretising the landscape and treating each point on it as a point source of smoke, which changes properties depending on whether the fire on that point is flaming or smouldering.

When modelling the wildfire and smoke injection as a series of points that are either inert, flaming or smouldering, issues may occur when modelling wildfires whose width is significantly smaller than the size of the pixel representing the point in the landscape. A typical pixel size for wildfire modelling, and that used by the LANDFIRE database of the United States, is 30 m on each side, while an average value for the width of a flaming front would be 5 mfor thick fuels

such as downed log forests, empirically. This means that as the wildfire progresses through the modelled pixel, only a part of the discretised landscape would be on fire at any given time. To model these effects in the subgrid, the emissions of each pixel are made variable depending on the rate of spread of the fire. This relation is depicted graphically in Fig. 7.8. Using this time progression of emissions within a pixel, a more realistic smoke injection method is employed, with the resulting flaming and smouldering emissions smoothly moving from point to point.

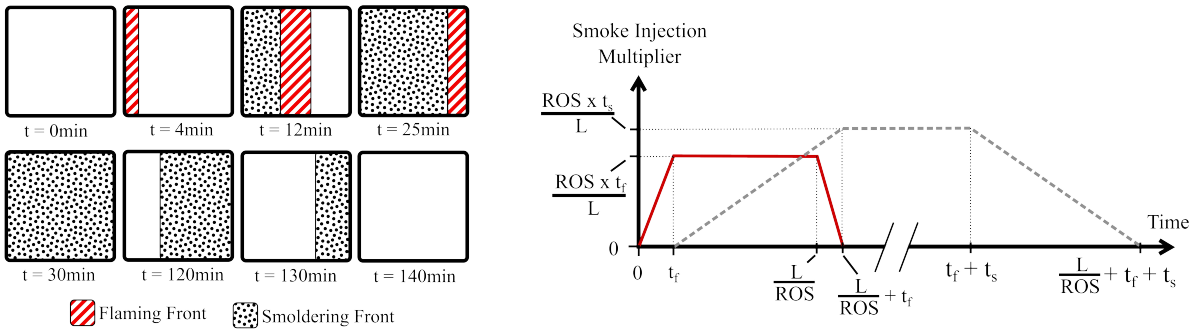


Figure 7.8: Right: A graphical illustration of the subgrid model of fire spread. Left: An example of the subgrid model fire spread. Flaming and Smouldering phases are shown to travel from left to right with the progress of time. To account for the fact that some part of the cell may only be flaming or smoldering, the smoke mass flow rate is limited via the Smoke Injection Multiplier, which can range between 0 and 1.

7.4 Benchmarking and Verification

As a first step to examine the behaviour of the model, a set of standard simple cases are ran, to analyse how the outputs of the models vary with input parameters. The simple cases can then be collated to a more complex case to examine if the final output matches the physical expectations. All results are of the ground-level smoke concentration, illustrated in Fig. 7.7. The model results are shown in Fig. 7.10

The first case is a wildfire starting from a point source and spreading along the direction of the wind over flat terrain and uniform fuel, in stable atmosphere. The second case is a repeat of the first with a line ignition. The third case is the same as the point source one, with temporally varying wind. The fourth case is the same as the point source one, with the top half of the landscape having one fuel model, and the bottom half having another fuel model. The fifth case is the same as the point source case with unstable atmosphere. The sixth case is the same as the first one, with a gradual increase in elevation occurring downwind of the ignition point. The final case is one with point source, varying fuel, temporally varying wind and ramping elevation. The results of each case verify that Galini's outputs match the expectations of a Gaussian plume model.

To provide a measure of comparison, the concentration of the smoke at ground-level for all the simple cases is given in μg of $PM2.5$ per m^3 of air. $PM2.5$ is considered in isolation in these simple cases for easier comparison to real values. As a comparison measure, more than $300\mu g/m^3$ of $PM2.5$ concentration is considered extremely unhealthy by the World Health Organization. When Galini is used for visibility estimation, both $PM2.5$ and $PM10$ are calculated. Converting these values to visibility, which might be the goal of a ground-level smoke model, can be done in many, competing ways, and as such is left outside the capabilities of the model.

The first of the simple cases, Point, sets a benchmark of the model, consisting of a point fire source in uniform wind, flat terrain and uniform fuel. The expected behaviour of the model is one that is very common in the literature and approaches a standard solution. Indeed, comparing the output of the model to an analytical solution of a Gaussian dispersion model with the same parameters yields a near perfect match, as shown in Fig. 7.9. The injection heights of the smoke in the flaming and the smouldering region are calculated as 250 and 30 m respectively. Compared to values found in the literature for the flaming phase (<2km), the injection height is very conservative. Considering Galini is focused on ground level condition, an injection height of several hundred meters to kilometers has a negligible effect to the ground level conditions compared to the smouldering fire. The injection height of the smouldering fire is rarely quoted in the literature, but some models elect to set the injection height at 0 m, lower than the calculated 30 m. More research is needed on the effective injection height of the smouldering fire smoke, along with the effect of the flaming and smouldering smoke mixing that may affect the injection height of the two.

The second simple case, Line, varies the ignition pattern of the fire and the following expansion of the wildfire. The line ignition of the fire is expected to approximate the ideal solution of a line source. Comparing the case output to the output of the analytical solution for a line source does yield comparable results, as shown in Fig. 7.9.

The third case, Transient Wind, displays the effect of transient wind on the smoke production and direction. The wind was set to vary in magnitude and direction, starting at a direction of 315^o and linearly shifting to 215^o and back within the span of 9 hours. The transient results are depicted in Fig. 7.11. Note that the generated fire that was driving the smoke was also simulated using this transient wind, so the fire front changes depending on the wind. The changing fire front results in a changing head and flank fire. The head fire would have a stronger convective plume, and the flank fires would have a weaker convective plume, possibly being entrained by the main head fire plume. Galini cannot model this behavior.

The fourth simple case, Two Fuels, shows the effect of different fuels on the smoke production and dissipation. Different fuels will have a primary effect on the wildfire propagation, as they will burn at different rates and produce different ROS values. In addition, different fuels have

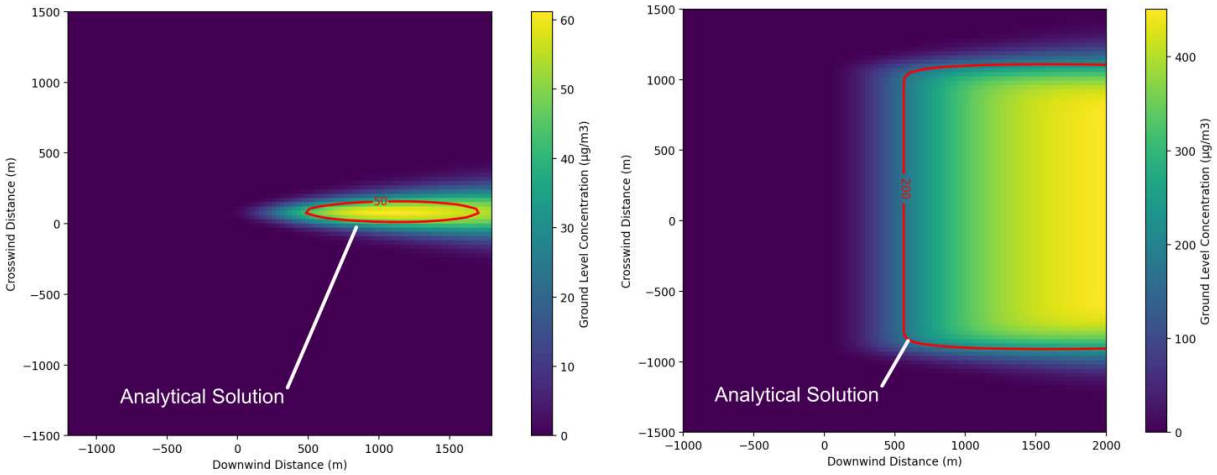


Figure 7.9: The verification of the Point and Line cases. In red is the analytical solution of the point and Line formulation of the Gaussian dispersion model respectively. Both are for SB fuel model 142, 16 kph wind, injection height of 50m.

differing amounts of fine and thick fuels, the two of which dictate the flaming and smouldering emissions respectively. It is expected that grasslands with low bulk density will not produce a lot of smoke in the smouldering phase and will not impede ground level visibility, as is found in the field. Conversely, forested areas with high bulk density and dense ground fuels will produce a lot of smoke in the smouldering phase. In this case study, the top half of the landscape contains Low Load Dry Climate Timber-Grass-Shrub (Dynamic), (Scott and Burgan Fuel Model 161), and the bottom half contains Moderate Load Dry Climate Shrub (Scott and Burgan Fuel Model 142). The two models were chosen as they have compatible rates of spread. As expected, the top fuel model which models forested areas produces denser smoke than the bottom fuel model, representing shrublands.

The fifth case study, Unstable, is identical to the first, with the atmospheric stability index set as "A", extremely unstable. Unstable atmospheric conditions are expected to promote smoke diffusion, covering a larger area with smoke, but restricting the areas where smoke is concentrated. The results do show that the smoke concentration at ground level is more diffuse downwind, covering more area but at a less concentration. The concentration immediately in front of the fire front is significantly higher compared to case 1 with Stable atmospheric conditions. This may be an indication that at different atmospheric conditions the health and visibility hazards may be shifted towards and away the fire front.

The sixth case, Ramp, employs a ramping elevation change halfway along the landscape, to display the effects of elevation on Galini. The results show that the smoke concentration jumps when the incline starts and stays high throughout the ramped elevation, only lowering due to atmospheric diffusion. The maximum concentration near the beginning of the ramp is almost 6 times higher than the maximum concentration of case 1. In effect the ground is modelled as compacting the smoke as it is driven over the ramp.

In the last case, Combined, a complex case was compiled of the previous cases, with a line ignition, multiple fuel, unstable atmosphere and a ramping landscape. The results show that due to the extremely unstable atmosphere, the change in concentration because of the ramp is negligible. This also shows that Galini can produce reasonable results if given a complicated case.

The Galini model uses the steady state solution of Gaussian dispersion to model the transient spread of wildfire. The application of the steady state solution can be used in this transient context if a criterion is satisfied, representing the ratios of the wildfire and smoke transport timescales.This steady state assumption makes Galini a very fast model, as was the goal when starting this project. Each time step of Galini lasts between 1s and 15s, depending on the size of the domain and the number of points in the landscape that are burning. The steady state formulation means that each time step can be calculated independently, without needing to calculate the smoke distribution of the precious time steps. As such, the model can be run with any timestep values, significantly reducing the required computational time to a few minutes for a multiple-hour wildfire. Current models that are used to estimate the smoke dispersion of a wildfire rely on computational fluid dynamics, and thus have issues of spatial and temporal resolution, provising solutions in the order of one simulated hour per hour, orders of magnitude slower than Galini.

A full derivation of the steady state criterion can be found in the appendix of the original publication [44]. The criterion to be satisfied is repeated in Eq. 7.4, where R is the rate of spread of the wildfire, and $\overline{u}$ is the wind speed at injection height.

$$\frac{4R}{\overline{u}} \ll 1 \tag{7.4}$$

To see if this criterion is satisfied in general in Galini, a small study was conducted. The Scott and Burgan fuel classification guide [108] includes typical relations of fuel rate of spread and windspeed at the height of the flames. Although the criterion of Eq. 7.4 is for wind speeds at the injection height of the smoke, the wind speed at ground level is used because of the availability of the data and the variability of the injection height windspeed. The criterion of Eq. 7.4 can then be applied to investigate which fuels broadly satisfy it. The results are shown in Fig. 7.12 and show that the criterion is broadly satisfied for most fuels, except the fastest-spreading grassland fuel types. Thus Galini can use the steady state assumption for the transient fire spread for most fuel types.

Each of the verification cases shows that Galini behaves as expected based on the solutions of the mathematical formulations it employs. When using such a model, one needs to be mindful of any limitations it may have, that may render it inaccurate or invalid when used in certain situations. The Gaussian dispersion model has been designed to work on wind-driven wildfire

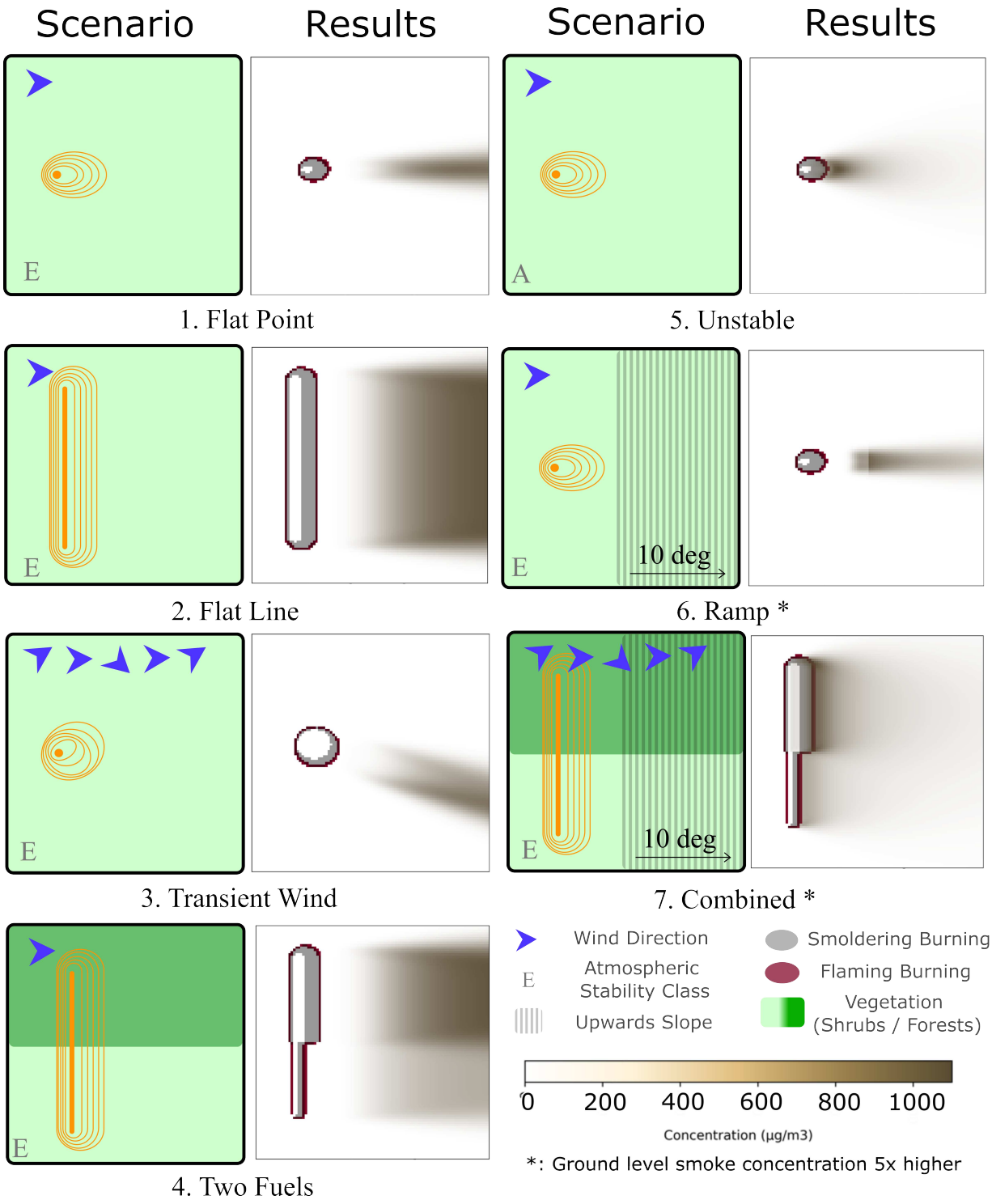


Figure 7.10: The verification scenarios (left column) and the results of Galini (right column). The hue of the grey-yellow areas represents the ground-level concentration of the smoke. The fire isochrones are given every hour. The smoke shown is an instantaneous snapshot of concentration at a timestep. Galini does not calculate accumulated smoke but solves each timestep independently. Readers are encouraged to seek the online version to clearly see the concentration gradient.

plumes. Wildfires may be buoyancy-driven and create a strongly convective, vertical smoke

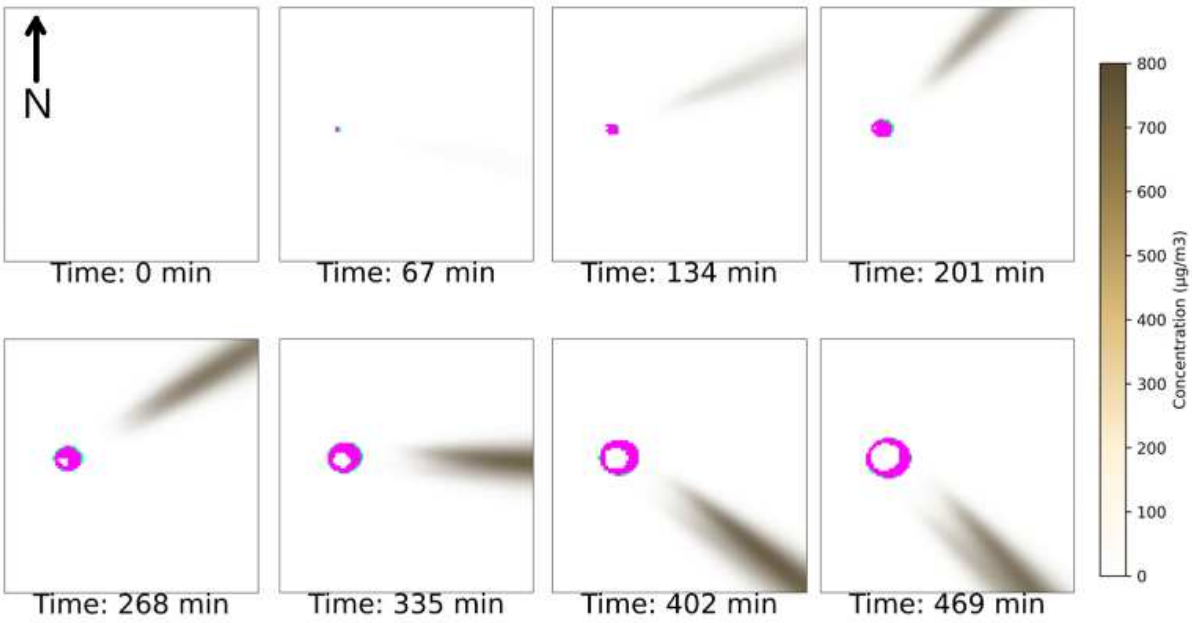


Figure 7.11: Scenario number 3, Transient Wind, with transient wind. The wind direction changes from southwest to northwest clockwise and back. The direction of the smoke plume changes with changing wind direction. The same colouring of smoke, flaming and smouldering areas as Fig. 7.10 applies.

plume that diffuses high in the atmosphere once it meets the atmospheric inversion layer. An empirical criterion for when this may happen may be the Byram convective number, a nondimensional number used to predict when erratic fire behavior may occur, but can be used to quantify the plume behavior since it depends on the atmosphere, wind, fireline intensity, and rate of spread [148], [149]. Strongly convective plumes do greater major health problems because of the long-range plume transport but fall outside of the types of plumes Galini tries to simulate. In a similar fashion, flow separation over obstacles such as mountains is a complex topic that requires physical modelling to fully capture. Some empirical rules can be developed and applied to mimic flow separation in the leeside of mountains, but any such attempt to do so would not yield conservative results. Complex topography may also induce strong spatial wind gradients, with valleys and mountains accelerating or decelerating the wind field. The Gaussian dispersion model fails to account for changing wind away from the source, and as such Galini cannot respond to such cases.

7.5 Conclusion

Galini includes the effect of different fuel, downwind elevation changes, and transient wind. It is a fast, computationally inexpensive wildfire smoke model with a focus on haze and ground-level concentration of smoke, for use in visibility studies, evacuation planning and related studies.

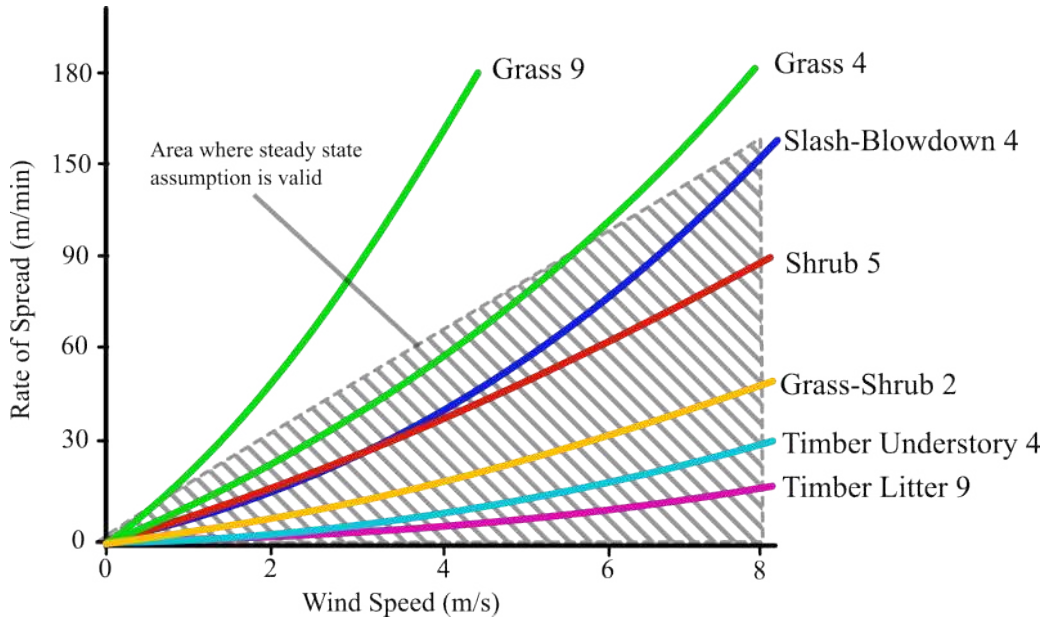


Figure 7.12: The typical rate of spread over midflame windspeed relations as given in the Scott and Burgan fuel model classification. Most fuels satisfy Equation 7.4 except the fastest spreading grassland fuel models. Not all fuel models shown, only the fastest ones in each fuel category.

Through a set of verification cases, each varying an elemental input of the model, it is shown that Galini is consistent with the expected smoke dispersion output. The results of Galini evolve along with the wildfire, providing transient results, accurate for all but very fast fires. The effect of downwind elevation changes is very pronounced, with very high smoke concentrations in areas downwind and uphill of the fire. The injection height has the most effect on ground-level smoke concentration, with the smoke temperature and initial velocity being the dominant factors of the smouldering and flaming phase respectively. Smouldering is shown to be the dominant ground-level smoke contributor, due to the longer burning period and the lower smoke injection height. The steady state solution is valid for most fuel models, except for the fastest grassland models. As with any model, limitations do exist on the kinds of phenomena it can model, as more complex atmospheric events are beyond the modelling capabilities of Galini. The model can be used as a very quick tool to estimate whether a wildfire may affect people and evacuees with its smoke.

Chapter 8

Conclusion

Wildfires are a complex and multidisciplinary problem. When wildfires threaten communities, evacuation is a drastic yet necessary option to ensure the safety of the population. The aim of this thesis is to use wildfire spread modeling to develop tools, models and methodologies to assist with evacuation planning, to ultimately ensure the long-term wildfire resilience of communities globally. To that effect, chapters 3 to 7 contributed to a stepwise buildup of a coupled wildfire-smoke-evacuation planning tool based on the probabilistic trigger boundary methodology.

Chapter 3 introduces k-PERIL, a probabilistic trigger boundary tool that helps communities plan their evacuations. The development of k-PERIL was a critical step in allowing communities to create data-driven, simulation-backed evacuation plans. While previous iterations of trigger boundaries could not be used for long-term planning, because of the limitation in simulating single wildfire and evacuation scenarios, probabilistic trigger boundaries can be used for planning as they do not rely on single wildfires and evacuation cases. Probabilistic trigger boundaries can be used to inform when an evacuation should be initiated, and which parts of the landscape should be monitored closely, based on the historic weather of the area, and thus can be applied on any future circumstances. Building up from the original PERIL paper, and to allow comparisons between it and k-PERIL, the Roxborough Park community was chosen as a case study, ultimately showing the match between the two models and highlighting the wider applicability of k-PERIL.

Chapter 4 expands on chapter 3 by tackling the issue of dire evacuations. Prior to this chapter, the phenomenon of dire evacuations was loosely defined, with no means of planning against them. The new methodology, based on the probabilistic nature of WASET and WRSET, allows for a strict definition of dire and late evacuations. The newly-introduced evacuation safety factor can be used to quantify the chances of an evacuation becoming dire based on historical analysis. This methodology can be combined with probabilistic trigger boundaries to establish a tool able

to predict and prevent dire evacuations. Evacuations starting when the wildfire is within the trigger boundary, or started within the trigger boundary, now have a quantified probability of becoming dire and placing people in danger. The area covered by the probabilistic trigger boundary must be made to prevent ignition of any kind, as any wildfire starting in this area will immediately lead to a dire evacuation. In the case of the Mati community, the probabilistic trigger boundaries show, based on historic wind and weather data, that the destructive wildfire of 2018 left the community with a 34% chance of dire evacuation upon ignition, and 100% chance of dire evacuation when the first spontaneous evacuations started. With the contents of the next chapters showing that the results strongly depend on the wildfire spread model used, these values may fluctuate and cannot be taken with decimal precision.

Chapter 5 discusses the effect of wildfire spread model choice on the perceived safety of communities. A set of simple cases, along with the 2018 Mati fire were chosen as benchmarks between 7 of the state-of-the-art wildfire spread models, using the exact same input parameters. This chapter shows that, even with the exact same inputs, each model yields different results, with significant implications on the community safety. The simple cases show that models interpret input variables like the wind and slope fundamentally differently, even with the same underlying wildfire rate of spread models. Farsite and ELMFIRE, for example, in the case of uniform wind, show the same windward wildfire spread extent, but ELMFIRE has 50% less flank- and backfire spread. The Machine Learning models create unrealistic outputs for the simple cases, showing that such tests stray far from their training sets and may not be an appropriate way to benchmark them. In the real case simulations, all models bar the FDS models showed acceptable agreement with the real fire scar, with similarity coefficients of more than 40%. The low overall score can be attributed to the exaggerated backfire all models predict, and by the inability of the models to allow fire spread within built-up areas. This is a critical issue with all wildfire spread models and one that needs to be addressed, to effectively estimate the wildfire risk communities face. Overall, different models use different assumptions and simplifications, which significantly affect the final results, in some cases by as much as 100%. An accurate estimate of the wildfire danger of an area must include a multitude of models and take a probabilistic approach, where all models' strengths are combined, and all their weaknesses are mutually covered.

Chapter 6 combines all previous work, and examines the use of ensemble wildfire spread modelling for probabilistic trigger boundary calculation. It was expected that, as different models predict different wildfire scars for the same input parameters, different models would also generate different trigger boundaries. The results support the hypothesis, showing that different models do predict different trigger boundaries. Ensemble modelling is required to combine the results of all models and yield the overall trigger boundary of the community. The Fort McMurray community studied in this chapter was found to be a high-risk community, as its required evacuation time is so large that the generated probabilistic trigger boundaries extend

beyond the range that a wildfire can be detected by the community. Any wildfire that can be spotted by the community automatically leads to an evacuation with some probability of it becoming dire. Such communities must take great care to reduce their evacuation time and improve their detection capabilities.

Finally, Chapter 7 fulfills an important role in the methodology of calculating probabilistic trigger boundaries, by creating a fast wildfire smoke dispersion model. While wildfire smoke has been shown to affect and delay evacuations, very few wildfire smoke dispersion models existthat can run at the same pace as the operational wildfire smoke models, and can be used today, and fewer still account for both the flaming and smoldering fronts. Galini was developed as a fast smoke spread model based on the gaussian dispersion theory, to provide quick estimates of the ground-level smoke concentration. Galini can provide results for any time during the wildfire in 1 s to 15 s , depending on the magnitude of the wildfire, must faster than traditional smoke dispersion models that compute in hour-long timescales. Compared to existing smoke models that can account for the near-fire ground level concentration, which traditionally solve to the tune of one simulated hour per computation hour, Galini is faster by two orders of magnitude. The addition of a ground effect term is critical in accurately estimating ground-level concentration before the smoke rises far from the ground. Verification and validation of the model are necessary steps for the development of Galini, and will be conducted based on the availability of equivalent models or data of ground-level smoke concentration.

Each of these chapters sequentially builds up to a final methodology for creating robust evacuation models, shown in Figure 8.1. The wildfire spread, its generated smoke, and the evacuation process are intrinsically interlinked, in both time and space. Studying each of the three separately is inadequate when planning for evacuations, as many of the coupled mechanisms are neglected, such as roads becoming impassable due to wildfire or smoke impingement, or fire-fighting efforts aiding the evacuation process. An intimately coupled system is required for accurate evacuation time estimations, and in turn for accurate probabilistic trigger boundaries. The final goal of this thesis is to establish a methodology to accurately create probabilistic trigger boundaries, to be used by communities to prevent dire evacuations, both in the event of a wildfire, and in long-term planning.

To that end, this thesis proposes a methodology of applying probabilistic trigger boundaries, ensemble modelling, and smoke modelling, with the goal of preventing dire evacuations, borrowing from the conclusions of the paper that initiated a similar methodology [47]. The methodology takes the form of a conceptual flowchart, shown in Figure 8.1, outlining how k-PERIL (Chapters 3 and 4), Galini (Chapter 7), and ensemble modelling (Chapters 5 and 6) should be used together in a platform like WUI-NITY. The bulk of the methodology is similar to that of k-PERIL, with the addition of both ensemble modelling and tight coupling of the wildfire model, Galini, and the evacuation model. This will allow the wildfire to dynamically affect

the smoke and evacuation processes, allowing complex effects like lane closure and tenability criteria to be modelled and be reflected in the final probabilistic trigger boundary.

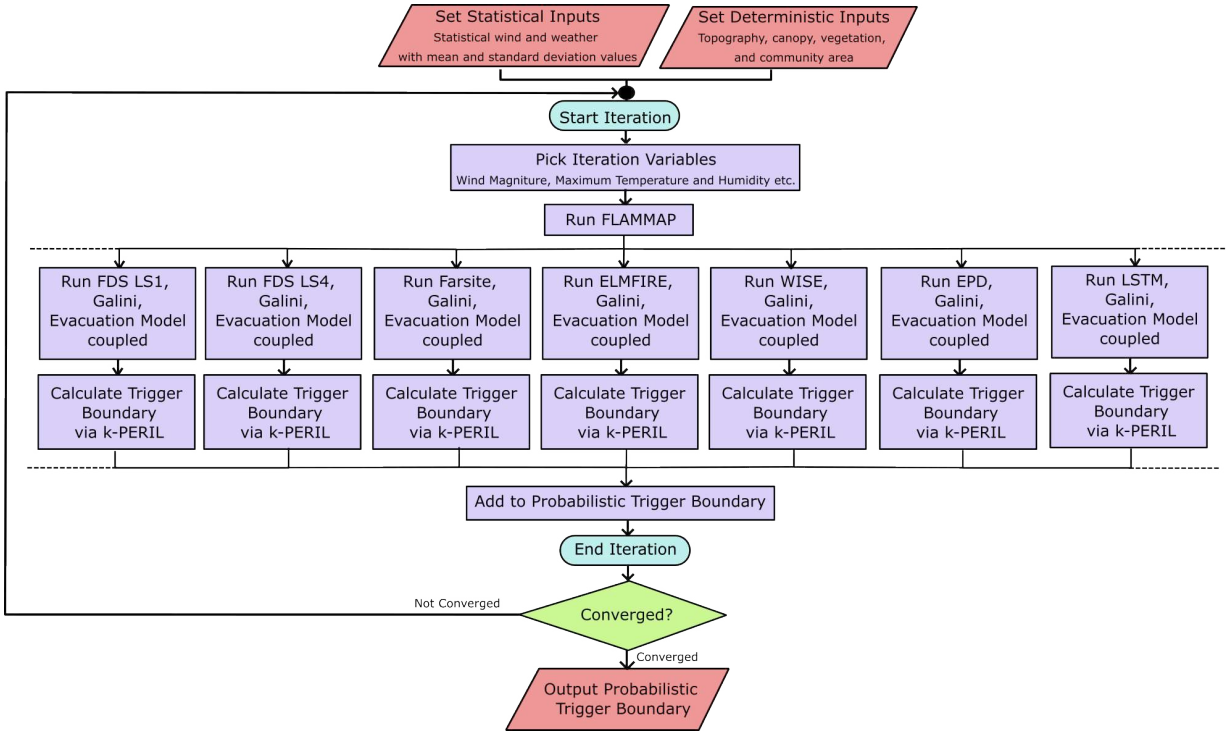


Figure 8.1: A conceptual flowchart of the future use of k-PERIL with the goal of creating probabilistic trigger boundaries to plan against dire evacuations. Ensemble modelling, coupled with smoke modelling and evacuation modelling, is a critical part of the procedure. Tight coupling between all three models is a future step that will create more accurate and actionable results.

The modelling methodology employed in all the models is semi-empirical, relying on a mixture of physical principles and experimental regressions to yield accurate results in a time span measured in seconds or minutes. The effect of model choice on perceived safety needs to be expanded upon, analyzing why different models yield different results, and further quantifying their applicability outside their calibrated areas. Wildfire smoke dispersion needs to be studied at ground-level, close to evacuees, to create more robust ground level models. More work needs to be aimed at understanding how wildfire models can be used with probabilistic trigger boundaries, and to understand how probabilistic trigger boundaries can be used practically from communities. Richard Rothermel, creator of the Rothermel model that the majority of examined wildfire models use, once remarked that it took him 10 years to create the model and another 10 years to understand the exact meaning and nature of the input parameters it requires [96]. Similarly, the concepts and methodologies of this thesis need to be applied to more communities, to be expanded upon and to be understood in depth before they can be actioned in real life.

A large range of case studies were conducted in this thesis. The communities of Roxborough

Park, Mati and Fort McMurray were all selected as case studies for each step in the development of probabilistic trigger boundaries. The reasoning behind choosing different case studies every time is twofold. One reason is to highlight the broad applicability wildfire models need to attain to be accurate, with wildfire-stricken communities existing in areas as diverse as north Canada, central US, and Mediterranean Greece. Another reason is to show that these methodologies should not only be used retroactively, in examination of wildfires that have already happened, but they should also be used for future planning to protect communities. The communities that were chosen do have experiences with wildfires or evacuation drills, which was integral in gathering all the necessary data for the methodologies and prove their effective through retroactive analysis. It still stands that these models can be used to aid in future preparations.

The work of this thesis sets solid foundations for the research within to be continued and expanded. In the realm of probabilistic trigger boundaries, the next step in its development will be to develop a more intimate coupling between wildfire and evacuation models. Instead of the WRSET being a prescribed statistical valuable, it can be influenced by the wildfire itself, thus identifying direction of wildfire encroachment that pose increased danger to the evacuation process. This is something that has not been done before and is only possible within the WUI-NITY project. In terms of model benchmarking, this work could be expanded to more models, particularly ones that are used by meteorological services and couple wildfire spread models and atmospheric interaction models. Comparisons of the predicted rates of spread with real recorded rates of spread of wildfires like the Mati fire would also provide valuable insights into the accuracy of them models. Finally, the Galini smoke model requires further verification and validation of the model itself and each of its submodels. While real driver-level concentration data is hard, if not impossible, to find, a comparison between Galini and a high-fidelity atmospheric model could provide valuable insights into the strengths and weaknesses of the model. Exploring the use of the Byram convective number as a criterion for the applicability of the model in plume-dominated or wind-driven wildfires is also a promising area of research. Overall, much research can be continued from the initla research steps of this thesis.

In conclusion, the aim of this thesis was to advance communities' capabilities to protect themselves from dire evacuations, through immediate response and long-term planning. Probabilistic trigger boundaries were found to be the best tool for predicting when an evacuation may become dire, and quantifying areas where the risk of an evacuation becoming dire is highest. Through the development of k-PERIL, Galini, and studies into dire evacuations and ensemble modelling, a concrete methodology is proposed that can create data-driven evacuation and management plans, to help communities improve their wildfire resilience. Creating and developing tools like these is a small but impactful step in ensuring that tragedies like the Mati fire, the Lahaina fire, the Camp fire and many other fatal wildfire never happen again.

Appendix A

Mati Fuel Types

Below is a table of the conversion of the fuel types in the Mati landscape. The conversion starts from the original CORINE Land Cover data, first converted to Scott and Burgan fuel models, then to Anderston fuel models and CFFDRS fuel models.

Table A.1: A conversion table for the Mati landscape in this study. The input data was the CORINE Land Cover Classes, which were first converted into Scott and Burgan models by manually inspecting the area. They were then converted to Anderson and CFFDRS fuel models using the respective guides.

CORINE Vegetation Model	**Scott and Burgan Fuel Model**	**Anderson Fuel Model**	**CFFDRS Fuel Model**
1 - Sealed	99 - Bare Ground	99 - Bare Ground	101 - Non-fuel
2 - Coniferous	165 - Very High Load, Dry Climate Timber-Shrub	10 - Timber (litter and understory)	3 - C-3 - Mature Jack or Lodgepole Pine
3 - Broadleaved Deciduous	165 - Very High Load, Dry Climate Timber-Shrub	10 - Timber (litter and understory)	3 - C-3 - Mature Jack or Lodgepole Pine
4 - Broadleaved Evergreen	165 - Very High Load, Dry Climate Timber-Shrub	10 - Timber (litter and understory)	3 - C-3 - Mature Jack or Lodgepole Pine
5 - Shrubs	144 - Low Load, Humid Climate Timber-Shrub	7 - Southern Rough	21 - C-7 - Ponderosa Pine - Douglas-Fir
6 - Permanent Herbaceous	103 - Low load, Very Coarse, Humid Climate Grass (Dynamic)	3 - Tall grass (2.5 feet)	33 - O-1a/O-1b - Grass
7 - Periodically Herbaceous	103 - Low load, Very Coarse, Humid Climate Grass (Dynamic)	3 - Tall grass (2.5 feet)	33 - O-1a/O-1b - Grass
8 - Lichens and Mosses	99 - Bare Ground	99 - Bare Ground	101 - Non-fuel
9 - Sparsely Vegetated	91 - Urban/Developed	91 - Urban/Developed	101 - Non-fuel
10 - Water	98 - Open Water	98 - Open Water	102 - Water
11 - Permanent Snow and Ice	92 - Snow/Ice	92 - Snow/Ice	101 - Non-fuel

Appendix B

SB to CFFDRS Fuel Models Complete Table

Table B.1: The complete table of Root Mean Square Errors (RMSE) of fits between Scott and Burgan Fuel Models and CFFDRS Fuel Models, with varying wind.

	CFFDRS Fuel Models														
RMSE	**C-1**	**C-2**	**C-3**	**C-4**	**C-5**	**C-6**	**C-7**	**D-1**	**S-1**	**S-2**	**S-3**	**O-1a**	**O-1b**	**M1**	**M2**
RMSE	**C-1**	**C-2**	**C-3**	**C-4**	**C-5**	**C-6**	**C-7**	**D-1**	**S-1**	**S-2**	**S-3**	**O-1a**	**O-1b**	**M1**	**M2**
GR1	3.7	3.8	3.7	3.8	3.1	3.1	3.1	3.7	3.6	3.2	3.7	4.2	4.2	3.4	3.7
GR2	3.2	3.2	3.2	3.2	4.3	3.1	4.6	8.0	3.0	3.0	3.0	3.8	3.9	2.9	3.1
GR3	3.0	2.9	3.0	3.0	5.1	3.3	5.4	9.8	2.7	3.2	2.7	3.6	3.8	2.9	2.8
GR4	3.9	3.1	3.8	3.1	10.6	6.9	11.2	19.3	3.6	6.4	3.4	3.1	3.4	5.1	3.7
GR5	3.2	2.8	3.2	2.8	7.6	4.8	8.1	14.2	2.9	4.5	2.8	3.4	3.6	3.7	3.0
GR6	4.2	3.3	4.1	3.2	11.5	7.5	12.2	20.9	3.9	7.0	3.6	3.1	3.3	5.6	3.9

(continued on next page)

RMSE (cont.)	C-1	C-2	C-3	C-4	C-5	C-6	C-7	D-1	S-1	S-2	S-3	O-1a	O-1b	M1	M2
GR7	5.9	4.4	5.8	4.2	16.9	11.3	17.8	29.9	5.6	10.5	5.1	2.9	3.0	8.3	5.6
GR8	4.7	3.5	4.6	3.3	13.8	9.0	14.5	24.8	4.4	8.4	4.0	2.8	3.1	6.6	4.4
GR9	9.8	7.3	9.6	6.9	27.0	18.5	28.4	46.8	9.5	17.3	8.7	3.2	2.9	13.8	9.4
GS1	3.8	3.9	3.8	3.9	3.1	3.2	3.0	3.2	3.7	3.3	3.8	4.2	4.3	3.5	3.8
GS2	3.5	3.5	3.5	3.6	3.2	2.9	3.2	4.8	3.3	2.9	3.4	4.0	4.1	3.1	3.4
GS3	3.2	3.3	3.2	3.3	3.8	2.8	4.0	6.9	3.0	2.8	3.1	3.8	4.0	2.9	3.1
GS4	3.3	3.3	3.3	3.4	3.4	2.8	3.6	6.0	3.1	2.8	3.2	3.9	4.0	2.9	3.2
SH1	4.4	4.5	4.4	4.5	4.2	4.3	4.2	4.0	4.4	4.3	4.4	4.5	4.5	4.4	4.4
SH2	4.4	4.4	4.4	4.4	4.2	4.3	4.2	3.9	4.4	4.3	4.4	4.5	4.5	4.3	4.4
SH3	4.4	4.4	4.4	4.4	4.1	4.2	4.1	3.8	4.4	4.2	4.4	4.5	4.5	4.3	4.4
SH4	3.3	3.4	3.3	3.4	3.4	2.8	3.5	5.8	3.2	2.8	3.2	3.9	4.1	3.0	3.3
SH5	3.0	2.8	3.0	2.8	6.4	4.0	6.8	12.1	2.7	3.8	2.7	3.4	3.6	3.2	2.8
SH6	3.5	3.6	3.5	3.7	2.8	2.8	2.8	3.6	3.4	2.9	3.5	4.1	4.2	3.1	3.5
SH7	3.1	3.2	3.1	3.2	3.7	2.7	3.9	6.9	2.9	2.7	3.0	3.8	4.0	2.7	3.0
SH8	3.5	3.6	3.5	3.7	2.9	2.9	2.9	3.9	3.4	2.9	3.5	4.1	4.2	3.2	3.5
SH9	3.0	2.8	3.0	2.8	6.0	3.8	6.4	11.4	2.7	3.6	2.7	3.5	3.7	3.1	2.8
TU1	4.4	4.4	4.4	4.4	4.2	4.3	4.2	3.9	4.4	4.3	4.4	4.5	4.5	4.4	4.4
TU2	3.9	4.0	3.9	4.0	3.2	3.4	3.2	2.9	3.9	3.5	3.9	4.3	4.3	3.7	3.9
TU3	3.4	3.4	3.4	3.5	3.2	2.8	3.3	5.3	3.2	2.8	3.3	4.0	4.1	3.0	3.3
TU4	3.9	4.0	3.9	4.0	3.2	3.4	3.2	3.1	3.8	3.4	3.9	4.3	4.3	3.6	3.9
TU5	4.1	4.2	4.1	4.2	3.6	3.8	3.5	3.0	4.1	3.8	4.1	4.4	4.4	4.0	4.1
TL1	4.5	4.5	4.5	4.5	4.5	4.5	4.5	4.4	4.5	4.5	4.5	4.6	4.6	4.5	4.5
TL2	4.5	4.5	4.5	4.5	4.4	4.4	4.4	4.3	4.5	4.4	4.5	4.5	4.6	4.5	4.5

(continued on next page)

RMSE (cont.)	C-1	C-2	C-3	C-4	C-5	C-6	C-7	D-1	S-1	S-2	S-3	O-1a	O-1b	M1	M2
TL3	4.5	4.5	4.5	4.5	4.4	4.4	4.4	4.2	4.5	4.4	4.5	4.5	4.6	4.5	4.5
TL4	4.5	4.5	4.5	4.5	4.3	4.3	4.3	4.1	4.4	4.4	4.5	4.5	4.5	4.4	4.4
TL5	4.3	4.4	4.3	4.4	4.0	4.1	4.0	3.7	4.3	4.2	4.3	4.5	4.5	4.2	4.3
TL6	4.3	4.3	4.3	4.3	3.8	4.0	3.8	3.4	4.2	4.0	4.2	4.4	4.5	4.1	4.2
TL7	4.4	4.5	4.4	4.5	4.2	4.3	4.2	4.0	4.4	4.3	4.4	4.5	4.5	4.4	4.4
TL8	4.3	4.3	4.3	4.3	3.8	4.0	3.8	3.4	4.2	4.0	4.3	4.4	4.5	4.1	4.2
TL9	4.1	4.2	4.1	4.2	3.5	3.7	3.5	3.0	4.1	3.8	4.1	4.4	4.4	3.9	4.1
SB1	4.2	4.3	4.3	4.3	3.8	4.0	3.8	3.4	4.2	4.0	4.2	4.4	4.5	4.1	4.2
SB2	3.8	3.9	3.8	3.9	3.0	3.2	3.0	3.2	3.7	3.3	3.8	4.2	4.3	3.5	3.8
SB3	3.3	3.4	3.3	3.4	3.6	2.8	3.7	6.2	3.1	2.9	3.2	3.9	4.0	2.9	3.2
SB4	3.3	2.9	3.2	2.9	7.5	4.8	7.9	13.8	2.9	4.5	2.9	3.4	3.6	3.7	3.1

Appendix C

SB to FCCS Fuel Model Conversion

Table C.1: The complete SB40 to FCCS conversion guide, based on the LANDFIRE database for the continental US.

SB Fuel	FCCS Closest	% Match	FCCS 2nd Closest	% Match	FCCS 3rd Closest	% Match
0	0	100.0%	-	-	-	-
91	0	100.0%	-	-	-	-
92	0	100.0%	-	-	-	-
93	1244	74.3%	1223	16.0%	0	9.2%
98	0	91.1%	307	6.0%	311	2.1%
99	0	99.8%	-	-	-	-
100	49	17.6%	311	17.6%	236	11.3%
101	519	11.0%	0	9.5%	500	7.6%
102	66	32.4%	1281	28.3%	1261	12.9%
103	66	48.4%	280	5.3%	469	4.8%
104	131	70.9%	2800112	18.6%	175	3.4%
105	131	27.4%	280	26.2%	335	20.2%
106	66	43.7%	131	42.9%	2800113	12.4%
107	0	37.5%	318	36.6%	443	22.3%
108	175	69.4%	131	10.6%	445	9.4%
120	401	18.0%	308	12.3%	540	11.8%
121	56	22.4%	69	18.8%	518	7.8%
122	308	19.0%	0	18.5%	210	11.4%
123	560112	63.3%	69	10.8%	560113	10.0%
124	445	100.0%	-	-	-	-

(continued on next page)

(continued from previous page)

SB Fuel	FCCS Closest	% Match	FCCS 2nd Closest	% Match	FCCS 3rd Closest	% Match
140	49	42.0%	233	41.9%	235	5.8%
141	69	29.7%	311	13.1%	308	10.9%
142	52	35.9%	62	16.3%	43	7.8%
143	36	32.6%	44	26.7%	440112	13.0%
144	69	73.9%	335	6.5%	157	4.8%
145	210	68.0%	44	26.6%	140	1.3%
146	470	33.9%	43	17.0%	467	7.7%
147	0	93.7%	154	5.9%	1430413	0.2%
148	1470313	65.0%	1470113	22.1%	1460412	2.7%
149	154	99.7%	140	0.1%	4550313	0.1%
160	10	28.1%	8	18.1%	2140132	7.7%
161	224	11.9%	59	10.1%	470	10.0%
162	0	32.5%	156	17.6%	142	9.7%
163	156	77.4%	191	6.8%	157	6.2%
164	59	19.9%	22	12.6%	52	11.2%
165	2	31.9%	0	29.6%	273	13.7%
180	49	73.6%	247	5.7%	334	2.7%
181	0	75.8%	154	15.1%	22	4.7%
182	283	18.6%	427	14.1%	22	7.4%
183	110	50.1%	0	6.0%	12	6.0%
184	305	43.2%	0	11.2%	287	8.1%
185	264	19.3%	321	8.1%	281	7.0%
186	154	49.1%	90	14.5%	157	11.6%
187	228	57.3%	26	14.8%	237	4.1%
188	90	35.1%	156	22.2%	52	11.9%
189	467	29.4%	8	29.0%	39	11.7%
200	1090412	65.2%	2870412	16.4%	4090412	9.8%
201	48	42.9%	273	24.6%	80133	18.6%
202	1100422	33.2%	1100432	21.6%	1100232	8.7%
203	2440432	63.7%	3560432	16.8%	4130432	5.9%

Appendix D

Details on automatically using the ensemble models

Starting with Farsite, all required files need to be placed in a folder, along with an input file specifying the required outputs, weather and fuel moisture data, and other simulation parameters. Farsite can then be used by running a command directly through the governing C# program. The outputs are the rate of spread magnitude and direction, which can directly be used to find the trigger boundary of the iteration.

WISE requires a more convoluted process to run. WISE is the new computational version of the Canadian Forest Fire Danger Rating System, based on the Prometheus model. Running Prometheus from the command line used the COM architecture, which was dated and was not supported by the developers. The version to replace it is WISE, used with a command line and with more capabilities. It is comprised of two main components, written in Java. The WISE Builder prepares the simulation files, and the WISE Manager stores all previous and currently running simulations. Once all the input parameters are established in the main C# program, another C# program is called to compile all the input parameters into one, and then pass them to a Javascript file. This Javascript file uses the Javascript API of WISE Builder to build the "job" file that is used to run the simulation. The same Javascript file begins the simulation and waits for the results.

In running WISE, an issue occurred where jobs submitted via the Javascript file would not start automatically. An error would occur, saying "Validation Failed". This was not a fault of the input file or the simulation setup, and was a bug that could be overcome by manually refreshing the simulation in WISE Manager. To enable automatic processing and bypass the manual refresh, the WISE simulator was run as soon as the "job" file was generated. This could be done by using the relevant executable file in command line directly, bypassing the Manager component, similar to Farsite. This would ultimately yield the rate of spread magnitude and

direction, which were used to calculate the trigger boundary.

ELMFIRE differs from all the other models as it can only be compiled and used in Linux, while all other models, and the main C# code, ran in Windows. The gap was bridged using the Windows Subsystem for Linux (WSL), allowing for a linux subsystem to work in windows. To use ELMFIRE, the required input files are copied into the linux subsystem, a file containing the model parameters is created, and the model is ran. The output is the rate of spread magnitude only, with no identified way to output the rate of spread direction. As such, the rate of spread direction is inferred from the arrival time output, by calculating the 2D gradient of arrival time at each point. The trigger boundary can then be calculated.

The Google models run in Python, with a number of restrictions. They can only simulate wildfires in a 126 x 126 landscape, with 30 m cell size, and with a fixed timestep of 15 min. The landscape used for the Fort McMurray simulations are 400 x 400 with a cell size of 200m. For the Google models to function, the landscape data are downscaled to 126 x 126, and the time step is automatically adjusted to 171 min. The input files are thus prepared and ran in Python. The output of the Google models are the isochrones of the fire at every time step, which cannot directly be used to calculate the trigger boundaries. Instead, linear interpolation is used to estimate the arrival time of each point from the wildfire isochrones. The 2D gradient of the arrival time is then used to get the rate of spread magnitude and direction.

Finally, FDS runs in Windows, but for the sake of time, the simulations of this study were ran in the Imperial High Performance Computing (HPC) system, allowing for parallelization. The main C# program prepared the simulations and saved them with the purpose of running them at a later time. The simulations were prepared using the QGIS2FDS plugin, allowing for easy conversion between geodata and FDS input file. The results of FDS are in a Fortran format that cannot easily be read by themselves, and require further processing in Python to get the arrival time of the simulation. Additional postprocessing is required in the same manner as the Google models to convert arrival time to rate of spread magnitude and direction. One issue that arises with FDS results is that the simulated fire creates multiple "islands" when the fire front encounters cells with slow rates of spread. These islands have much higher arrival times than their neighbors. Finding the rate of spread via central differenciation, as is done with the Google models, exaggerates the effect of the islands. To compensate, the rate of spread is calculated with forward and backward differentiation, and the highest value is saved. The trigger boundary can then be calculated.

Appendix E

Code Repositories

All the code used in this thesis can be found in the following repositories:

1. k-PERIL: `https://zenodo.org/records/16420487`
2. Ensemble Modelling (With automated running of the 7 models): `https://zenodo.org/records/16420542`
3. Galini: `https://zenodo.org/uploads/16357373`

Bibliography

[1] V. Samborska and H. Ritchie, "Wildfires: Explore global and country-level data on the extent of wildfires and how they've changed over time.," *Our World in Data*, Apr. 2024.

[2] A. L. Westerling, "Increasing western US forest wildfire activity: Sensitivity to changes in the timing of spring," *Philosophical Transactions of the Royal Society B: Biological Sciences*, vol. 371, no. 1696, pp. 20 150 178–20 150 178, Jun. 2016. DOI: 10.1098/rstb.2015.0178.

[3] J. San-Miguel-Ayanz, R. Boca, P. Maianti, *et al.*, Eds., *Forest fires in Europe, Middle East and North Africa 2023*, eng. Luxembourg: Publications Office, 2024, ISBN: 978-92-68-21495-4. DOI: 10.2760/8027062.

[4] G. Xanthopoulos and M. Athanasiou, "Attica Region, Greece July 2018: A tale of two res and a seaside tragedy," *Wildfire*, Apr. 2019.

[5] A. Maranghides and E. D. Link, "WUI fire evacuation and sheltering considerations: Assessment, Planning, and Execution (ESCAPE)," Tech. Rep., Aug. 2023. DOI: 10.6028/NIST.TN.2262. [Online]. Available: https://nvlpubs.nist.gov/nistpubs/TechnicalNotes/NIST.TN.2262.pdf.

[6] S. Kerber and D. Alkonis, "Lahaina Fire Incident Analysis Report," UL Research Institutes, Tech. Rep., 2024, Artwork Size: 0 Bytes, 0 Bytes. DOI: 10.60752/102376.26858962. [Online]. Available: https://ulri.figshare.com/articles/report/Lahaina_Fire_Incident_Analysis_Report/26858962 (visited on 01/29/2025).

[7] O. O. Woolcott, "Los Angeles County in flames: Responsibilities on fire," en, *The Lancet Regional Health - Americas*, vol. 42, p. 101 005, Feb. 2025, ISSN: 2667193X. DOI: 10.1016/j.lana.2025.101005. [Online]. Available: https://linkinghub.elsevier.com/retrieve/pii/S2667193X25000158 (visited on 01/29/2025).

[8] B. Teague, *2009 Victorian Bushfires Royal Commission: final report*, eng. Melbourne: The Commission, 2010, OCLC: 652409884, ISBN: 978-0-9807408-2-0.

[9] David L. Peterson, Sarah M. McCaffrey, and Toral Patel-Weynand, *Wildland Fire Smoke in the United States*, D. L. Peterson, S. M. McCaffrey, and T. Patel-Weynand, Eds. Cham: Springer International Publishing, 2022, ISBN: 978-3-030-87044-7. DOI: 10.1007/978-3-030-87045-4.

[10] J. K. Balch, V. Iglesias, A. L. Mahood, *et al.*, "The fastest-growing and most destructive fires in the US (2001 to 2020)," en, *Science*, vol. 386, no. 6720, pp. 425–431, Oct. 2024, ISSN: 0036-8075, 1095-9203. DOI: 10.1126/science.adk5737. [Online]. Available: https://www.science.org/doi/10.1126/science.adk5737 (visited on 11/01/2024).

[11] Joint Research Centre (JRC), "Advance report on Forest Fires in Europe, Middle East and North Africa 2023," Tech. Rep., 2024.

[12] H. Misal, "Economic, social and institutional drivers of wildfire management," PhD Thesis, Imperial College London, London, UK, 2024.

[13] D. L. Swain, A. F. Prein, J. T. Abatzoglou, *et al.*, "Hydroclimate volatility on a warming Earth," en, *Nature Reviews Earth & Environment*, vol. 6, no. 1, pp. 35–50, Jan. 2025, ISSN: 2662-138X. DOI: 10.1038/s43017-024-00624-z. [Online]. Available: https://www.nature.com/articles/s43017-024-00624-z (visited on 01/29/2025).

[14] J. K. Balch, J. T. Abatzoglou, M. B. Joseph, *et al.*, "Warming weakens the night-time barrier to global fire," *Nature*, vol. 602, no. 7897, pp. 442–448, Feb. 2022, Publisher: Nature Research. DOI: 10.1038/s41586-021-04325-1.

[15] P. Krebs, G. B. Pezzatti, S. Mazzoleni, L. M. Talbot, and M. Conedera, "Fire regime: History and definition of a key concept in disturbance ecology," en, *Theory in Biosciences*, vol. 129, no. 1, pp. 53–69, Jun. 2010, ISSN: 1431-7613, 1611-7530. DOI: 10.1007/s12064-010-0082-z. [Online]. Available: http://link.springer.com/10.1007/s12064-010-0082-z (visited on 01/16/2025).

[16] S. L. Manzello, Ed., *Encyclopedia of Wildfires and Wildland-Urban Interface (WUI) Fires*, en. Cham: Springer International Publishing, 2020, ISBN: 978-3-319-52089-6 978-3-319-52090-2. DOI: 10.1007/978-3-319-52090-2. [Online]. Available: http://link.springer.com/10.1007/978-3-319-52090-2 (visited on 01/16/2025).

[17] V. C. Radeloff, D. P. Helmers, H. A. Kramer, *et al.*, "Rapid growth of the US wildland-urban interface raises wildfire risk," en, *Proceedings of the National Academy of Sciences*, vol. 115, no. 13, pp. 3314–3319, Mar. 2018, ISSN: 0027-8424, 1091-6490. DOI: 10.1073/pnas.1718850115. [Online]. Available: https://pnas.org/doi/full/10.1073/pnas.1718850115 (visited on 01/16/2025).

[18] D. Drysdale, *An Introduction to Fire Dynamics*. Wiley, Aug. 2011, ISBN: 978-0-470-31903-1. DOI: 10.1002/9781119975465.

[19] M. Finney, S. McAllister, T. Grumstrup, and J. Forthofer, *Wildland Fire Behaviour*. CSIRO Publishing, 2021, ISBN: 978-1-4863-0909-2. DOI: 10.1071/9781486309092.

[20] S. McAllister, J.-Y. Chen, and A. C. Fernandez-Pello, *Fundamentals of Combustion Processes*. New York, NY: Springer New York, 2011, ISBN: 978-1-4419-7942-1. DOI: 10.1007/978-1-4419-7943-8.

[21] F. X. Jervis and G. Rein, "Experimental study on the burning behaviour of *Pinus halepensis* needles using smallscale fire calorimetry of live, aged and dead samples," en, *Fire and Materials*, vol. 40, no. 3, pp. 385–395, Apr. 2016, ISSN: 0308-0501, 1099-1018. DOI: 10.1002/fam.2293. [Online]. Available: https://onlinelibrary.wiley.com/doi/10.1002/fam.2293 (visited on 01/29/2025).

[22] "Development and structure of the Canadian Forest Fire Behavior Prediction System," Natural Resources Canada, Canadian Forestry Service, Ottawa, Canada, Tech. Rep. ST-X-3, 1992, p. 64.

[23] M. Finney, "FARSITE: A fire area simulator for fire managers," Forest Service, U.S. Department of Agriculture, Albany, CA: Pacific Southwest Research Station, General Technical Report PSW-GTR-158, Feb. 1994.

[24] K. Mcgrattan, "Fire Modeling: Where Are We? Where Are We Going?" Tech. Rep., 2005.

[25] G. Rein, "The six Layers of Protection in Fire Engineering," Aug. 2022, Publisher: Zenodo Version Number: ver 1. DOI: 10.5281/ZENODO.7036280. [Online]. Available: https://zenodo.org/record/7036280 (visited on 01/28/2025).

[26] T. M. Giannaros, V. Kotroni, and K. Lagouvardos, "IRIS Rapid response fire spread forecasting system: Development, calibration and evaluation," en, *Agricultural and Forest Meteorology*, vol. 279, p. 107 745, Dec. 2019, ISSN: 01681923. DOI: 10.1016/j.agrformet.2019.107745. [Online]. Available: https://linkinghub.elsevier.com/retrieve/pii/S0168192319303612 (visited on 01/17/2025).

[27] E. Ronchi, J. Wahlqvist, A. Rohaert, *et al.*, "WUI-NITY 2: The integration, verification, and validation of the wildfire evacuation platform WUI-NITY," Tech. Rep., 2021. [Online]. Available: www.nfpa.org/foundation.

[28] E. D. Kuligowski, N. A. Waugh, J. Sutton, and T. J. Cova, "Ember Alerts: Assessing Wireless Emergency Alert Messages in Wildfires Using the Warning Response Model," *Natural Hazards Review*, vol. 24, no. 2, May 2023, Publisher: American Society of Civil Engineers (ASCE). DOI: 10.1061/nhrefo.nheng-1724.

[29] E. Ronchi, S. D. Wong, and M. Theodori, "Case studies of large outdoor fires involving evacuations," 2021. DOI: 10.5281/zenodo.4504853. [Online]. Available: https://www.researchgate.net/publication/350372895.

[30] T. J. Cova, D. Li, L. K. Siebeneck, and F. A. Drews, "Toward Simulating Dire Wildfire Scenarios," *Natural Hazards Review*, vol. 22, no. 3, Aug. 2021, Publisher: American Society of Civil Engineers (ASCE). DOI: 10.1061/(asce)nh.1527-6996.0000474.

[31] A. J. Tepley, M.-A. Parisien, X. Wang, J. A. Oliver, and M. D. Flannigan, "Wildfire evacuation patterns and syndromes across Canada's forested regions," en, *Ecosphere*, vol. 13, no. 10, e4255, Oct. 2022, ISSN: 2150-8925, 2150-8925. DOI: 10.1002/ecs2.4255. [Online]. Available: https://esajournals.onlinelibrary.wiley.com/doi/10.1002/ecs2.4255 (visited on 01/17/2025).

[32] M. Athanasiou and G. Xanthopoulos, "The behaviour of the deadly wildre of July 23, 2018 in Northeastern Attica, Greece," *Proceedings of the 20th Panhellenic Forestry Conference*, 2021.

[33] K. Lagouvardos, V. Kotroni, T. M. Giannaros, and S. Dafis, "Meteorological conditions conducive to the rapid spread of the deadly wildfire in eastern attica, Greece," *Bulletin of the American Meteorological Society*, vol. 100, no. 11, pp. 2137–2145, 2019, Publisher: American Meteorological Society. DOI: 10.1175/BAMS-D-18-0231.1.

[34] A. Gourbatsis, "Technical Report (Preliminary)," Greek, Hellenic Fire Service, Athens, Greece, Incident Report, 2018.

[35] The Global Fire Monitoring Center (GFMC), "Committee for the potenial wildfire management of firests and countryside in Greece. (Originally:)," Greek, Athens, Greece, Government Report, Jan. 2019.

[36] E. Ronchi, S. Gwynne, G. Rein, R. Wadhwani, P. Intini, and A. Bergstedt, "E-Sanctuary: Open Multi-Physics Framework for Modelling Wildfire Urban Evacuation FINAL REPORT BY," Tech. Rep., 2017.

[37] E. Ronchi, J. Wahlqvist, S. Gwynne, *et al.*, "WUI-NITY: A platform for the simulation of wildland-urban interface fire evacuation," Tech. Rep., 2020. [Online]. Available: www.nfpa.org/foundation.

[38] E. Ronchi, J. Wahlqvist, A. Rohaert, *et al.*, "WUI-NITY 3: Multi-method traffic movement data collection for WUI fire evacuation modelling Final Report by," Tech. Rep., 2023. [Online]. Available: www.nfpa.org/foundation.

[39] E. Ronchi, A. Rohaert, J. Wahlqvist, N. Wetterberg, and P. Intini, "Progress Report 1: Resilience and Adaptation to Climatic Extreme Wildfires (RACE Wildfires)," Tech. Rep. [Online]. Available: http://www.brand.lth.se/english.

[40] E. Ronchi, J. Wahlqvist, A. Ardinge, *et al.*, "The verification of wildlandurban interface fire evacuation models," en, *Natural Hazards*, vol. 117, no. 2, pp. 1493–1519, Jun. 2023, ISSN: 0921-030X, 1573-0840. DOI: 10.1007/s11069-023-05913-2. [Online]. Available: https://link.springer.com/10.1007/s11069-023-05913-2 (visited on 01/28/2025).

[41] A. Rohaert, N. Janfeshanaraghi, E. Kuligowski, and E. Ronchi, "The analysis of traffic data of wildfire evacuation: The case study of the 2020 Glass Fire," *Fire Safety Journal*, vol. 141, Dec. 2023, Publisher: Elsevier Ltd. DOI: 10.1016/j.firesaf.2023.103909.

[42] S. M. V. Gwynne, E. Ronchi, J. Wahlqvist, *et al.*, "Roxborough Park Community Wildfire Evacuation Drill: Data Collection and Model Benchmarking," en, *Fire Technology*, vol. 59, no. 2, pp. 879–901, Mar. 2023, ISSN: 0015-2684, 1572-8099. DOI: 10.1007/s10694-023-01371-1. [Online]. Available: https://link.springer.com/10.1007/s10694-023-01371-1 (visited on 01/16/2025).

[43] N. Kalogeropoulos, H. Mitchell, E. Ronchi, S. Gwynne, and G. Rein, "Design of stochastic trigger boundaries for rural communities evacuating from a wildfire," *Fire Safety Journal*, vol. 140, Oct. 2023, Publisher: Elsevier Ltd. DOI: 10.1016/j.firesaf.2023.103854.

[44] N. Kalogeropoulos, A. Castagna, and G. Rein, "A Gaussian Dispersion Model for Haze Spread with Downwind Terrain Effects," in *Submitted to the International Symposium of Fire and Explosion Hazards (ISFEH 11)*, Rome, Italy, 2025.

[45] N. Kalogeropoulos, H. Mitchell, E. Kuligowski, E. Ronchi, and G. Rein, "Quantifying dire evacuations in case of wildfire using trigger boundaries and case study of the 2018 Mati wildfire in Greece," *Safety Science*, vol. 181, Jan. 2025, Publisher: Elsevier B.V. DOI: 10.1016/j.ssci.2024.106691.

[46] N. Kalogeropoulos and G. Rein, *Benchmarking of Semi-Empirical and Machine Learning Models of Wildfire Spread Outside their Calibration Region*, Oral Presentation, Corfu, Greece, Jun. 2025.

[47] H. Mitchell, S. Gwynne, E. Ronchi, N. Kalogeropoulos, and G. Rein, "Integrating wildfire spread and evacuation times to design safe triggers: Application to two rural communities using PERIL model," *Safety Science*, vol. 157, Jan. 2023, Publisher: Elsevier B.V. DOI: 10.1016/j.ssci.2022.105914.

[48] E. Ronchi and S. Gwynne, *Computational Evacuation Modeling in Wildfires*, 2020.

[49] T. W. Juliano, F. Szasdi-Bardales, N. P. Lareau, *et al.*, "Brief communication: The Lahaina Fire disaster how models can be used to understand and predict wildfires," en, *Natural Hazards and Earth System Sciences*, vol. 24, no. 1, pp. 47–52, Jan. 2024, ISSN: 1684-9981. DOI: 10.5194/nhess-24-47-2024. [Online]. Available: https://nhess.copernicus.org/articles/24/47/2024/ (visited on 01/17/2025).

[50] M. Dandoulaki, M. Lazoglou, N. Pangas, and K. Serraos, "Disaster Risk Management and Spatial Planning: Evidence from the Fire-Stricken Area of Mati, Greece," *Sustainability (Switzerland)*, vol. 15, no. 12, Jun. 2023, Publisher: MDPI. DOI: 10.3390/su15129776.

[51] K. Katzilieris, E. I. Vlahogianni, and H. Wang, "Evacuation behavior of affected individuals and households in response to the 2018 Attica wildfires: From empirical data to models," en, *Safety Science*, vol. 153, p. 105 799, Sep. 2022, ISSN: 09257535. DOI:

10.1016/j.ssci.2022.105799. [Online]. Available: https://linkinghub.elsevier.com/retrieve/pii/S0925753522001382 (visited on 01/17/2025).

[52] George G. Spanos, "Urban Fires Case Study: Mati, Eastern Attica, Greece 23.7.2018 and its Management. Personal Rescue and Emergency Evacuation Through Survivors' testimonies," Tech. Rep., 2021.

[53] S. Grajdura, X. Qian, and D. Niemeier, "Awareness, departure, and preparation time in no-notice wildfire evacuations," *Safety Science*, vol. 139, Jul. 2021, Publisher: Elsevier B.V. DOI: 10.1016/j.ssci.2021.105258.

[54] S. Grajdura, S. Borjigin, and D. Niemeier, "Fast-moving dire wildfire evacuation simulation," *Transportation Research Part D: Transport and Environment*, vol. 104, Mar. 2022, Publisher: Elsevier Ltd. DOI: 10.1016/j.trd.2022.103190.

[55] M. Diakakis, G. Xanthopoulos, and L. Gregos, "Analysis of forest fire fatalities in Greece: 19772013," en, *International Journal of Wildland Fire*, vol. 25, no. 7, pp. 797–809, Jun. 2016, ISSN: 1049-8001, 1448-5516. DOI: 10.1071/WF15198. [Online]. Available: https://www.publish.csiro.au/WF/WF15198 (visited on 01/17/2025).

[56] N. Krusel and S. N. Petris, "A Study Of Civilian Deaths In the 1983 Ash Wednesday Bushfires Victoria, Australia," Tech. Rep. 300.032.0202, 1998. [Online]. Available: www.cfa.vic.gdv.au.

[57] T. Toledo, I. Marom, E. Grimberg, and S. Bekhor, "Analysis of evacuation behavior in a wildfire event," *International Journal of Disaster Risk Reduction*, vol. 31, pp. 1366–1373, Oct. 2018, Publisher: Elsevier Ltd. DOI: 10.1016/j.ijdrr.2018.03.033.

[58] I. Zikeloglou, E. Lekkas, S. Lozios, and M. Stavropoulou, "Is early evacuation the best and only strategy to protect and mitigate the effects of forest fires in WUI areas? A qualitative research on the residents response during the 2021 forest fires in NE Attica, Greece," *International Journal of Disaster Risk Reduction*, vol. 88, Apr. 2023, Publisher: Elsevier Ltd. DOI: 10.1016/j.ijdrr.2023.103612.

[59] E. D. Kuligowski, X. Zhao, R. Lovreglio, *et al.*, "Modeling evacuation decisions in the 2019 Kincade fire in California," *Safety Science*, vol. 146, Feb. 2022, Publisher: Elsevier B.V. DOI: 10.1016/j.ssci.2021.105541.

[60] L. H. Folk, E. D. Kuligowski, S. M. Gwynne, and J. A. Gales, "A Provisional Conceptual Model of Human Behavior in Response to Wildland-Urban Interface Fires," *Fire Technology*, vol. 55, no. 5, pp. 1619–1647, Sep. 2019, Publisher: Springer New York LLC. DOI: 10.1007/s10694-019-00821-z.

[61] K. Haynes, K. Short, G. Xanthopoulos, D. Viegas, L. M. Ribeiro, and R. Blanchi, "Wildfires and WUI Fire Fatalities," in *Encyclopedia of Wildfires and Wildland-Urban Interface (WUI) Fires*, Springer International Publishing, 2020, pp. 1–16. DOI: 10.1007/978-3-319-51727-8_92-1.

[62] D. M. Molina-Terrén, G. Xanthopoulos, M. Diakakis, *et al.*, "Analysis of forest fire fatalities in Southern Europe: Spain, Portugal, Greece and Sardinia (Italy)," *International Journal of Wildland Fire*, vol. 28, no. 2, pp. 85–98, 2019, Publisher: CSIRO. DOI: 10.1071/WF18004.

[63] K. Haynes, J. Handmer, J. McAneney, A. Tibbits, and L. Coates, "Australian bushfire fatalities 1900-2008: Exploring trends in relation to the 'Prepare, stay and defend or leave early' policy," *Environmental Science and Policy*, vol. 13, no. 3, pp. 185–194, May 2010. DOI: 10.1016/j.envsci.2010.03.002.

[64] D. Weber, E. Moskwa, G. M. Robinson, D. K. Bardsley, J. Arnold, and M. A. Davenport, "Are we ready for bushfire? Perceptions of residents, landowners and fire authorities on Lower Eyre Peninsula, South Australia," *Geoforum*, vol. 107, pp. 99–112, Dec. 2019, Publisher: Elsevier Ltd. DOI: 10.1016/j.geoforum.2019.10.006.

[65] J. Whittaker, M. Taylor, and C. Bearman, "Why don't bushfire warnings work as intended? Responses to official warnings during bushfires in New South Wales, Australia," *International Journal of Disaster Risk Reduction*, vol. 45, May 2020, Publisher: Elsevier Ltd. DOI: 10.1016/j.ijdrr.2020.101476.

[66] J. Auld, V. Sokolov, A. Fontes, and R. Bautista, "Internet-based stated response survey for no-notice emergency evacuations," *Transportation Letters*, vol. 4, no. 1, pp. 41–53, 2012, Publisher: Maney Publishing. DOI: 10.3328/TL.2012.04.01.41-53.

[67] Y. C. Chiu, H. Zheng, J. Villalobos, and B. Gautam, "Modeling no-notice mass evacuation using a dynamic traffic flow optimization model," *IIE Transactions (Institute of Industrial Engineers)*, vol. 39, no. 1, pp. 83–94, Jan. 2007. DOI: 10.1080/07408170600946473.

[68] J. Sorensen and B. Vogt, "Description of Survey Data Regarding the Chemical Repackaging Plant Accident West Helena, Arkansas," en, Tech. Rep. ORNL/TM-13722, 5889, Mar. 1999, ORNL/TM–13 722, 5889. DOI: 10.2172/5889. [Online]. Available: http://www.osti.gov/servlets/purl/5889-1rboIG/webviewable/ (visited on 01/17/2025).

[69] M. Meit, I. Redlener, T. W. Briggs, M. Kwanisai, D. Culp, and D. M. Abramson, "Rural and Suburban Population Surge Following Detonation of an Improvised Nuclear Device: A New Model to Estimate Impact," en, *Disaster Medicine and Public Health Preparedness*, vol. 5, no. S1, S143–S150, Mar. 2011, ISSN: 1935-7893, 1938-744X. DOI: 10.1001/dmp.2011.20. [Online]. Available: https://www.cambridge.org/core/product/identifier/S1935789300003852/type/journal_article (visited on 01/17/2025).

[70] D. J. Zeigler and J. H. Johnson, "Evacuation Behavior in response to Nuclear Power Plant Accidents," en, *The Professional Geographer*, vol. 36, no. 2, pp. 207–215, May 1984, ISSN: 0033-0124, 1467-9272. DOI: 10.1111/j.0033-0124.1984.00207.x. [Online]. Available: http://www.tandfonline.com/doi/abs/10.1111/j.0033-0124.1984.00207.x (visited on 01/17/2025).

[71] N. Golshani, R. Shabanpour, A. Mohammadian, J. Auld, and H. Ley, "Analysis of evacuation destination and departure time choices for no-notice emergency events," *Transportmetrica A: Transport Science*, vol. 15, no. 2, pp. 896–914, Nov. 2019, Publisher: Taylor and Francis Ltd. DOI: 10.1080/23249935.2018.1546778.

[72] B. Wolshon, E. Urbina, and M. Levitan, *National Review of Hurricane Evacuation Plans and Policies*. Baton Rouge, Louisiana: LSU Hurricane Center, 2001.

[73] B. Wolshon and E. M. Iii, "Emergency Planning in the Urban-Wildland Interface: Subdivision-Level Analysis of Wildfire Evacuations," *Journal of Urban Planning and Development*, 2007. DOI: 10.1061/ASCE0733-94882007133:173.

[74] M. Ciarla and K. Townsend, *2023 HURREVAC Training Webinar Series Day 3 Evacuation Timing Features*, Jun. 2023.

[75] D. Li, T. J. Cova, and P. E. Dennison, "Using reverse geocoding to identify prominent wildfire evacuation trigger points," *Applied Geography*, vol. 87, pp. 14–27, Oct. 2017, Publisher: Elsevier Ltd. DOI: 10.1016/j.apgeog.2017.05.008.

[76] P. E. Dennison, T. J. Cova, and M. A. Mortiz, "WUIVAC: A wildland-urban interface evacuation trigger model applied in strategic wildfire scenarios," *Natural Hazards*, vol. 41, no. 1, pp. 181–199, Apr. 2007. DOI: 10.1007/s11069-006-9032-y.

[77] T. J. Cova, P. E. Dennison, D. Li, F. A. Drews, L. K. Siebeneck, and M. K. Lindell, "Warning Triggers in Environmental Hazards: Who Should Be Warned to Do What and When?" *Risk Analysis*, vol. 37, no. 4, pp. 601–611, Apr. 2017, Publisher: Blackwell Publishing Inc. DOI: 10.1111/risa.12651.

[78] A. L. Sullivan, "Wildland surface fire spread modelling, 1990 - 2007. 3: Simulation and mathematical analogue models," *International Journal of Wildland Fire*, vol. 18, no. 4, pp. 387–387, 2009. DOI: 10.1071/WF06144.

[79] A. L. Sullivan, "Wildland surface fire spread modelling, 1990 - 2007. 2: Empirical and quasi-empirical models," *International Journal of Wildland Fire*, vol. 18, no. 4, pp. 369–369, 2009. DOI: 10.1071/WF06142.

[80] A. L. Sullivan, "Wildland surface fire spread modelling, 1990 - 2007. 1: Physical and quasi-physical models," *International Journal of Wildland Fire*, vol. 18, no. 4, pp. 349–349, 2009. DOI: 10.1071/WF06143.

[81] C. Tymstra, R. W. Bryce, B. M. Wotton, S. W. Taylor, and O. B. Armitage, "Development and Structure of Prometheus: The Canadian Wildland Fire Growth Simulation Model," Natural Resources Canada, Edmonton, Alberta, Information Report NOR-X-417, 2010.

[82] C. Lautenberger, "Wildland fire modeling with an Eulerian level set method and automated calibration," *Fire Safety Journal*, vol. 62, no. PART C, pp. 289–298, 2013, Publisher: Elsevier Ltd. DOI: 10.1016/j.firesaf.2013.08.014.

[83] J. Burge, M. R. Bonanni, R. L. Hu, and M. Ihme, "Recurrent Convolutional Deep Neural Networks for Modeling Time-Resolved Wildfire Spread Behavior," *Fire Technology*, vol. 59, no. 6, pp. 3327–3354, Nov. 2023, Publisher: Springer. DOI: 10.1007/s10694-023-01469-6.

[84] A. Bergstedt, "A review of traffic models for wildland-urban interface wildfire evacuation.," Lund University, Lund, Sweden, Tech. Rep. 5555, 2017.

[85] P. Intini, E. Ronchi, S. Gwynne, and A. Pel, "Traffic Modeling for WildlandUrban Interface Fire Evacuation," *Journal of Transportation Engineering, Part A: Systems*, vol. 145, no. 3, Mar. 2019, Publisher: American Society of Civil Engineers (ASCE). DOI: 10.1061/jtepbs.0000221.

[86] A. Forrister, E. D. Kuligowski, Y. Sun, *et al.*, "Analyzing Risk Perception, Evacuation Decision and Delay Time: A Case Study of the 2021 Marshall Fire in Colorado," en, *Travel Behaviour and Society*, vol. 35, p. 100 729, Apr. 2024, ISSN: 2214367X. DOI: 10.1016/j.tbs.2023.100729. [Online]. Available: https://linkinghub.elsevier.com/retrieve/pii/S2214367X23001801 (visited on 01/17/2025).

[87] N. Wetterberg, E. Ronchi, and J. Wahlqvist, "Individual Driving Behaviour in Wildfire Smoke," en, *Fire Technology*, vol. 57, no. 3, pp. 1041–1061, May 2021, ISSN: 0015-2684, 1572-8099. DOI: 10.1007/s10694-020-01026-5. [Online]. Available: https://link.springer.com/10.1007/s10694-020-01026-5 (visited on 01/17/2025).

[88] J. C. Larsen, P. E. Dennison, T. J. Cova, and C. Jones, "Evaluating dynamic wildfire evacuation trigger buffers using the 2003 Cedar Fire," *Applied Geography*, vol. 31, no. 1, pp. 12–19, Jan. 2011. DOI: 10.1016/j.apgeog.2010.05.003.

[89] J. Ramirez, S. Monedero, C. A. Silva, and A. Cardil, "Stochastic decision trigger modelling to assess the probability of wildland fire impact," *Science of the Total Environment*, vol. 694, Dec. 2019, Publisher: Elsevier B.V. DOI: 10.1016/j.scitotenv.2019.07.311.

[90] M. Pishahang, A. Ruiz-Tagle, E. Lopez Droguett, M. Ramos, and A. Mosleh, "WISE: A Probabilistic Wildfire Safe Egress Planning Framework and Software Platform," Honolulu, Jun. 2022.

[91] M. A. Finney, "FARSITE: Fire Area Simulator-model development and evaluation," en, U.S. Department of Agriculture, Forest Service, Rocky Mountain Research Station, Ft. Collins, CO, Tech. Rep. RMRS-RP-4, 1998, RMRS–RP–4. DOI: 10.2737/RMRS-RP-4. [Online]. Available: https://www.fs.usda.gov/treesearch/pubs/4617 (visited on 11/04/2024).

[92] G. D. Richards, "The properties of elliptical wildfire growth for time dependent fuel and meteorological conditions," *Combustion Science and Technology*, vol. 95, no. 1-6, pp. 357–383, Dec. 1993. DOI: 10.1080/00102209408935341.

[93] C. E. Van Wagner, "A Simple Fire-Growth Model For personal use only," Tech. Rep., 1969.

[94] H. E. Anderson, "Predicting wind-driven wild land fire size and shape.," USDA Forest Service, Intermountain Forest and Range Experiment Station, Odgen, Utah, Research Paper INT-RP-305, 1983.

[95] R. C. Rothermel, "A mathematical model for predicting fire spread in wildland fuels.," US Forest Service, Odgen, Utah, Research Paper INT-115, 1972.

[96] P. L. Andrews, "The Rothermel surface fire spread model and associated developments: A comprehensive explanation," en, U.S. Department of Agriculture, Forest Service, Rocky Mountain Research Station, Ft. Collins, CO, Tech. Rep. RMRS-GTR-371, 2018, RMRS–GTR–371. DOI: 10.2737/RMRS-GTR-371. [Online]. Available: https://www.fs.usda.gov/treesearch/pubs/55928 (visited on 11/04/2024).

[97] T. H. Cormen, C. E. Leiserson, R. L. Rivest, and C. Stein, *Introduction to algorithms*, eng, Third edition. Cambridge, Massachusetts London, England: MIT Press, 2009, ISBN: 978-0-262-03384-8 978-0-262-27083-0.

[98] *ACS Demographic And Housing Estimates, 2021: ACS 5-Year Estimate Data Profiles*, 2020.

[99] R. Lovreglio, E. Kuligowski, S. Gwynne, and K. Boyce, "A pre-evacuation database for use in egress simulations," en, *Fire Safety Journal*, vol. 105, pp. 107–128, Apr. 2019, ISSN: 03797112. DOI: 10.1016/j.firesaf.2018.12.009. [Online]. Available: https://linkinghub.elsevier.com/retrieve/pii/S0379711218302212 (visited on 01/17/2025).

[100] D. Purser and M. Bensilum, "Quantification of behaviour for engineering design standards and escape time calculations," en, *Safety Science*, vol. 38, no. 2, pp. 157–182, Jul. 2001, ISSN: 09257535. DOI: 10.1016/S0925-7535(00)00066-7. [Online]. Available: https://linkinghub.elsevier.com/retrieve/pii/S0925753500000667 (visited on 01/17/2025).

[101] R. Lovreglio, E. Ronchi, and D. Borri, "The validation of evacuation simulation models through the analysis of behavioural uncertainty," *Reliability Engineering and System Safety*, vol. 131, pp. 166–174, 2014, Publisher: Elsevier Ltd. DOI: 10.1016/j.ress.2014.07.007.

[102] Y. Matvienko, "The simplified approach for estimating probabilistic safety factors in fracture mechanics," en, *Engineering Failure Analysis*, vol. 117, p. 104 814, Nov. 2020, ISSN: 13506307. DOI: 10.1016/j.engfailanal.2020.104814. [Online]. Available: https://linkinghub.elsevier.com/retrieve/pii/S1350630720305574 (visited on 01/17/2025).

[103] A. Haldar and S. Mahadevan, *Probability, reliability, and statistical methods in engineering design*. New York ; Chichester [England]: John Wiley, 2000, OCLC: ocm42621802, ISBN: 978-0-471-33119-3.

[104] A. Grandison, "Determining Confidence Intervals, and Convergence, for Parameters in Stochastic Evacuation Models," *Fire Technology*, vol. 56, no. 5, pp. 2137–2177, Sep. 2020, Publisher: Springer. DOI: 10.1007/s10694-020-00968-0.

[105] M. A. Finney, "An Overview of FlamMap Fire Modeling Capabilities," U.S. Department of Agriculture, Forest Service, Portland, OR, Proceedings RMRS-P-41, Mar. 2006.

[106] G. Xanthopoulos, V. Varela, P. Fernandes, L. Ribeiro, and F. Guarnieri, "Decision support systems and tools: A state of the art," EUFIRELAB, Project Deliverable D-06-02, 2002.

[107] G. Büttner, J. Feranec, G. Jaffrain, European Environment Agency, and European Commission, Eds., *Corine land cover update 2000*, eng. Copenhagen: EEA, 2002, ISBN: 978-92-9167-511-1.

[108] J. H. Scott and R. E. Burgan, "Standard fire behavior fuel models: A comprehensive set for use with Rothermel's surface fire spread model," en, U.S. Department of Agriculture, Forest Service, Rocky Mountain Research Station, Ft. Collins, CO, Tech. Rep. RMRS-GTR-153, 2005, RMRS–GTR–153. DOI: 10.2737/RMRS-GTR-153. [Online]. Available: https://www.fs.usda.gov/treesearch/pubs/9521 (visited on 11/04/2024).

[109] K. Lagouvardos, V. Kotroni, A. Bezes, *et al.*, "The automatic weather stations NOANN network of the National Observatory of Athens: Operation and database," en, *Geoscience Data Journal*, vol. 4, no. 1, pp. 4–16, Jun. 2017, ISSN: 2049-6060, 2049-6060. DOI: 10.1002/gdj3.44. [Online]. Available: https://rmets.onlinelibrary.wiley.com/doi/10.1002/gdj3.44 (visited on 01/17/2025).

[110] M. R. Siam, H. Wang, M. K. Lindell, C. Chen, E. I. Vlahogianni, and K. Axhausen, "An interdisciplinary agent-based multimodal wildfire evacuation model: Critical decisions and life safety," *Transportation Research Part D: Transport and Environment*, vol. 103, Feb. 2022, Publisher: Elsevier Ltd. DOI: 10.1016/j.trd.2021.103147.

[111] K. Sinolakis, N. Kalligeris, V. Skanavis, *et al.*, *The deadly dire of the 23rd July in Mati: Wildfire and Evacuation Simulation (Originally: 23 :)*, Athens, Greece, 2018.

[112] P. Intini, J. Wahlqvist, N. Wetterberg, and E. Ronchi, "Modelling the impact of wildfire smoke on driving speed," *International Journal of Disaster Risk Reduction*, vol. 80, Oct. 2022, Publisher: Elsevier Ltd. DOI: 10.1016/j.ijdrr.2022.103211.

[113] C. Miller and A. A. Ager, "A review of recent advances in risk analysis for wildfire management," en, *International Journal of Wildland Fire*, vol. 22, no. 1, p. 1, 2013, ISSN: 1049-8001. DOI: 10.1071/WF11114. [Online]. Available: http://www.publish.csiro.au/?paper=WF11114 (visited on 11/01/2024).

[114] G. D. Papadopoulos and F.-N. Pavlidou, "A Comparative Review on Wildfire Simulators," *IEEE Systems Journal*, vol. 5, no. 2, pp. 233–243, Jun. 2011, ISSN: 1932-8184, 1937-9234. DOI: 10.1109/JSYST.2011.2125230. [Online]. Available: http://ieeexplore.ieee.org/document/5738359/ (visited on 11/01/2024).

[115] Y. R. Driss, M. J. Suggs, and A. D. Ray, "Methods of Numerical Integration of Whitham's F -Curve," en, 2018, Publisher: Unpublished. DOI: 10.13140/RG.2.2.31338.13761. [Online]. Available: http://rgdoi.net/10.13140/RG.2.2.31338.13761 (visited on 11/01/2024).

[116] D. G. Green, A. M. Gill, and I. R. Noble, "Fire Shapes and the Adequacy of Fire-Spread Models," Tech. Rep. 03043800/83, 1983, Volume: 20, pp. 33–45.

[117] C. Lautenberger, "Mapping areas at elevated risk of large-scale structure loss using Monte Carlo simulation and wildland fire modeling," en, *Fire Safety Journal*, vol. 91, pp. 768–775, Jul. 2017, ISSN: 03797112. DOI: 10.1016/j.firesaf.2017.04.014. [Online]. Available: https://linkinghub.elsevier.com/retrieve/pii/S0379711217301017 (visited on 01/16/2025).

[118] V. Mallet, D. E. Keyes, and F. E. Fendell, "Modeling wildland fire propagation with level set methods," *Computers and Mathematics with Applications*, vol. 57, no. 7, pp. 1089–1101, Apr. 2009. DOI: 10.1016/j.camwa.2008.10.089.

[119] B. M. Wotton, "Interpreting and using outputs from the Canadian Forest Fire Danger Rating System in research applications," en, *Environmental and Ecological Statistics*, vol. 16, no. 2, pp. 107–131, Jun. 2009, ISSN: 1352-8505, 1573-3009. DOI: 10.1007/s10651-007-0084-2. [Online]. Available: http://link.springer.com/10.1007/s10651-007-0084-2 (visited on 03/27/2025).

[120] K. B. McGrattan, "Fire dynamics simulator (version 4) : Technical reference guide," en, National Institute of Standards and Technology, Gaithersburg, MD, Tech. Rep. NIST SP 1018, 2006, Edition: 0, NIST SP 1018. DOI: 10.6028/NIST.SP.1018. [Online]. Available: https://nvlpubs.nist.gov/nistpubs/Legacy/SP/nistspecialpublication1018.pdf (visited on 03/27/2025).

[121] H. E. Anderson, "Aids to Determining Fuel Models For Estimating Fire Behavior," US Forest Service, Odgen. Utah, Tech. Rep. General Technical Report INT-122, 1982. [Online]. Available: https://doi.org/10.2737/INT-GTR-122.

[122] K. B. McGrattan and G. P. Forney, "Fire Dynamics Simulator User Manual (Version 6.9.1)," National Institute of Standards and Technology, Gaithersburg, MD, Tech. Rep., 2004. DOI: 10.6028/NIST.SP.1019. [Online]. Available: https://nvlpubs.nist.gov/nistpubs/Legacy/SP/nistspecialpublication1019.pdf.

[123] R. Ziel, "Michigan Field Guide for CFFDRS Fire Behavior Prediction (FBP) System," Tech. Rep., 2015.

[124] T. Gneiting and A. E. Raftery, "Weather Forecasting with Ensemble Methods," en, *Science*, vol. 310, no. 5746, pp. 248–249, Oct. 2005, ISSN: 0036-8075, 1095-9203. DOI: 10.1126/science.1115255. [Online]. Available: https://www.science.org/doi/10.1126/science.1115255 (visited on 03/27/2025).

[125] H. Wu and D. Levinson, "The ensemble approach to forecasting: A review and synthesis," en, *Transportation Research Part C: Emerging Technologies*, vol. 132, p. 103 357, Nov. 2021, ISSN: 0968090X. DOI: 10.1016/j.trc.2021.103357. [Online]. Available: https://linkinghub.elsevier.com/retrieve/pii/S0968090X21003594 (visited on 03/27/2025).

[126] J. Vaillant, *Fire weather: a true story from a hotter world*, eng, Paperback edition. London: Sceptre, 2024, ISBN: 978-1-3997-2023-6.

[127] R. Massey, B. Rogers, L. Berner, *et al.*, *Arctic-Boreal Vulnerability Experiment (ABoVE)Deciduous Fractional Cover and Tree Canopy Cover for Boreal North America, 1992-2015*, en, Artwork Size: 0 MB Medium: COG Pages: 0 MB Version Number: 1, 2023. DOI: 10.3334/ORNLDAAC/2296. [Online]. Available: https://daac.ornl.gov/cgi-bin/dsviewer.pl?ds_id=2296 (visited on 01/30/2025).

[128] N. Phelps, H. Cameron, A. M. Forbes, T. Schiks, D. Schroeder, and J. L. Beverly, "The Alberta Wildland Fuels Inventory Program (AWFIP): Data description and reference tables," en, *Annals of Forest Science*, vol. 79, no. 1, p. 28, Dec. 2022, ISSN: 1286-4560, 1297-966X. DOI: 10.1186/s13595-022-01144-w. [Online]. Available: https://annforsci.biomedcentral.com/articles/10.1186/s13595-022-01144-w (visited on 01/30/2025).

[129] R. M. Nelson Jr, "Prediction of diurnal change in 10-h fuel stick moisture content," en, *Canadian Journal of Forest Research*, vol. 30, no. 7, pp. 1071–1087, Jul. 2000, Publisher: Canadian Science Publishing, ISSN: 0045-5067, 1208-6037. DOI: 10.1139/x00-032. [Online]. Available: http://www.nrcresearchpress.com/doi/10.1139/x00-032 (visited on 07/24/2025).

[130] M. LLP, "A Review of the 2016 Horse River Wildfire: Alberta Agriculture and Forestry Preparedness and Response," Dorestry Divistion, Alberta Agriculture and Forestry, Edmonton, Alberta, Tech. Rep., Mar. 2017.

[131] F. C. Rego and F. X. Catry, "Modelling the effects of distance on the probability of fire detection from lookouts," en, *International Journal of Wildland Fire*, vol. 15, no. 2, p. 197, 2006, ISSN: 1049-8001. DOI: 10.1071/WF04016. [Online]. Available: http://www.publish.csiro.au/?paper=WF04016 (visited on 03/05/2025).

[132] O. Kucuk, O. Topaloglu, A. O. Altunel, and M. Cetin, "Visibility analysis of fire lookout towers in the Boyabat State Forest Enterprise in Turkey," en, *Environmental Monitoring and Assessment*, vol. 189, no. 7, p. 329, Jul. 2017, ISSN: 0167-6369, 1573-2959. DOI: 10.1007/s10661-017-6008-1. [Online]. Available: http://link.springer.com/10.1007/s10661-017-6008-1 (visited on 03/05/2025).

[133] D. J. Rasbash and D. D. Drysdale, "Fundamentals of Smoke Production*," Tech. Rep., 1982, Volume: 5, pp. 77–86.

[134] E. A. Lancet, G. Asaeda, R. Zeig-Owens, and D. J. Prezant, "Emergency Medical Services Use in New York City Amidst Record-Breaking Fine Particulate Matter Levels from the Canadian Wildfires, June 2023," en, *Annals of Emergency Medicine*, vol. 84, no. 2, pp. 223–225, Aug. 2024, ISSN: 01960644. DOI: 10.1016/j.annemergmed.2024.03.028. [Online]. Available: https://linkinghub.elsevier.com/retrieve/pii/S0196064424001987 (visited on 03/27/2025).

[135] J. Casal, *Evaluation of the Effects and Consequences of Major Accidents in Industrial Plants*. Elsevier, 2018, ISBN: 978-0-444-63883-0. DOI: 10.1016/C2016-0-00740-4.

[136] A. R. Riebau, D. G. Foxt, M. L. Sestak, B. Dailey, and S. F. Archer, "SIMPLE APPROACH SMOKE ESTIMATION MODEL," Tech. Rep., 1988, Issue: 4 Volume: 22, pp. 783–788.

[137] J. Mandel, S. Amram, J. D. Beezley, *et al.*, "Recent advances and applications of WRFSFIRE," *Natural Hazards and Earth System Sciences*, vol. 14, no. 10, pp. 2829–2845, Oct. 2014. DOI: 10.5194/nhess-14-2829-2014.

[138] Y. Hu, W. Cui, and G. Rein, "Haze emissions from smouldering peat: The roles of inorganic content and bulk density," en, *Fire Safety Journal*, vol. 113, p. 102 940, May 2020, ISSN: 03797112. DOI: 10.1016/j.firesaf.2019.102940. [Online]. Available: https://linkinghub.elsevier.com/retrieve/pii/S0379711219304230 (visited on 11/25/2024).

[139] D. C. Lutes, "FOFEM 6.4: First Order Fire Effects Model user guide.," USDA Forest Service, Rocky Mountain Research Station, Missoula, MT, User Guide, 2017, p. 86.

[140] R. D. Ottmar, D. V. Sandberg, C. L. Riccardi, and S. J. Prichard, "An overview of the Fuel Characteristic Classification Systemă Quantifying, classifying, and creating fuelbeds for resource planningThis article is one of a selection of papers published in the Special Forum on the Fuel Characteristic Classification System.," en, *Canadian Journal of Forest Research*, vol. 37, no. 12, pp. 2383–2393, Dec. 2007, Publisher: Canadian Science Publishing, ISSN: 0045-5067, 1208-6037. DOI: 10.1139/x07-077. [Online]. Available: http://www.nrcresearchpress.com/doi/10.1139/X07-077 (visited on 07/24/2025).

[141] J. Z. Holland, *A Meteorological Survey of the Oak Ridge Area: Final Report Covering the Period 1948-52*. Oak Ridge, TN: United States Atomic Energy Commission, Technical Information Service, 1953.

[142] K. Anderson, A. Pankratz, and C. Mooney, "A Thermodynamic Approach to Estimating Smoke Plume Heights," in *Proceedings of Ninth Symposium on Fire and Forest Meteorology*, 2011.

[143] N. Moisseeva and R. Stull, "Wildfire smoke-plume rise: A simple energy balance parameterization," *Atmospheric Chemistry and Physics*, vol. 21, no. 3, pp. 1407–1425, Feb. 2021, Publisher: Copernicus GmbH. DOI: 10.5194/acp-21-1407-2021.

[144] G. Briggs, "Plume Rise: A Critical Survey," en, Tech. Rep. TID–25075, 4743102, Jan. 1969, TID–25 075, 4 743 102. DOI: 10.2172/4743102. [Online]. Available: http://www.osti.gov/servlets/purl/4743102-l7XJH8/ (visited on 11/07/2024).

[145] Z. Ke, Y. Wang, Y. Zou, Y. Song, and Y. Liu, "Global Wildfire PlumeRise Data Set and Parameterizations for Climate Model Applications," en, *Journal of Geophysical Research: Atmospheres*, vol. 126, no. 6, e2020JD033085, Mar. 2021, ISSN: 2169-897X, 2169-8996. DOI: 10.1029/2020JD033085. [Online]. Available: https://agupubs.onlinelibrary.wiley.com/doi/10.1029/2020JD033085 (visited on 03/28/2025).

[146] L. Lavdas, "Program VSMOKE–Users Manual," Department of Agriculture, Forest Service, Southern Research Station, Asheville, NC: U.S, Technical Report, 1996.

[147] S. Heier, *Grid integration of wind energy conversion systems*, eng, 2nd ed. Chichester: Wiley, 2006, ISBN: 978-0-470-86899-7.

[148] A. Sullivan, "Convective Froude number and Byrams energy criterion of Australian experimental grassland fires," en, *Proceedings of the Combustion Institute*, vol. 31, no. 2, pp. 2557–2564, Jan. 2007, Publisher: Elsevier BV, ISSN: 1540-7489. DOI: 10.1016/j.proci.2006.07.053. [Online]. Available: https://linkinghub.elsevier.com/retrieve/pii/S1540748906000654 (visited on 07/24/2025).

[149] R. Nelson, "Byram Derivation of the Energy Criterion for Forest and Wildland Fires," en, *International Journal of Wildland Fire*, vol. 3, no. 3, p. 131, 1993, Publisher: CSIRO Publishing, ISSN: 1049-8001. DOI: 10.1071/wf9930131. [Online]. Available: http://www.publish.csiro.au/?paper=WF9930131 (visited on 07/24/2025).